

# JOINT TRANSPORTATION RESEARCH PROGRAM

INDIANA DEPARTMENT OF TRANSPORTATION  
AND PURDUE UNIVERSITY



## Hydraulic Fracture Test to Determine Aggregate Freeze-Thaw Durability



**Belayneh Desta**

**Nancy M. Whiting**

**Mark B. Snyder**

## RECOMMENDED CITATION

Desta, B., Whiting, N. M., & Snyder, M. B. (2014). *Hydraulic fracture test to determine aggregate freeze-thaw durability* (Joint Transportation Research Program Publication No. FHWA/IN/JTRP-2014/15). West Lafayette, IN: Purdue University. <http://dx.doi.org/10.5703/1288284315515>

## AUTHORS

### **Belayneh Desta**

Graduate Research Assistant  
Lyles School of Civil Engineering  
Purdue University

### **Nancy M. Whiting**

Concrete Research Scientist  
Lyles School of Civil Engineering  
Purdue University  
(765) 463-2000  
[whiting@purdue.edu](mailto:whiting@purdue.edu)  
*Corresponding Author*

### **Mark B. Snyder, PhD**

Engineering Consultant

## JOINT TRANSPORTATION RESEARCH PROGRAM

The Joint Transportation Research Program serves as a vehicle for INDOT collaboration with higher education institutions and industry in Indiana to facilitate innovation that results in continuous improvement in the planning, design, construction, operation, management and economic efficiency of the Indiana transportation infrastructure. [https://engineering.purdue.edu/JTRP/index\\_html](https://engineering.purdue.edu/JTRP/index_html)

Published reports of the Joint Transportation Research Program are available at: <http://docs.lib.purdue.edu/jtrp/>

## NOTICE

The contents of this report reflect the views of the authors, who are responsible for the facts and the accuracy of the data presented herein. The contents do not necessarily reflect the official views and policies of the Indiana Department of Transportation or the Federal Highway Administration. The report does not constitute a standard, specification, or regulation.

## COPYRIGHT

Copyright 2014 by Purdue University. All rights reserved.

Print ISBN: 978-1-62260-324-4

ePUB ISBN: 978-1-62260-325-1

<b>1. Report No.</b> FHWA/IN/JTRP-2014/15	<b>2. Government Accession No.</b>	<b>3. Recipient's Catalog No.</b>	
<b>4. Title and Subtitle</b> Hydraulic Fracture Test to Determine Aggregate Freeze-Thaw Durability		<b>5. Report Date</b> August 2014	<b>6. Performing Organization Code</b>
<b>7. Author(s)</b> Belayneh Desta, Nancy M. Whiting, Mark B. Snyder		<b>8. Performing Organization Report No.</b> FHWA/IN/JTRP-2014/15	
<b>9. Performing Organization Name and Address</b> Joint Transportation Research Program Purdue University 550 Stadium Mall Drive West Lafayette, IN 47907-2051		<b>10. Work Unit No.</b>  <b>11. Contract or Grant No.</b> SPR-3402	
<b>12. Sponsoring Agency Name and Address</b> Indiana Department of Transportation State Office Building 100 North Senate Avenue Indianapolis, IN 46204		<b>13. Type of Report and Period Covered</b> Final Report  <b>14. Sponsoring Agency Code</b>	
<b>15. Supplementary Notes</b> Prepared in cooperation with the Indiana Department of Transportation and Federal Highway Administration.			
<b>16. Abstract</b>  The freeze-thaw durability of carbonate aggregates can vary greatly from durable to highly susceptible to freeze-thaw distress. Using nondurable aggregate in concrete pavement exposed to freeze-thaw cycles may lead to serious distress and greatly decrease the pavement's service life. The testing needed to identify freeze-thaw durable aggregates can take several months to complete. The main objective of this study was to develop a reliable, quick test method for determining the freeze-thaw resistance of carbonate quarried aggregates in Indiana using the Hydraulic Fracture Test (HFT) equipment.  Aggregate samples collected from 18 quarried carbonate sources from across Indiana that represented a range of freeze-thaw performance were subjected to HFT using the existing MnDOT HFT equipment and the newly developed INDOT HFT equipment. Aggregates from the same sources also were used to produce concrete beams that were subjected to the INDOT modified AASHTO T161-B freeze-thaw test (ITM 210) which evaluates the dilation of concrete beams exposed to freeze-thaw cycles. The experimental data were analyzed statistically and linear regression models were developed to predict the average percent dilation and the durability factor of freeze-thaw test beams using parameters obtained from HFT results. Comparing the modeled and measured test results, the favored model predicts dilations based on the INDOT HFT results. These modeled dilations, when compared to measured dilations gave an adjusted R <sup>2</sup> value of 0.85, indicating the model has a high degree of certainty. The modified INDOT HFT equipment, refined test procedures and data analysis developed during this study are recommended as screening tools for predicting AASHTO T161/ASTM C666 FT test results in 8-days. Further testing is recommended to refine and validate the models before they are fully implemented as an acceptance standard.			
<b>17. Key Words</b>  freeze-thaw resistance, HFT, D-cracking, dilation, durability factor		<b>18. Distribution Statement</b>  No restrictions. This document is available to the public through the National Technical Information Service, Springfield, VA 22161.	
<b>19. Security Classif. (of this report)</b>  Unclassified	<b>20. Security Classif. (of this page)</b>  Unclassified	<b>21. No. of Pages</b>  80	<b>22. Price</b>

## EXECUTIVE SUMMARY

### HYDRAULIC FRACTURE TEST TO DETERMINE AGGREGATE FREEZE-THAW DURABILITY

#### Introduction

Carbonate rocks are the primary sources used as coarse aggregate for concrete paving in Indiana. The freeze-thaw durability of carbonates can vary greatly from durable to highly susceptible to freeze-thaw distress. Using nondurable aggregates in concrete exposed to moisture and freeze-thaw cycles can lead to serious distress and greatly decrease a pavement's service life. The testing needed to identify freeze-thaw durable aggregates can take 90 days or more to complete. The main objective of this study was to develop a reliable, quick test method for determining the freeze-thaw resistance of carbonate aggregates quarried in Indiana using the 8-day Hydraulic Fracture Test (HFT).

The underlying theory behind this accelerated test method suggests that the HFT simulates the state of stresses developing in concrete aggregates exposed to freezing and thawing environments by inducing hydraulic pressure in aggregate particles. Oven-dry aggregates are placed in a test chamber; the chamber is then flooded with water and pressurized using a compressed nitrogen gas to force water into the pores of the aggregate. When the applied pressure is released rapidly, compressed air trapped within the aggregate pores expands, expelling water from pores and creating internal stresses in the aggregate particles, which is believed to be similar to the pressures that can develop in aggregate particles as water in the pores freezes and expands. The degree of fracturing that develops is believed to be an indication of potential freeze-thaw durability of the aggregate. Aggregate fracturing is measured as mass change over several different sieves after 50 pressurization-depressurization cycles.

Aggregate samples were identified and collected from 18 quarried carbonate sources in Indiana that represent a range of freeze-thaw performance: durable (Group A), nondurable (Group B), and of variable or unknown performance (Group C). Samples of aggregate from all 18 sources were subjected to basic characterization tests (e.g., specific gravity and absorption capacity) and HFT testing using both the small MnDOT HFT chamber and newly developed Indiana Department of Transportation (INDOT) HFT chamber. Aggregates from the same sources were also used to produce concrete beams that were subjected to the INDOT modified AASHTO T161-B freeze-thaw test, ITM210 Class AP Coarse Aggregate, to evaluate the dilation of beams exposed to freeze-thaw cycles.

#### Findings

The dilation and the durability factor (DF) measurements of the ITM210 concrete beams correlated well after 350 cycles of freezing and thawing ( $R^2=0.91$ ) (as shown in Figure 5.4). As expected, all aggregate sources in Group A passed the freeze-thaw test while all sources in Group B tested as nondurable based on INDOT's acceptance criteria of less than 0.060% expansion.

The experimental data was analyzed statistically, and linear regression models were developed to predict the average percent

dilation and the durability factor (DF) of freeze-thaw test beams using parameters obtained from HFT results. The percent dilation predicted by the model developed using the MnDOT HFT results showed a good correlation with the measured dilations, resulting in an  $R^2$  value of 0.836 and an adjusted  $R^2$  value of 0.71. The DF models showed poor correlation between predicted and measured DF. The MnDOT HFT equipment with the dilation model developed is considered a good screening tool.

The model developed to predict percent dilation using INDOT HFT equipment results provided an excellent correlation between the measured dilation and predicted dilation with an  $R^2=0.892$  and an adjusted  $R^2$  value of 0.853, indicating the model has a high degree of certainty. This model predicted the durability of 14 out of 18 sources correctly. Of the four sources incorrectly identified, one was a durable source, A3, but had a predicted dilation of 0.1068%, clearly above the INDOT 0.060% acceptance criterion (as shown in Table 7.1). Three sources (B3, B6 and C7) tested as nondurable, with measured dilations ranging from 0.081% to 0.085%, but were predicted to be marginally durable with dilations ranging from 0.055% to 0.0597%, just below the acceptance criterion (as seen in Figure 6.4). This dilation model appears to lose some sensitivity in predicting the performance of sources in the mid-range values that failed with measured dilations at or below 0.085%.

The model developed to predict ITM210 DF using INDOT HFT results also had a very good correlation between the measured and predicted durability factor with  $R^2=0.875$ , and adjusted  $R^2 = 0.812$ . INDOT has not developed acceptance criteria based on DF; therefore, the model's accuracy to predict durability could not be evaluated. This DF model is recommended for further development.

#### Implementation

The refined INDOT HFT equipment, procedures and analysis appear to provide a quick method to evaluate the freeze-thaw resistance of carbonate aggregates quarried in Indiana predicting the 90-day AASHTO T161/ASTM C666 FT test results in 8 days. At this time it is recommended that the INDOT HFT equipment and the developed regression model to predict dilation be used as a screening test employing the following criteria:

- If the HFT results in a predicted dilation lower than 0.050%, then the aggregate is expected to be durable.
- If the HFT results in a predicted dilation greater than 0.060%, then the aggregate is likely nondurable. Actual freeze-thaw durability testing (ITM210) can be performed to confirm.
- If HFT results in a predicted dilation between 0.050% and 0.060%, then freeze-thaw durability testing (ITM210) is required to determine the aggregate durability.

Of the 18 aggregate sources tested, if the above pass/fail criteria for HFT are used, the developed model correctly identified all nondurable aggregates and all but one durable aggregate. Continued testing of additional sources according to both ITM210 and the HFT is recommended. Refining the HFT model should be revisited once additional test data are available before the HFT can be used as a specified acceptance standard.

## CONTENTS

1. INTRODUCTION . . . . .	1
1.1 Background . . . . .	1
1.2 Research Objectives . . . . .	1
1.3 Scope of Work . . . . .	1
2. LITERATURE REVIEW . . . . .	2
2.1 Original SHRP C-391 Study . . . . .	2
2.2 Development of AASHTO Provisional Standard TP12 . . . . .	3
2.3 HFT Testing by Different Agencies . . . . .	3
2.4 Further Developments in Hydraulic Fracture Test . . . . .	4
3. HFT EQUIPMENT AND TEST PROCEDURES . . . . .	5
3.1 MnDOT HFT Equipment . . . . .	5
3.2 INDOT HFT Equipment . . . . .	7
4. AGGREGATE SELECTION . . . . .	12
4.1 Geologic and Geographic Distribution . . . . .	12
4.2 Performance Quality . . . . .	12
5. TEST RESULTS AND ANALYSIS . . . . .	15
5.1 Aggregate Test Results . . . . .	15
5.2 Concrete Freeze-Thaw Test Results . . . . .	17
6. REGRESSION MODEL DEVELOPMENT . . . . .	20
6.1 Models Developed Using MnDOT HFT Results . . . . .	20
6.2 Models Developed Using INDOT HFT Results . . . . .	22
6.3 Summary of Model Development . . . . .	25
7. SUMMARY AND DISCUSSIONS . . . . .	26
8. CONCLUSIONS AND RECOMMENDATIONS . . . . .	27
9. IMPLEMENTATION STRATEGIES AND RECOMMENDATIONS FOR FUTURE RESEARCH . . . . .	28
9.1 Implementation Strategy . . . . .	28
9.2 Recommendations for Future Research . . . . .	29
REFERENCES . . . . .	29
APPENDICES . . . . .	30
Appendix A. Literature Review . . . . .	30
Appendix B. HFT Equipment Calibration and Standard Test Procedures . . . . .	33
Appendix C. HFT Results . . . . .	40
Appendix D. Materials Used for Batching Concrete and Fresh Concrete Properties . . . . .	52
Appendix E. Regression Model Development . . . . .	53
Appendix F. Recycled Concrete Aggregate Testing and Analyses . . . . .	65
Appendix G. INDOT HFT Equipment and Modifications . . . . .	70

## LIST OF TABLES

Table	Page
<b>Table 3.1</b> Aggregate gradation for HFT test using MnDOT HFT equipment	7
<b>Table 3.2</b> Aggregate gradation used for HFT test using INDOT HFT chamber	11
<b>Table 4.1</b> Aggregate source information	15
<b>Table 5.1</b> Bulk specific gravity and absorption results of aggregates used in the study	16
<b>Table 5.2</b> MnDOT HFT result of a particular source (source B3)	17
<b>Table 5.3</b> INDOT HFT result of a particular source (source B3)	17
<b>Table 5.4</b> Summary of dilation and DF measured after 350 cycles	18
<b>Table 6.1</b> Summary of freeze-thaw and MnDOT HFT results	21
<b>Table 6.2</b> Summary of freeze-thaw and INDOT HFT chamber results	23
<b>Table 6.3</b> Measured and predicted dilation by Equation 6.4	23
<b>Table 6.4</b> Measured and predicted DF by Equation 6.5	25
<b>Table 6.5</b> Summary of regression analysis models	26
<b>Table 7.1</b> Summary of measured versus predicted values (INDOT HFT)	27
<b>Table B.1</b> Target release rate calibration data	34
<b>Table B.2</b> Aggregate gradation used for HFT test using INDOT's HFT chamber	35
<b>Table C.1</b> MnDOT HFT result of aggregate source A1	40
<b>Table C.2</b> MnDOT HFT result of aggregate source A2	40
<b>Table C.3</b> MnDOT HFT result of aggregate source A3	40
<b>Table C.4</b> MnDOT HFT result of aggregate source A4	41
<b>Table C.5</b> MnDOT HFT result of aggregate source A5	41
<b>Table C.6</b> MnDOT HFT result of aggregate source A6	41
<b>Table C.7</b> MnDOT HFT result of aggregate source B1	41
<b>Table C.8</b> MnDOT HFT result of aggregate source B2	42
<b>Table C.9</b> MnDOT HFT result of aggregate source B3	42
<b>Table C.10</b> MnDOT HFT result of aggregate source B4	42
<b>Table C.11</b> MnDOT HFT result of aggregate source B5	42
<b>Table C.12</b> MnDOT HFT result of aggregate source B6	43
<b>Table C.13</b> MnDOT HFT result of aggregate source C1	43
<b>Table C.14</b> MnDOT HFT result of aggregate source C3	43
<b>Table C.15</b> MnDOT HFT result of aggregate source C4	43
<b>Table C.16</b> MnDOT HFT result of aggregate source C5	44
<b>Table C.17</b> MnDOT HFT result of aggregate source C6	44
<b>Table C.18</b> MnDOT HFT result of aggregate source C7	44
<b>Table C.19</b> INDOT HFT result of aggregate source A1	45
<b>Table C.20</b> INDOT HFT result of aggregate source A2	45
<b>Table C.21</b> INDOT HFT result of aggregate source A3	45
<b>Table C.22</b> INDOT HFT result of aggregate source A4	46
<b>Table C.23</b> INDOT HFT result of aggregate source A5	46
<b>Table C.24</b> INDOT HFT result of aggregate source A6	46

<b>Table C.25</b> INDOT HFT result of aggregate source B1	46
<b>Table C.26</b> INDOT HFT result of aggregate source B2	47
<b>Table C.27</b> INDOT HFT result of aggregate source B3	47
<b>Table C.28</b> INDOT HFT result of aggregate source B4	47
<b>Table C.29</b> INDOT HFT result of aggregate source B5	47
<b>Table C.30</b> INDOT HFT result of aggregate source B6	48
<b>Table C.31</b> INDOT HFT result of aggregate source C1	48
<b>Table C.32</b> INDOT HFT result of aggregate source C3	48
<b>Table C.33</b> INDOT HFT result of aggregate source C4	48
<b>Table C.34</b> INDOT HFT result of aggregate source C5	49
<b>Table C.35</b> INDOT HFT result of aggregate source C6	49
<b>Table C.36</b> INDOT HFT result of aggregate source C7	49
<b>Table C.37</b> HFT result of RCA source R-1	50
<b>Table C.38</b> HFT result of RCA source R-2	50
<b>Table C.39</b> HFT result of RCA source R-3	50
<b>Table C.40</b> HFT result of RCA source R-4	51
<b>Table C.41</b> HFT result of RCA source R-5	51
<b>Table C.42</b> HFT result of RCA source R-6	51
<b>Table D.1</b> Mix design parameters and concrete materials	52
<b>Table D.2</b> Plastic concrete properties for ITM210 mixtures using quarried aggregate	52
<b>Table D.3</b> Plastic concrete properties for ITM210 mixtures using RCA	52
<b>Table E.1</b> Table shows an example of HFT results and related PCMR values (source B3)	53
<b>Table E.2</b> Studentized residual values for all sources	54
<b>Table E.3</b> Comparison of measured and predicted dilation	55
<b>Table E.4</b> Measured and predicted DF values for Model M4	57
<b>Table E.5</b> Studentized residual for all aggregate sources	60
<b>Table E.6</b> Measured and predicted dilation values	61
<b>Table E.7</b> Measured and predicted DF values	64
<b>Table F.1</b> Sources of recycled concrete for RCA	65
<b>Table F.2</b> RCA properties	66
<b>Table F.3</b> Summary of HFT and freeze-thaw test results used as model inputs	66
<b>Table F.4.</b> Measured and predicted values for dilation and DF using models developed from testing quarried carbonate sources	67
<b>Table F.5</b> Measured and predicted dilation and DF using models developed from RCA test results	68

## LIST OF FIGURES

Table	Page
<b>Figure 1.1</b> D-cracking in concrete pavement	1
<b>Figure 3.1</b> MnDOT small HFT chamber ready to fill with aggregate	5
<b>Figure 3.2</b> MnDOT small HFT chamber ready for testing	6
<b>Figure 3.3</b> Comparison of pressure release profiles for calibrating MnDOT HFT equipment	6
<b>Figure 3.4</b> ITM 401 pressure chamber, with a close-up view of the top on the right	8
<b>Figure 3.5</b> Old INDOT HFT equipment, as received before any modifications	8
<b>Figure 3.6</b> Initial modifications to the INDOT HFT equipment	8
<b>Figure 3.7</b> Damage to exhaust muffler resulting from ejection of aggregate fragments and dust through the release valve system	9
<b>Figure 3.8</b> Side-by-side views of the INDOT HFT equipment	9
<b>Figure 3.9</b> Conceptual diagram of INDOT HFT equipment	9
<b>Figure 3.10</b> Annotated photo of fully assembled INDOT HFT test equipment	10
<b>Figure 3.11</b> Target pressure release rate profile for calibrating HFT apparatus	10
<b>Figure 3.12</b> Pressure release profiles for various pressure settings	11
<b>Figure 4.1</b> Conceptual map of the general geologic structures dominating Indiana's bedrock	12
<b>Figure 4.2</b> Bedrock geology of Indiana compared to the distribution of aggregate source	13
<b>Figure 4.3</b> Location of aggregate quarries sampled for testing	14
<b>Figure 5.1</b> Aggregate gradation plots for HFT and ITM 210 tests	16
<b>Figure 5.2</b> Mass changes of material retained on each sieve after 50 HFT cycles (source B3)	17
<b>Figure 5.3</b> Mass changes on each sieve after 50 HFT cycles (source B3)	18
<b>Figure 5.4</b> Percent dilation versus durability factor	19
<b>Figure 5.5</b> Plot of percent dilation compared against INDOT's acceptance criteria	19
<b>Figure 5.6</b> Plot of durability factor results compared with $DF=86$	19
<b>Figure 6.1</b> Measured versus predicted dilation by Equation 6.2 (without A4 and B2 and B5)	21
<b>Figure 6.2</b> Locations of the outliers (A4, B2, and B5) in reference to the measured and predicted dilation by the recommended model	22
<b>Figure 6.3</b> Measured versus predicted dilation with outliers A3 and B2	24
<b>Figure 6.4</b> Comparing measured and predicted dilation with acceptance criteria	24
<b>Figure 6.5</b> Predicted DF using Equation 6.5 versus measured values	25
<b>Figure B.1</b> Target release rate calibration curve developed for original SHRP equipment	33
<b>Figure B.2</b> Example of variability of pressure release rates with constant chamber and actuator pressure, INDOT chamber	34
<b>Figure B.3</b> Pressure release profiles for chamber pressure of 1300 psi using three different pressure settings to trigger the release valve	35
<b>Figure B.4</b> Double boiler used to soak aggregate sample	36
<b>Figure B.5</b> Example of a suitable rock tumbler	36
<b>Figure B.6</b> Basket containing the aggregate as removed from the chamber	36
<b>Figure B.7</b> INDOT HFT equipment set up	37
<b>Figure B.8</b> Aggregate specimen in HFT chamber with open mesh basket lid in place	38
<b>Figure B.9</b> INDOT HFT chamber with water fill and drain valves A, B, and C	38
<b>Figure B.10</b> Hydraulic Fracture data sheet	39
<b>Figure E.1</b> JMP output of Model M1	54
<b>Figure E.2</b> Predicted dilation versus measured dilation plot of Model II	54

<b>Figure E.3</b> JMP output of Model M2	55
<b>Figure E.4</b> JMP output of Model M3	55
<b>Figure E.5</b> Comparison of dilation models	56
<b>Figure E.6</b> JMP output of Model M4	56
<b>Figure E.7</b> Measured and predicted DF values	57
<b>Figure E.8</b> JMP output of Model I1	58
<b>Figure E.9</b> JMP output for Model I2	58
<b>Figure E.10</b> Measured dilation versus predicted dilation by Model I1	59
<b>Figure E.11</b> Scatter plot diagram	59
<b>Figure E.12</b> Histogram of residuals for Model I1	60
<b>Figure E.13</b> Normal probability plot of residuals	60
<b>Figure E.14</b> Residual plot showing the location of outlier observations 3 (A3) and 8 (B2)	60
<b>Figure E.15</b> Residual plot for Model I2	61
<b>Figure E.16</b> Comparison of model outputs, measured dilations and the 0.06% dilation criteria	62
<b>Figure E.17</b> Comparison of models with 0.05% dilation criteria	62
<b>Figure E.18</b> JMP output for Model I3	63
<b>Figure E.19</b> JMP output for Model I4	63
<b>Figure E.20</b> JMP output for Model 5	64
<b>Figure E.21</b> Comparison of DF model outputs to actual DF measurements	64
<b>Figure F.1</b> Dilation versus FT cycles for source R-6	67
<b>Figure F.2</b> DF versus FT cycles of RCA	67
<b>Figure F.3</b> Plot of dilation compared against INDOT's acceptance criteria	67
<b>Figure F.4</b> Plot of durability factor results of RCA	67
<b>Figure F.5</b> JMP output of Model RCA1	67
<b>Figure F.6</b> Measured versus predicted dilation for Model RCA1	68
<b>Figure F.7</b> JMP output of Model RCA2	69
<b>Figure F.8</b> Measured versus predicted dilation for Model RCA2	69
<b>Figure G.1</b> Letter transferring ownership of the HFT equipment to Purdue	71
<b>Figure G.2</b> Schematic side view of the top of the modified INDOT HFT chamber	72
<b>Figure G.3</b> Schematic view of the new cover for the modified INDOT HFT chamber	72
<b>Figure G.4</b> Diagrammatic representation of inside of the lid with the angle of the slope highly exaggerated	73
<b>Figure G.5</b> Annotated photo of INDOT HFT equipment fully assembled, ready for testing	73
<b>Figure G.6</b> INDOT HFT chamber showing water fill and drain assembly	73
<b>Figure G.7</b> INODT HFT chamber showing excess water drain line and valve	73
<b>Figure G.8</b> INDOT HFT chamber showing exhaust pipe, nitrogen cylinders, pressure regulators and side table	74
<b>Figure G.9</b> INDOT HFT chamber filled with aggregate with lid assembly resting on slide table	74

## 1. INTRODUCTION

### 1.1 Background

Aggregates are approximately 75% of the total volume of concrete and hence play a key role in concrete durability. D-cracking in concrete pavements occurs when frost-susceptible coarse aggregates exposed to cycles of freezing and thawing crack, and those cracks propagate into the concrete paste (Stark, 1976). D-cracking in concrete pavements manifests on the pavement surface as closely spaced parallel cracks at longitudinal joints, transverse joints and the edges of pavement slabs, as shown in Figure 1.1.

Different mechanisms have been postulated to describe the D-cracking mechanism. In 1945, Powers originated the hydraulic pressure hypothesis, which theorizes that, upon freezing the growing volume of ice creates pressure that forces the water in the smallest saturated pores out to larger voids, a free surface or area not yet fully saturated. This movement of water through a low-permeability porous media causes hydraulic pressure. This pressure may cause rupture in the aggregate or concrete (Janssen & Snyder, 1994; Powers, 1975).

D-crack-susceptible aggregates are typically sedimentary rocks, either siliceous or carbonate (Neville, 2012). Carbonate rock formations (limestone and dolostone) are the primary aggregate sources available for concrete paving in Indiana. The freeze-thaw durability of carbonates can vary greatly from durable to highly susceptible to freeze-thaw distress. Using nondurable aggregates in concrete in a slab on grade that is exposed to freeze-thaw cycles may lead to serious distress in the concrete pavement, greatly decreasing pavement life. Indiana Department of Transportation (INDOT) developed a successful program that identifies quality, freeze-thaw



**Figure 1.1** D-cracking in concrete pavement (Photo credit: Portland Cement Association).

durable aggregates (i.e., AP aggregates). The acceptance criteria includes preparing concrete beams containing the aggregate in question and freeze-thaw testing of concrete beams in accordance with Indiana Test Method, ITM 210-Class AP Coarse Aggregate (a modified version of ASTM C-666/AASHTO T 161-Resistance of Concrete to Rapid Freezing and Thawing, Procedure B).

The processing and testing needed to identify the AP quality of a single aggregate source can take several months, and the natural variability within aggregate sources may require frequent testing to ensure durability. The Indiana Department of Transportation (INDOT) tests all their concrete aggregate sources that are part of their Certified Aggregate Producer (CAP) Program every one to three years, depending on source variability and historical test results. A simple and rapid method of assessing the susceptibility of aggregates to freezing and thawing would allow a quick review of material quality, greatly ease the testing burden and reduce the length of time INDOT, contractors and aggregate producers have to wait for approval to use a particular aggregate source in concrete.

The Hydraulic Fracture Test (HFT) was originally developed under the first Federal Strategic Highway Research Program (SHRP) in the early 1990's as an eight-day test method of identifying concrete aggregate freeze-thaw durability (Janssen & Snyder, 1994). Subsequently, AASHTO developed a provisional standard TP12-93 modified and reapproved as TP12-96 "Method for Determining the Hydraulic Fracture of Coarse Aggregate," but it fell out of favor because the equipment available and method for interpreting the results at that time had marginally acceptable accuracy. Additional research sponsored by different state transportation agencies continued to refine the equipment and data analyses, increasing the accuracy and repeatability of the HFT and provided a foundation for the work completed in this study (Hietpas, 1998; Janssen & Snyder, 1994; Rettner & Embacher, 2009; Snyder et al., 1996). A more detailed history of research efforts on HFT are discussed in Chapter 2.

### 1.2 Research Objectives

The original objective of this study was to develop a reliable, quick test method for determining the freeze-thaw resistance of carbonate quarried aggregates in Indiana using existing Hydraulic Fracture Test (HFT) equipment and procedures refined by other state agencies. As the study progressed it became apparent that modifications to the old INDOT HFT equipment and adjustments to the testing procedures could lead to improved test results. Henceforth the research objectives were expanded to include redesigning the INDOT HFT equipment and refining the existing testing and analysis procedures.

### 1.3 Scope of Work

The scope of the study included identifying and collecting aggregate samples from 18 sources that

represent a range of freeze-thaw performance: durable, nondurable and of variable or unknown performance. Representative samples from all aggregate sources were tested in accordance with ITM 210-Class AP Coarse Aggregate, and the Hydraulic Fracture Tests using both the small MnDOT HFT chamber and the redesigned INDOT HFT chamber. The test results were analyzed statistically and regression analyses were performed to develop models of ITM 210 test results as a function of HFT results.

## 2. LITERATURE REVIEW

The Hydraulic Fracture Test (HFT) was developed at the University of Washington as the Washington Hydraulic Fracture Test (WHFT) in the early 1990s under the first Strategic Highway Research Program (SHRP) (Janssen & Snyder, 1994). Since that time several agencies have sponsored research to validate and refine HFT test procedures or equipment. Eventually the “W” in WHFT was dropped and HFT became the accepted designation. The key findings and recommendations of the studies that led to the evolution of the HFT equipment and procedures are discussed in this Chapter. Section 2.1 describes the original SHRP study and the basic concepts behind the HFT; Section 2.2 discusses the AASHTO provisional standard that was developed; Section 2.3 discusses the research that followed the SHRP study as agencies looked at adopting the HFT procedures; and Section 2.4, summarizes the research related to more recent refinement of equipment, testing procedures and analysis. More thorough discussions of these publications are presented in Appendix A.

### 2.1 Original SHRP C-391 Study (Janssen & Snyder, 1994)

The development of HFT equipment and testing procedures were published as part of SHRP C391 *Resistance of Concrete to Freezing and Thawing* and promoted as relatively inexpensive and capable of identifying the freeze-thaw durability of several aggregate samples in eight days.

#### 2.2.1 Theory Behind the HFT

The HFT was intended to simulate the internal hydraulic pressures created in aggregate particles that are exposed to cyclical freezing and thawing. Similar to the model Powers (1975) describes for freeze-thaw durable concrete, when the internal pressures exceed the strength of the aggregate the particle fractures (as described in Section 1.1). The HFT simulates the freeze-thaw process by forcing water into the pores of aggregate particles using pressurized nitrogen gas. Then the pressure is rapidly released inducing pressure that causes the air that had been compressed and trapped within the aggregate pores to expand. Internal hydraulic pressure is created as the trapped air tries to

escape expelling water from the aggregate pores. The amount of aggregate fracturing that results from the HFT test was compared to the AASHTO T161 (ASTM C666) Standard Test Method for Resistance of Concrete to Rapid Freezing and Thawing results to develop acceptance criteria (Embacher & Snyder, 2003; Janssen & Snyder, 1994; Rettner & Embacher, 2009).

#### 2.1.2 Original Research

The WHFT chamber used in the C-391 study (Janssen & Snyder, 1994) was similar to the current small MnDOT HFT chamber except it had no neoprene pads, the pressure release was a manually operated trigger and the exhaust was an open valve with no muffler attached. Sample preparation and the HFT testing process were similar to that performed under the current study (as described in Section 3.1) except that the HFT chamber in C-391 was operated at 1150 psi.

In the C-391 study, 13 aggregate sources from five different states were tested, and two aggregate sizes were tested from each source: 1/2 to 3/4 in. (12.5 to 19.0 mm) and 3/4 to 1.25 in. (19.0 to 31.5 mm). The change in mass and change in the number of particles were recorded after 50 HFT cycles (10 cycles per day). The freeze-thaw durability of the aggregates was assigned based on their reported field performance histories.

Analysis of HFT results included calculation of three parameters: percent fracture (PF), Hydraulic Fracture Index (HFI) and percent mass lose (ML). The HFI value is based on a change in particle count and related to the estimated number of cycles needed to reach 10 percent fracturing. The HFI related well with the reported durability for 11 of the 13 aggregates using  $HFI > 100$  to indicate a freeze-thaw durable aggregate.

The inter-laboratory variability of HFI results showed good agreement between the two labs that participated. Results also showed that as the number of particles tested increased the coefficient of variation of HFI values decreased leading to a minimum sample size recommendation of 600–800 particles to adequately represent the aggregate source. The need for a sample size that was larger than the small WHFT could accommodate led to the development of the large WHFT chamber that held nearly five times the volume of the original, (small) WHFT chamber. The C-391 study emphasized that both chambers should be calibrated to have similar pressure release rates to ensure similar amounts of aggregate fracture are produced. The pressure release rate documented was 30,350 psi/sec (through the central, linear, portion of the pressure release rate curve). However the critical pressure release rate and the parameters necessary to ensure that equipment remained in calibration were not determined until later, under the Michigan Department of Transportation investigation (Snyder et al., 1996). Further details of the WHFT chamber, test procedures, analysis and validation of the test are descriptions in Appendix C and in the C391 report (Janssen & Snyder, 1994).

## 2.2 Development of AASHTO Provisional Standard TP12

The HFT testing had been accepted as a provisional standard procedure under AASHTO TP12-93 “Method for Determining the Hydraulic Fracture of Coarse Aggregate” and later refined as TP12-96, but never became accepted as a full standardized procedure. TP12-93 recommended using the large chamber developed under C391 but recognized the chamber developed by Purdue University as an alternative (also known as the original INDOT chamber). The importance of testing 600–800 particles was mentioned in TP-93, but because of the capacity of the larger chamber replicates were not required. The release rate was mentioned as non-mandatory information only.

Changes that occurred to the provisional standard and published as TP12-96 recommended that the small chamber be used with neoprene pads on the inside of the upper and lower lid; required calibration of the release rate and recommended testing replicate samples to achieve test results for a total of 600–800 particles. SHRP C391, TP12-93 and TP-96 all recommended testing at 1150 psi, the mass and particle counts were determined in two size fractions: retained on the 3/8 in. sieve, and passing 3/8 in. but retained on the #4 sieves.

Results continued to be reported as HFI but unlike C391 and TP12-93, the HFI in TP-96 was based on the number of cycles needed to produce 5% fracture (not 10%). Several investigations examined the applicability of this temporary standard as an acceptance test for aggregate freeze-thaw durability, but most of the reports did not specify whether the 1993 or the 1996 standardized procedures were followed.

## 2.3 HFT Testing by Different Agencies

### 2.3.1 Michigan Department of Transportation (MDOT) (Snyder et al., 1996)

MDOT further developed the HFT equipment, test procedures and acceptance criteria. Nine aggregates sources with a range of freeze-thaw performance were tested in the HFT and MTM115 (MDOT’s version of AASHTO T161 Procedure B). The research examined the effects of varying the chamber pressures, chamber sizes, release rate and with/without neoprene pads lining the inside of the lower and upper lids of the small chamber.

Outcome of this research included changes in the HFT equipment such as: changing the release valve from a plug valve to a ball valve; automating the release mechanism by adding an actuator to electro-pneumatically operated the pressure release ball valve; and lining the inside of the chamber with a thin neoprene pad to minimize or eliminate mechanical crushing of the aggregate. Changes to the analysis process recommended calculating the HFI based on number of cycles necessary to produce 5% fracturing (not 10%). The MDOT research suggested an HFI value greater than

100 indicated freeze-thaw durable aggregate. This research recognized that the HFT was unable to fracture chert particles, which can contribute to freeze-thaw problems and MDOT concluded that the HFT in its current form could not consistently predict the freeze-thaw test results according to MDOT test procedure (MTM115). Although MDOT concluded that the HFT was not ready for implementation (Snyder et.al, 1996) much of the work under this project led to the changes made in AASHTO TP12 between the 1993 and 1996 versions.

### 2.3.2 Kansas Department of Transportation (KDOT) (Zubery, Hossain, & Clowers, 1997)

KDOT, in conjunction with Kansas State University examined the freeze-thaw durability of 32 different Kansas aggregates sources by comparing the HFT Hydraulic Fracture Index (HFI) to the results from ASTM C666 and several other types of tests. This study concluded that the HFI correlated poorly with ASTM C666 test results and would not replace the existing ASTM C666 procedure. However the HFI showed a significant correlation with the KDOT-modified freeze-thaw test on unconfined aggregates.

### 2.3.3 New York State Department of Transportation (NYSDOT)

NYSDOT developed a more automated HFT chamber that was pressurized to 1200 psi using air, not nitrogen, and used a pneumatically actuated ball valve with electronic trigger for the pressure release system. The pressure release rate peaked between 0.01 and 0.02 seconds at approximately 35,000 psi/s slightly higher the 30,350 psi/sec reported for the SHRP WHFT chamber and required under TP12-96. Eight samples were tested in HFT, magnesium-sulfate soundness tests and aggregate freeze-thaw in brine tests. Results, reported as mass loss for all tests, indicated that the HFT resulted in significantly less mass loss than either magnesium-sulfate soundness or aggregate freeze-thaw test. NYSDOT concluded that the HFT could not be used as a prescreening test for determining aggregate freeze-thaw durability.

### 2.3.4 Illinois Department of Transportation (IDOT) (Issa & Bendok, 2000)

IDOT sponsored a study under which a fully automated larger chamber was developed that used air to drive the water into aggregate voids instead of nitrogen. Aggregates from twenty-one different sources were tested using both the small chamber and the IDOT developed larger HFT chambers. HFT results were compared with ASTM C666 freeze-thaw results and concluded that the HFI correctly predicted freeze-thaw durability 76% of the time if the HFI was based on a percent fracture of 2% (not 10% or 5%, as recommended in C391 or TP12-96, respectively). The study

concluded that the larger automated chamber had the potential to be used as a screening test prior to ASTM C666 test.

### 2.3.5 Interlaboratory Evaluation of AASHTO TP12 (UDOT, 1998)

An interlaboratory round-robin study, sponsored by FHWA and directed by CTL, examined the within-lab and between-lab precision of the HFT procedures as outlined in AASHTO TP12. Nine of the 10 testing labs that participated used the small HFT chamber, and the tenth lab used a larger chamber designed by Gilson which held more than twice the volume of aggregate as the small chamber. Four aggregate sources were tested in the HFT; five replicates of each source by each lab. Each lab also tested each source using AASHTO T161 reporting results as durability factor (DF). Several labs chose to run other “optional” aggregate tests as well including: LA abrasion, magnesium-sulfate soundness, insoluble residue and others. This testing benefitted from the changes introduced by the MDOT research and adopted by TP12-96 including neoprene lining in the small chambers, an automated pressure release valve and the HFI based on 5% fracture.

Researchers found that the results from the other ‘optional’ tests had no correlation with either the DF or the HFT results. There was not a linear relationship between Hydraulic Fracture Index (HFI) and DF, but a high HFI (>120) correlated well with durable aggregates (DF>80). On the other hand, a low HFI (<120) correlated with both high and low DF. There was no correlation between total percent mass loss and DF; however, the researchers recognized that newly published work by Hietpas (1998) was showing an improved correlation with percent mass loss if measured as a loss on specific sieves and not just a total over the 3/8 in. sieve. Unfortunately the work by Hietpas (1998) was not yet available at the time of the round-robin testing.

Unlike the recommendations in TP12-96, each of the five replicate test results was analyzed as a unique data point, even though most test samples contained less than 200 particles. The 150–200 particle sample size was a much smaller than recommended to obtain a low coefficient of variation in testing and to adequately represent a source (per the SHRP C391 study). Not surprisingly the experimental results from the small chamber showed a wide range of variability, whereas test results from the larger chamber had a lower coefficient of variation and combining two small-chamber test results of the same source improved the coefficient of variability.

The study recommended that AASHTO TP12 could be used as a screening test to identify freeze-thaw durable aggregate but should not be used as an acceptance test or as an alternate test to AASHTO T161 until additional work addresses some of the concerns identified (UDOT, 1998).

## 2.4 Further Developments in Hydraulic Fracture Test

Up through the late 1990’s the HFT results were based on particle count of material passing and retained on the 3/8 in. sieve, and reported as HFI. More recent research introduced a new method for analyzing and reporting results.

### 2.4.1 University of Minnesota Study (Hietpas, 1998)

The work in this study further validated the calibration procedure developed under the MDOT study and refined both the HFT equipment and analysis procedures. The equipment modifications included increasing the size of the release valve and pipes from 1/2 in. (12.5 mm) to 3/4 in. (19 mm) to obtain the recommended release rate. The HFT modifications to the analysis procedures included adding several sieves to better characterize the effects of HFT on the change in particle sizes.

Seven aggregate sources with particle sizes that ranged from 3/4 to 1.25 in. (19 to 32 mm) were tested in the small chamber (per to TP12-96) and linear regression models were developed to correlate the data obtained from the HFT to dilation data obtained using AASHTO T161-C (similar to Procedure B, except beams were wrapped in cloth). The cumulative percent mass retained on the 5/8 in., 1/2 in., 3/8 in. and #4 sieves were used to develop a model to predict the dilation per 100 freeze-thaw cycles. The predicted verses measured freeze-thaw test results had a very high  $R^2$  value of 0.95. Due to the small number of aggregate sources tested, it was necessary to further refine and validate the models using a larger data set (more aggregate sources). Results of the modified large HFT chamber suggested that the large chamber had the potential to replace replicate tests using the small chamber.

### 2.4.2 Minnesota Department of Transportation (MnDOT) Study (Embacher & Snyder, 2003)

The main focus of this MnDOT study was to follow-up the study by Hietpas (1998), and test a larger range of aggregate sizes and sources to further develop and refine the HFT testing and analysis. Particle counts and masses retained were used to develop models to predict freeze-thaw dilation using the following aggregate size fractions: 3/4 to 1.5 in. (19.0 to 37.5 mm), 1/2 to 3/4 in. (12.5 to 19.0 mm), and #4 to 1/2 in. (4.75 to 12.5 mm). Each HFT result was based on a minimum of 600 particles in each size range which required the combination of replicate tests in the small chamber. All 20 aggregate sources were tested in AASHTO T161, Procedure C (beams wrapped in cloth, provisional method), and dilation and durability factor (DF) values were determined. Regression models developed to predict dilation and DF from the HFT results had good correlations with measured AASHTO T161-C results, especially for the larger aggregate size fraction.

The best correlation between predicted and actual dilation measurements was with the HFT results for 3/4 in. to 1.5 in. size fraction with an  $R^2$  value of 0.978.

This study further developed the large HFT chamber that would enable the minimum 600 particles to be tested together, and eliminate the need for replicate tests. To achieve the recommended release rate the release valve and pipes were increased from 1/2 in. (12.5 mm) to 3/4 in. (19 mm), as with the 1998 study, and a larger actuator was used that could achieve the 205 psi needed, as determined by the calibration process. Four of the 20 aggregate sources that had been tested in the small chamber were tested in the improved larger chamber with promising results.

#### 2.4.3 Minnesota Department of Transportation Implementation Study (Snyder, 2005)

This report documents equipment set-up, calibration and use of both the small and large HFT chambers. It provides step-by-step procedures for HFT testing and data analysis.

#### 2.4.4 Minnesota Department of Transportation Study (Rettner & Embacher, 2009)

To further validate the use of the large HFT chamber MnDOT sponsored a study that tested 12 aggregate sources in the HFT, both the large and small chambers, and in AASHTO T161, Procedure A (Procedure C was never accepted as a standardized procedure). The regression models developed by Embacher and Snyder (2003) were used to compare HFT-based predicted freeze-thaw dilations and DF to measured results.

Problems obtaining appropriate release rates led to testing with release rates that were lower than the recommended rate, and lower than the rate used in previous studies. The small chamber was pressurized to 1300 psi and the large chamber was pressurized to 1350 psi, with 150 psi for both of the actuators controlling the pressure release valve.

The results from this study did not find a good correlation between HFT and freeze-thaw test for either chamber using the existing regression models, and concluded that new models would need to be developed to correlate HFT to AASHTO T161, Procedure A.

### 3. HFT EQUIPMENT AND TEST PROCEDURES

This chapter describes both the MnDOT and INDOT HFT equipment, the modifications made to the INDOT chamber, chamber calibration procedures, sample preparation and test procedures.

#### 3.1 MnDOT HFT Equipment

The two HFT chambers developed under the original SHRP study differ primarily in the size (depth) of the 10 in. diameter cylindrical chamber. The small chamber has a 2 in. internal depth while the large chamber has a

10 in. internal depth (Snyder, 2005). Throughout this report any reference to the MnDOT HFT chamber refers to the small chamber, unless stated otherwise.

The MnDOT HFT equipment used in this study was on loan under an inter-agency agreement between the Indiana Department of Transportation and the Minnesota Department of Transportation. The MnDOT equipment included several modifications from the original SHRP WHFT equipment, including electronic switches, a muffler, neoprene liners, and others as detailed in Chapter 2.

The MnDOT HFT equipment consists of several different parts. The chamber and several of the valves, hoses and attachments can be seen in Figure 3.1, in which the empty chamber is shown in the horizontal position prior to filling with aggregate. Once filled with aggregate, the top plate is secured in place with 16 high-strength steel bolts, and the chamber is swiveled into the vertical position ready for filling and pressurizing (as seen Figure 3.2). A muffler was attached to the valve labeled (a) in Figure 3.1 to reduce the noise and water splash experienced when the pressure is released. Next the chamber is filled with water, pressurized with nitrogen to a pressure determined during the calibration process (see section 3.1.1), held at that pressure for the designated time period. Then pressure release is triggered quickly using a pneumatically actuated ball valve, which is triggered by an operator-controlled electric switch (labeled (b) in Figure 3.2). Additional test procedures are detailed in (Appendix B) and MnDOT HFT equipment details are available in other publications (Snyder, 2005).

##### 3.1.1 Calibration of MnDOT HFT Equipment

The original SHRP study showed that pressure release rates from the HFT chamber significantly affect aggregate fracture rate, which, in turn, is related to aggregate durability. Higher pressure release rates corresponded to higher fracture rates (Janssen & Snyder, 1994; Snyder, 2005).

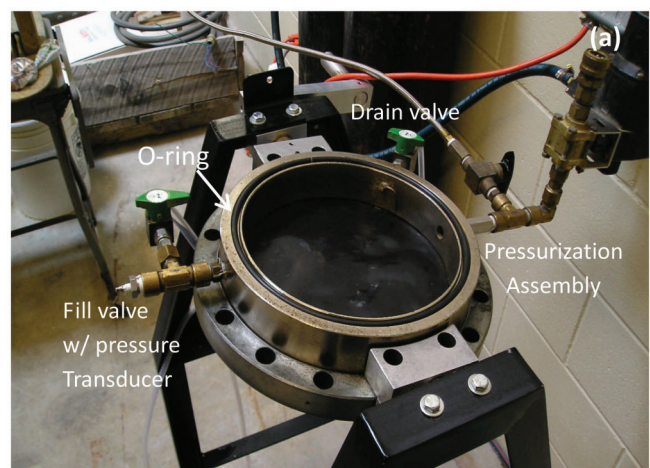


**Figure 3.1** MnDOT small HFT chamber ready to fill with aggregate (Snyder, 2005).

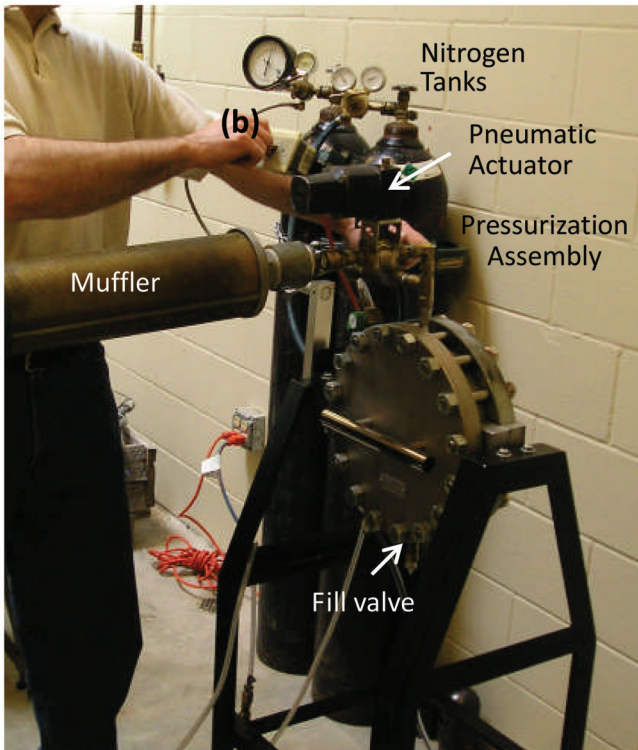


**Figure 3.2** MnDOT small HFT chamber ready for testing (Snyder, 2005).

Prior to any testing in the current study, the HFT equipment was calibrated. HFT equipment “calibration” is more accurately described as adjusting the chamber pressure and exhaust valve actuator pressure to obtain pressure release rate, measured as an average pressure change versus time curve, that closely matches

the “standard” that was adopted in the Minnesota HFT research (Snyder, 2005; Snyder et al., 1996). While the target is to match the entire pressure release profile as closely as possible, it is believed that it is particularly important to match the specific average release rate at the 0.01 sec interval (Snyder, 2005). Calibrating the pressure release rate to match the established standard rate is important in order to produce aggregate fracture rates consistent with those used to develop the freeze-thaw prediction models.

Details on the calibration process are published in Snyder, 2005 and the exact processes used in this study is detailed in Appendix B. Figure 3.3 shows a plot of the best results obtained using the calibration process completed under this project for the MnDOT equipment, compared to the ideal “standard” rate (labeled target release Rate in Figure 3.3). The first number in the legend indicate chamber pressure (which varied from 1300 to 1400 psi for this data set), followed by the pressure used to activate the actuator, which was 150 psi for all tests. As is evident from this plot, the “standard” release rate curve was never duplicated under this study.

Much of the original WHFT and MnDOT HFT procedures and analysis were based on chamber pressures at 1150 psi (Janssen & Snyder, 1994; Snyder et al., 1996; Hietpas, 1998; Embacher & Snyder, 2003). Under this study it was not possible to obtain acceptable release rates with chamber pressures at 1150 psi using the MnDOT equipment. Rettner and Embacher (2009) found similar results with this same equipment. Similar to Rettner and Embacher (2009) pressure settings of 1300+150 psi were chosen for testing because they produce a release rate profile fairly similar to the target profile without significantly exceeding the developed operating pressure of 1150 psi.

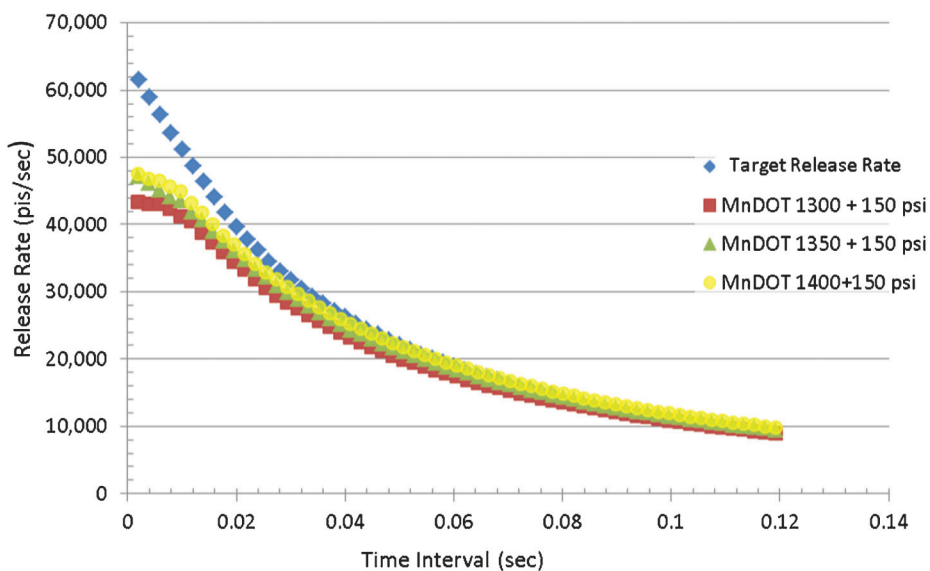


**Figure 3.3** Comparison of pressure release profiles for calibrating MnDOT HFT equipment.

### 3.1.2 MnDOT HFT Equipment Test Procedure

The Hydraulic Fracture Test (HFT) was performed on all 18 project aggregate sources using the MnDOT HFT equipment. Representative samples were obtained from each aggregate source. Source materials were separated by sieving into two size ranges: 1/2 to 3/4 in. (12.5 to 19.0 mm) and 3/4 to 1 in. (19.0 to 25 mm). The aggregates were recombined according to the proportion shown in Table 3.1 to more accurately reflect the proportion of these aggregate sizes used to fabricate the concrete beams used in the freeze-thaw test.

As suggested by previous research (Janssen & Snyder, 1994) a minimum sample size of 600 particles was used to represent each aggregate source. Because of the relatively small size of the MnDOT chamber, it was necessary to test three replicate samples of each aggregate source in order to test at least 600 particles of the gradation given in Table 3.1.

Each replicate sample was subjected to 50 cycles of pressurization and depressurization using chamber and actuator pressures of 1300 and 150 psi respectively. After each 10 cycles, the samples were oven-dried overnight, cooled to room temperature, sieved through 3/4 in., 5/8 in., 1/2 in., 5/8 in., 5/16 in., 1/4 in., and #4 sieves and the mass retained on each sieve was recorded. Additional HFT test procedure details are described in Appendix B.

## 3.2 INDOT HFT Equipment

The original INDOT HFT chamber was constructed by the Purdue Machine Shop over 20 years ago. This chamber was modeled after another pressure chamber (shown in Figure 3.4) that is used for ITM 401 High Pressure Air Content of Hardened Portland Cement Concrete, which tests for the air content in hardened concrete cores. Both test chambers are "...specially designed stainless steel seamless tube secured with [welded to] a stainless steel plate, at the bottom, and a stainless steel lid, at the top" (per section 5.1 of ITM 401), and were designed to contain water under pressures of 5000 psi.

The original INDOT HFT equipment, as shown in Figure 3.5, had been used for HFT research by CSR American Aggregates in the 1990's, a company later acquired by Martin Marietta Materials (per verbal communications with David John). Prior to any modifications of the INDOT HFT equipment the ownership

TABLE 3.1  
Aggregate gradation for HFT test using MnDOT HFT equipment

Sieve size	Percentage passing
1 in. (25 mm)	100
3/4 in. (19 mm)	89
1/2 in. (12.5 mm)	0

of the equipment was transferred to Purdue (see letter of property transfer as Figure G.1, Appendix G).

The chamber was filled while in an upright position, then the chamber was manually rotated back 90 degrees so that the chamber lay horizontally and the release valve assembly pointed upwards (as seen in Figure 3.5). A pipe assembly was attached to the release valve, but beyond that the operation of the equipment for HFT testing was unknown. Several people were contacted both from within INDOT and outside of INDOT but no one recalled exactly how the equipment worked.

### 3.2.1 Initial INDOT HFT Equipment Modifications

The initial alteration of the INDOT equipment included adding valves and attachments (as shown in Figure 3.6) so that the equipment operated more similarly to the MnDOT equipment. The modifications to the INDOT chamber included:

- Changes to allow the chamber to be pressurized using nitrogen
- Addition of an automatic pressure release system—a ball valve, controlled with a pneumatic actuator that was triggered with an electric switch
- Addition of a muffler over the exhaust valve to reduce noise and water spray during decompression

Sample preparation was performed in the same manner as under the MnDOT HFT testing, except that one large 30 lb. sample was tested instead of the three smaller replicates needed for testing with the MnDOT HFT equipment. All other test procedures were similar to those used with the MnDOT HFT equipment.

Rotating the heavy INDOT HFT equipment 90 degrees between filling and testing was difficult, and the larger opening of the release valve became problematic as aggregate dust and fragments were sometimes ejected through the exhaust port. After replacing the muffler twice before completing the first 50 cycles (see damaged muffler in Figure 3.7) and having a 'near miss' with a flying aggregate particle when the operator forgot to rotate the chamber 90 degrees before releasing the pressure, it was decided that major alterations were necessary before continuing to use the INDOT HFT equipment.

### 3.2.2 Advanced INDOT Equipment Modifications

The research team consulted with Professor Don Janssen, originator of the WHFT equipment, and worked with the Purdue Machine Shop to modify the INDOT HFT chamber to address safety concerns; to make the equipment easier to use; and to improve on the quick release of the chamber pressure. The changes to the chamber included:

- The chamber height was reduced to 12 in. depth with the chamber top just above the existing side port (which was plugged).



**Figure 3.4** ITM 401 pressure chamber, with a close-up view of the top on the right.

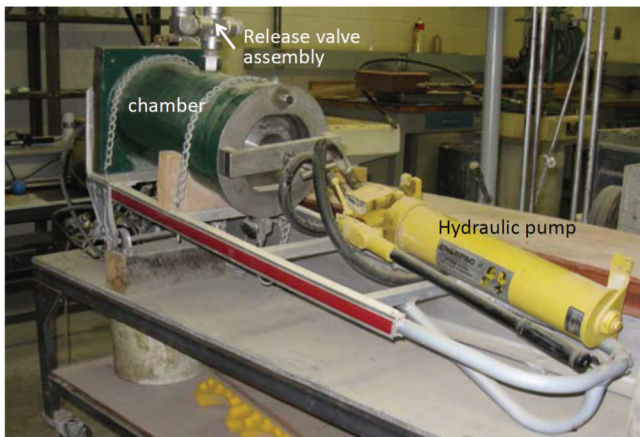


**Figure 3.5** Old INDOT HFT equipment, as received before any modifications.

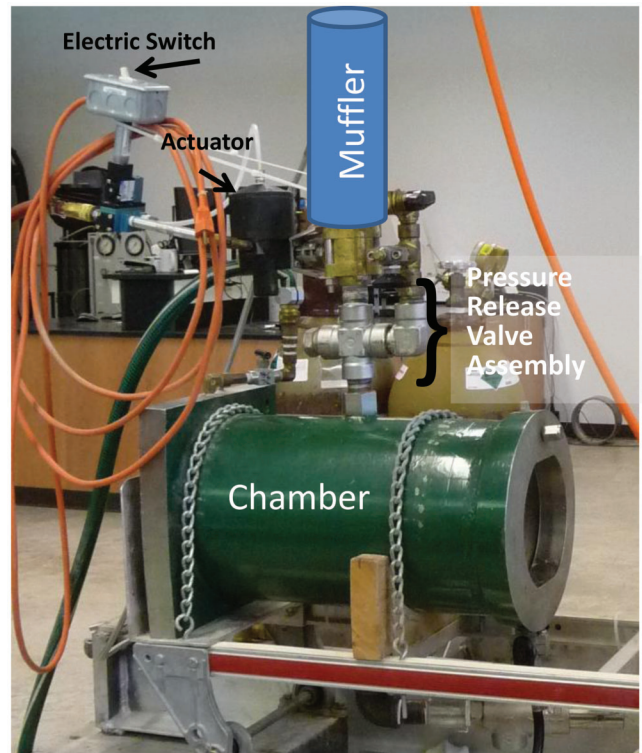


**Figure 3.6** Initial modifications to the INDOT HFT equipment.

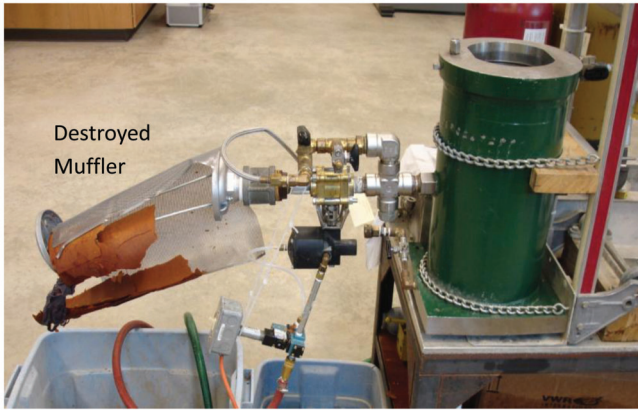


**Figure 3.7** Damage to exhaust muffler resulting from ejection of aggregate fragments and dust through the release valve system.

- A new stainless steel flange and lid were fabricated with an O-ring for sealing (see schematic in Appendix G, Figure G.2 and G.3).
- The inside of the lid was constructed with a slight conical taper towards the center to help eliminate trapped air. The center of the lid was fabricated with a larger, 1.5 in. diameter threaded opening at the tip of the taper to facilitate a quicker release of pressure (see Appendix G, Figure G.3 and G.4).
- The lid and flange were drilled to fit twelve 3/4 in. grade-8, high-strength hex bolts and nuts for closing and securing the system (Appendix G Figure G.3). The flange was welded to the chamber.
- The pressure release assembly was moved to the top of the lid. A larger, high-pressure 1.5 in. ball valve with a more robust pneumatic actuator (maximum capacity of 200 psi) was added to the pressure release assembly.
- The system was designed for an operating pressure of 1500 psi; the vessel was pressure-tested to 3000 psi.

A side-by-side comparison of the chamber after initial and more advanced modification is shown in Figure 3.8.

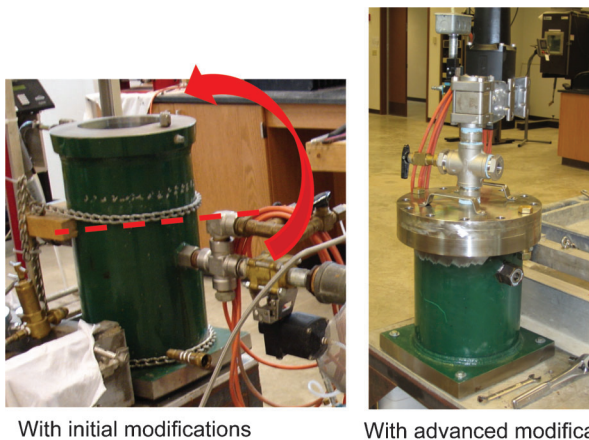


**Figure 3.8** Side-by-side views of the INDOT HFT equipment.

### 3.2.3 Current INDOT HFT Equipment Description

The current INDOT HFT equipment consists of two main assemblages: the pressure chamber assembly and the lid assembly. The water supply and drainage lines and associated valves are connected to the pressure chamber assembly, while the nitrogen supply line, water overflow/drainage line and exhaust pipe with associated valve and actuator assemblies are connected to the lid assembly (as shown in a conceptual diagram in Figure 3.9).

After placing the aggregate sample in the chamber, the lid and pressure chamber assemblies are bolted together with the twelve high-strength bolts. The chamber is then filled with water and pressurized with nitrogen gas. Figure 3.10 shows the INDOT HFT equipment fully assembled ready for testing.

The individual parts of the HFT equipment shown in Figure 3.10 are described in detail in Appendix G.

### 3.2.4 Calibration of INDOT HFT Equipment

The original SHRP study showed that aggregate fracture rate is related to durability of aggregates and is significantly affected by the pressure release rate from the HFT chamber (Alford & Janssen, 1995; Janssen & Snyder, 1994). Higher pressure release rates may produce unusually high aggregate fracture rates which may require recalibrating the models that relate fracture test results to freeze-thaw test results. Lower pressure release rates may produce lower aggregate fracture rates that make it difficult to distinguish between durable and nondurable aggregate sources.

The INDOT HFT equipment was calibrated in a similar manner as the MnDOT chamber had been as discussed in Section 3.1.1. The goal of this task was to establish the actuator pressure and the chamber pressures that consistently produced release rates curves similar to the “standard” that was adopted in the Minnesota HFT research (shown in Figure 3.11). While the target is to match the entire pressure release profile

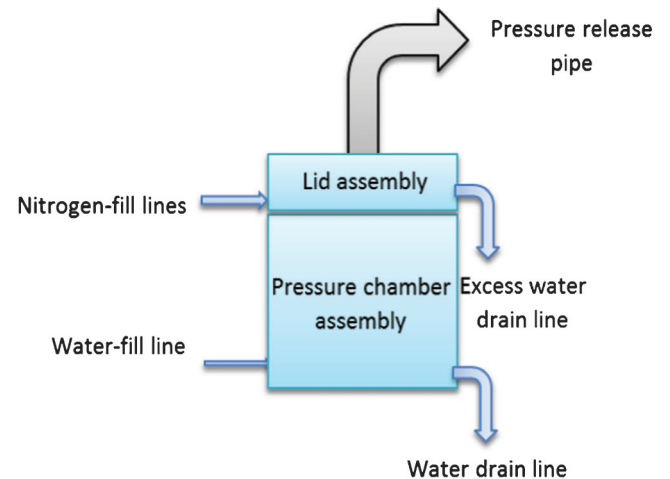


**Figure 3.9** Conceptual diagram of INDOT HFT equipment.

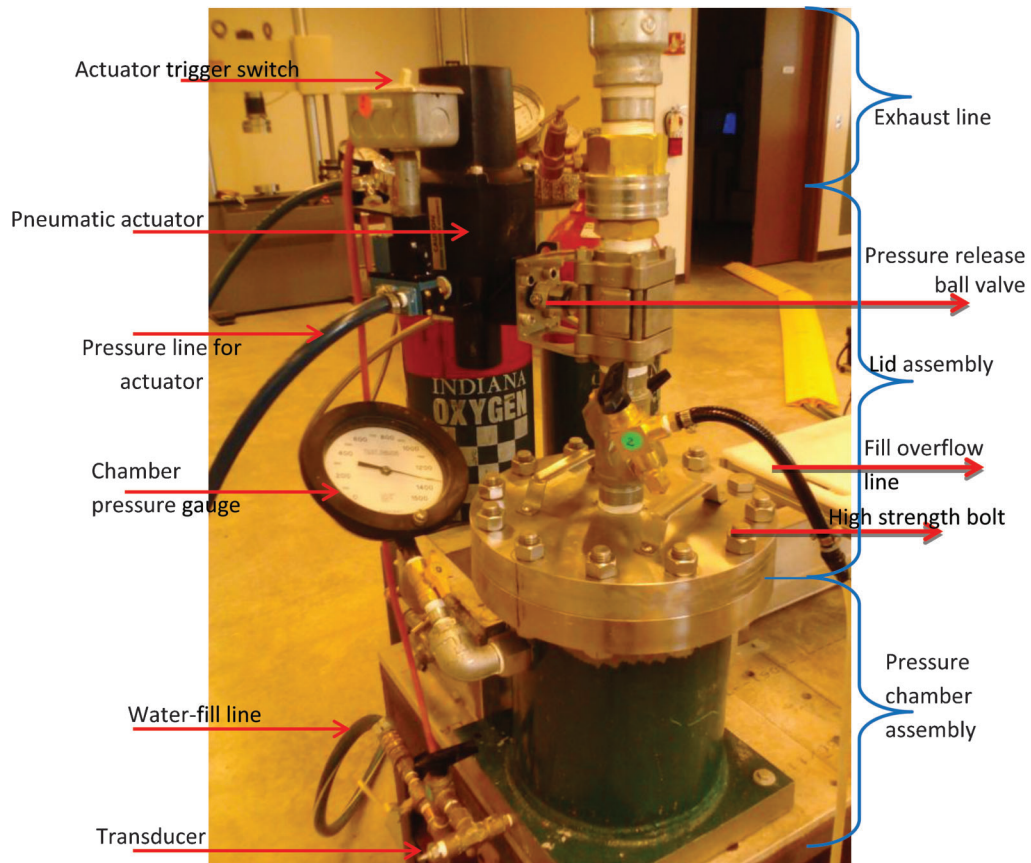


Figure 3.10 Annotated photo of fully assembled INDOT HFT test equipment.

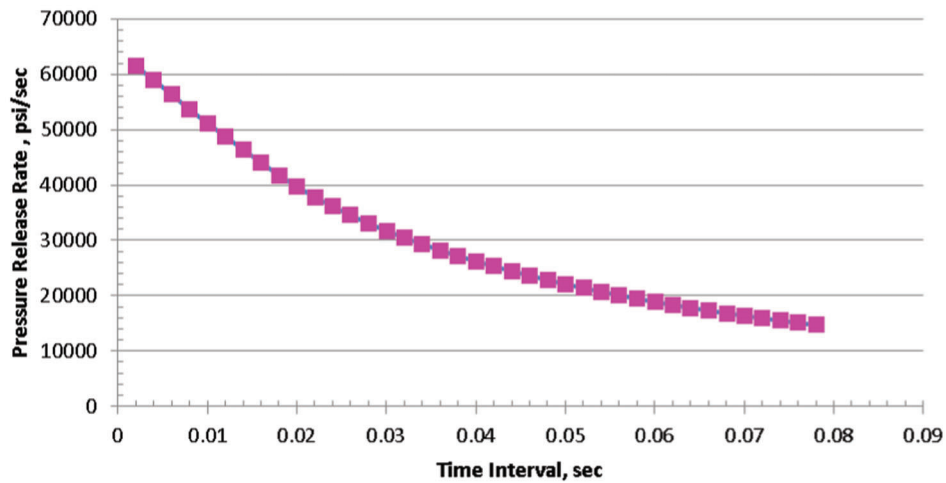


Figure 3.11 Target pressure release rate profile for calibrating HFT apparatus (Snyder, 2005).

as closely as possible, it is believed that it is particularly important to match the release rate at the 0.01 sec interval (Snyder, 2005).

During the calibration process of the INDOT HFT chamber, the pressure release rate was monitored using a pressure transducer mounted on the chamber as shown in Figure 3.10. The transducer was then connected to a dynamic signal analyzer, which collected the signal data, converted it to pressure change values, and output the data for analysis in an Excel spreadsheet.

Dozens of combinations of chamber and actuator pressures were tried with different exhaust line configurations (with and without a bend in the line). Although the equipment is capable of operating using higher pressures, it was found that the chamber could be kept at the same operating pressure used for the MnDOT chamber (1300 psi) and only the actuator pressure needed to be adjusted until a good match with the target pressure release rate profile was achieved.

A series of test runs were performed with the actuator pressure set at values that ranged from 150 to 200 psi while the chamber pressure was held at 1300 psi and resulting profiles were compared to the target profile. Each actuator-chamber pressure combination was repeated five times to ensure repeatability. The resulting pressure release rate profiles were compared to the target release rate profile.

Figure 3.12 shows examples of the pressure release profiles obtained and compared to the target pressure release rate. This figure shows that the INDOT HFT equipment is capable of releasing pressures at a faster rate than those achieved with the original MnDOT HFT chamber. The pressure release rate obtained for the INDOT equipment with a chamber pressure of 1300 psi and an actuator pressure of 175 psi was the closest match to the target pressure profile and closely matched the release rate at the critical time of 0.01 second. In addition, the coefficient of variation of the

TABLE 3.2  
Aggregate gradation used for HFT test using INDOT HFT chamber

Sieve size	Percentage passing
1 in. (25 mm)	100
3/4 in. (19 mm)	89
5/8 in. (16 mm)	40
1/2 in. (12.5 mm)	0

five repeated measures for the 1300 psi and 175 psi actuator-pressure combination at 0.01 second was found to be very low (1.87%). Therefore, a chamber pressure of 1300 psi, and actuator pressure of 175 psi were selected to test all the aggregates in the INDOT chamber for this research.

### 3.2.5 INDOT HFT Equipment Test Procedure

Representative samples from each aggregate source were obtained and prepared in a similar manner as for the MnDOT chamber previously described in Section 3.1.2 except for two key differences:

1. Only one sample of approximately 28 lb. was tested (compared to three replicates of approximately 8 lb. each), and
2. The percentage of aggregate passing the 3/4 in. sieve remained the same, but, unlike the MnDOT HFT tests, the amount of material retained on the 5/8 sieve was controlled (as shown in Table 3.2).

The actual HFT test procedures used were similar to those described for the MnDOT HFT procedures except that 175 psi was used for the actuator pressure. Detailed instructions on the INDOT HFT testing procedures are given in Appendix B.

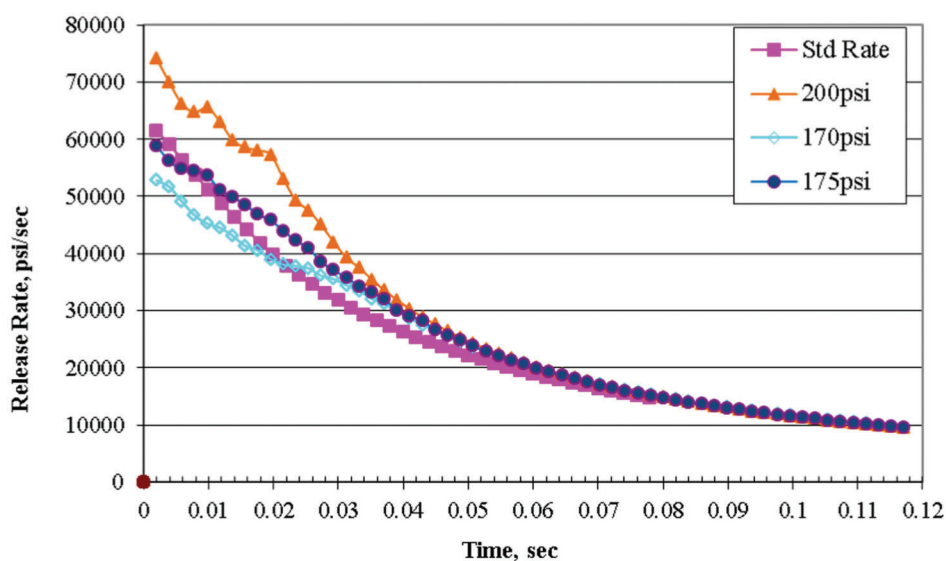


Figure 3.12 Pressure release profiles for various actuator pressure settings.

## 4. AGGREGATE SELECTION

The U.S. Geological Survey (USGS) 2009 publication indicated that Indiana ranked 8th in the nation for crushed stone production, with 94 limestone and dolostone (a.k.a. carbonate rock) quarry operations producing 44,100,000 metric tons that year. Approximately 5% or 2,080,000 metric tons of that quarried coarse aggregate was used in concrete construction (U.S. Geological Survey, 2009).

Crushed carbonate rock is the primary aggregate source used in concrete paving in Indiana and must pass a series of rigorous tests to obtain the AP classification required by INDOT for use in concrete paving. Not all aggregate sources qualify. Although the number of Class AP approved aggregate sources in Indiana varies with time, approximately 63 quarries and 10 gravel sources have appeared on INDOT's AP approved source list in recent years.

### 4.1 Geologic and Geographic Distribution

The bedrock geology in Indiana is dominated by sedimentary rocks formed from the sediments deposited by the fluctuating inland seas that dominated the landscape more than 300 million years ago (m.y.a.). The younger of these rock formations, of the Mississippian and Pennsylvanian age, form two geologic basins: the Michigan Basin in northeastern Indiana and the Illinois Basin in southwestern Indiana (as shown in Figure 4.1) (Hasenmueller & Hasenmueller, n.d.). Between these two



**Figure 4.1** Conceptual map of the general geologic structures dominating Indiana's bedrock (Hasenmueller & Hasenmueller, 2011).

basins stretches an arch, an uplifted section of much older sedimentary rock formations from the Ordovician to Devonian Periods (from approximately 485–420 m.y.a.) (Indiana Geological Survey, n.d.).

Comparing the bedrock map to the map delineating the aggregate sources in Indiana, and more specifically the crushed stone sources (both shown in Figure 4.2), it can be seen that a majority of the aggregate quarries mine the older Silurian and Devonian formations. The exception is a strip of quarries through the Mississippian deposits in the southwestern half of Indiana, nominally north and south of Bloomington.

The Indiana Geological Survey (IGS) and other researchers have made progress identifying rock characteristics and formations related to variable performance statewide (Schuster, 1957; Shaffer & Wenning, 2009; Smith, Brookley, & McGregor, 1954). However, a direct correlation between the geologic formation, or other easily indefinable characteristics, and the aggregate freeze-thaw performance in concrete pavements has not yet been identified. Several sources that have AP approved material have borderline ITM210 test results, particularly in the Louisville formation. One stockpile may pass AP approval and the next may fail, which may result in problems during a specific project (per verbal conversations with INDOT's chief geologist, R. Rees).

### 4.2 Performance Quality

Given the large number of potential aggregate sources available to INDOT for concrete paving mixtures, the variability between and within sources, and the scope of this study, careful selection of the aggregate sources for testing was important. Through a collaborate effort with INDOT's chief geologist aggregate samples were judiciously selected and collected to represent the varied geology and performance statewide (as shown in Figure 4.3 and Table 4.1). All sources selected were quarried carbonate aggregates.

Aggregate were identified and collected from 14 different carbonate quarries. If samples were taken from the same quarry but at different times during production or taken from the same quarry but different ledges a new sample designation was assigned. Aggregate sources will remain anonymous throughout this report but are grouped into three performance levels:

- A. freeze-thaw durable, AP approved aggregate sources
- B. Non-freeze-thaw durable, known to fail AP criteria
- C. Variable durability performance or of unknown performance

A total of 18 aggregate sources were collected, six from each of the above categories A, B and C. Sample C2 was not a quarried aggregate, removed from the study and C7 was added to complete the suite of 18 quarried aggregate sources. (Source C2 was a Recycled Concrete Aggregate source and added to the testing discussed in Appendix F).

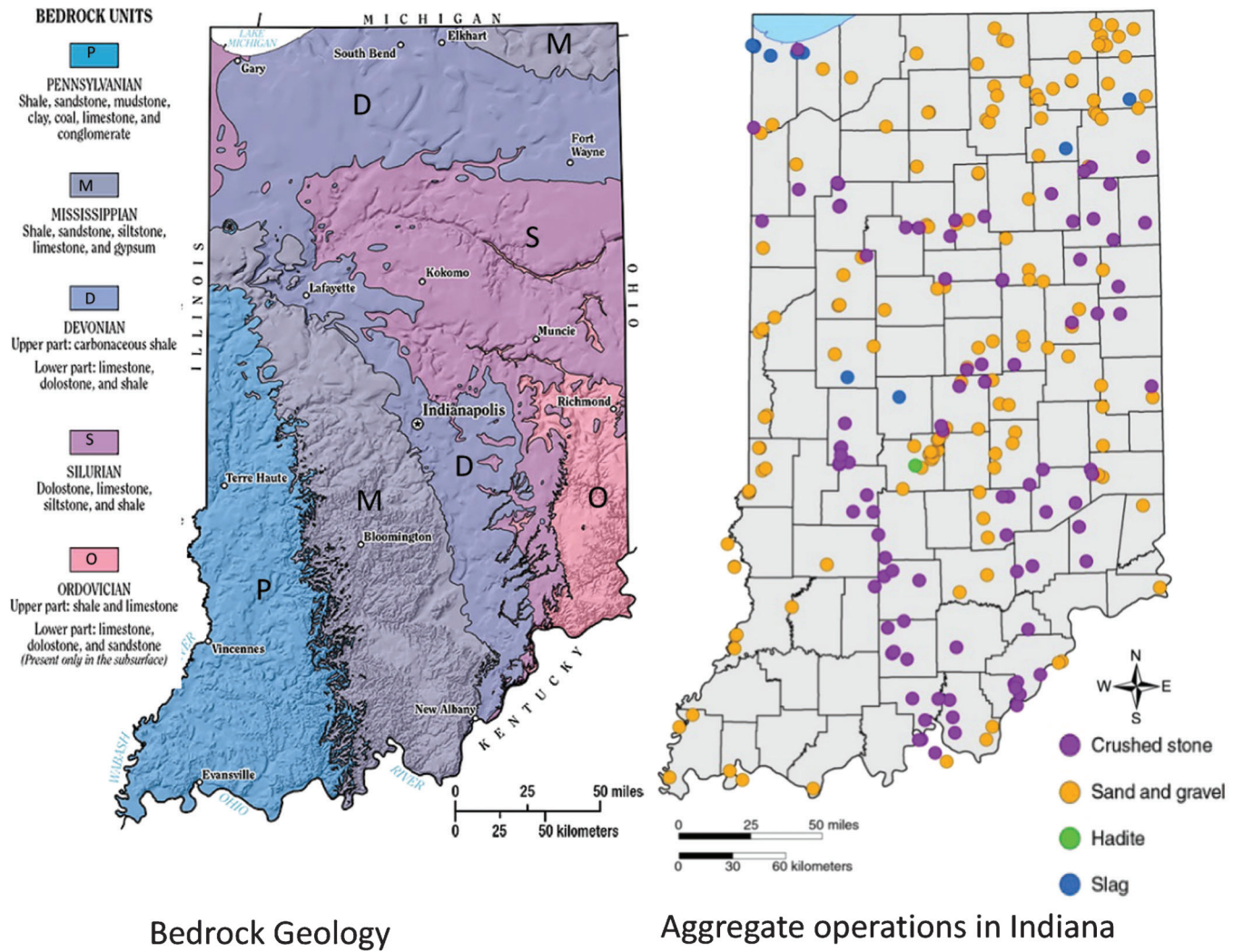


**Figure 4.2** Bedrock geology of Indiana compared to the distribution of aggregate source (taken from IGS website <http://igs.indiana.edu/> (Hasenmueller & Hasenmueller, n.d.; Indiana Geological Survey, n.d.)).

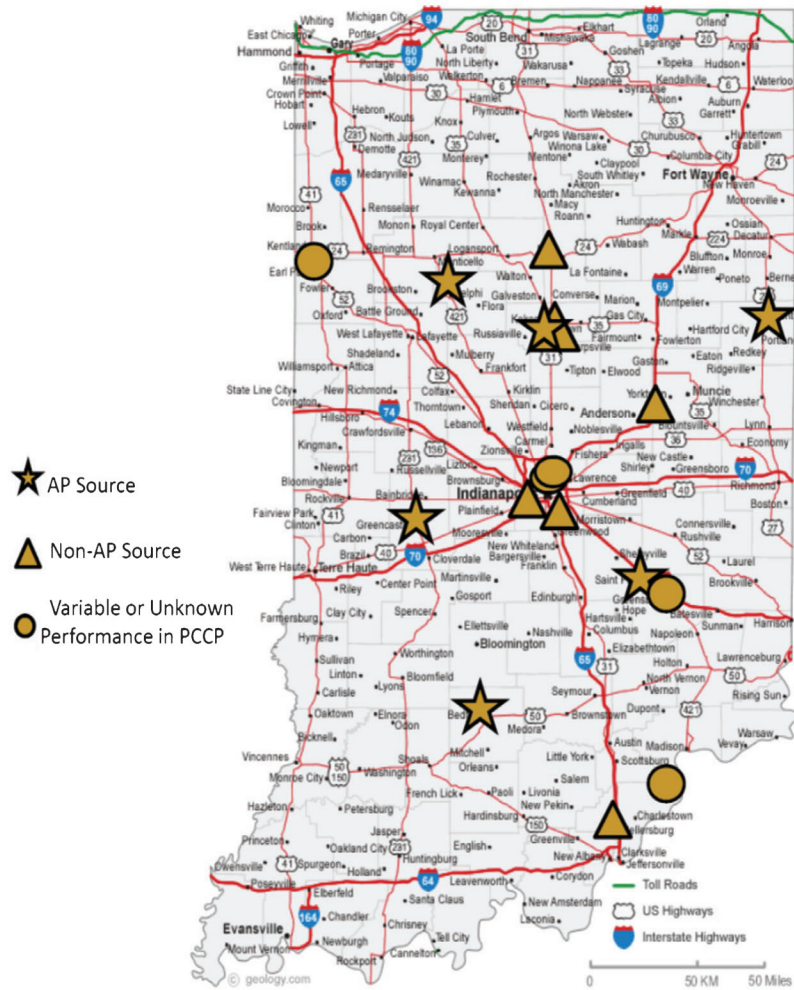


Figure 4.3 Location of aggregate quarries sampled for testing.

TABLE 4.1  
Aggregate source information

Source	Formation	Geologic period	Year collected
A1	Salamonie Dolomite	Silurian	2010
A2	St. Genevieve Fm	Mississippian	
A3	Reefal Fm	Silurian	
B1	Mississinewa	Silurian	
B2	Mississinewa	Silurian	
B3	N.Vernon, Jeffersonville	Devonian	
B4	Mississinewa, Louisville Fm	Silurian	
C1	Louisville Fm; Salamonie Fm	Silurian-Ordovician	2011
A4	St. Genevieve Fm	Mississippian	
A5	Wabash Fm; Kokomo Lmst	Silurian	
B5	Wabash-Liston Creek	Silurian	
B6	N.Vernon, Jeffersonville	Devonian	
C3	Louisville Fm	Silurian	
C4	Louisville Fm	Silurian	
A6	Salamonie Fm; Laurel Mbr	Silurian	2012
C5	Jeffersonville Geneva Dolo	Silurian	
C6	Mississinewa, Louisville Fm, Salamonie Fm	Silurian	
C7	N.Vernon, Jeffersonville	Devonian	

Fm= Formation; Mbr= Member; Lmst= limestone; Dolo= dolostone.

## 5. TEST RESULTS AND ANALYSIS

Samples of aggregate from all 18 sources were subjected to basic characterization tests (e.g., specific gravity and absorption capacity) and HFT testing using both the MnDOT HFT chamber and INDOT HFT chamber. In addition, concretes prepared from these aggregate samples were subjected to tests, including freeze-thaw testing.

This chapter presents the results of all of the tests performed on the 18 aggregates sources and the concrete incorporating these aggregates. The experimental findings are presented in two sections: aggregate test results (Section 5.1) and freeze-thaw test results of concrete made with aggregates from each source (Section 5.2).

### 5.1 Aggregate Test Results

The aggregate samples from each of the 18 sources were separated into their component size fractions using the following screen sizes: 1 in., 3/4 in., 5/8 in., 1/2 in., 3/8, and #4. The size fractions for each source were then proportions to produce the specific gradations required for each test (as is discussed in sections 5.1.1 through 5.1.3).

Figure 5.1 shows the aggregate particle size distributions that were used for ITM 210 and HFT tests under this study. The ITM 210 freeze-thaw test of concrete prisms requires a specific gradation to prepare the concrete that incorporates coarse aggregate from No. 4 (4.75 mm) through 1 in. (25 mm). It is generally agreed that the larger-sized fraction of the coarse aggregate is most responsible for producing aggregate-related freeze-thaw damage in concrete (Stark & Klieger, 1973), and previous research showed the HFT results of the larger

size fractions provided the best correlation with concrete freeze-thaw results (Embacher & Snyder, 2003). Therefore only 1/2-in.-plus material was tested in the HFT. The aggregate gradation used in HFT testing was selected to reflect the relative proportions of the 3/4-in.-plus and 1/2-in.-plus materials tested in ITM210. (Section 3.1.2 and 3.2.5 presents additional details related to aggregate gradations used for HFT testing in this study.)

#### 5.1.1 Specific Gravity and Absorption

All 18 aggregate sources were tested for absorption and specific gravity according to AASHTO T85 using the same gradation used in batching ITM210 concrete specimens. As shown in Table 5.1 the specific gravities ranged from 2.48 to 2.75, and the absorption values ranged from 0.88 to 5.20% with both the highest and lowest absorptions tested being AP aggregate. An increase in absorption capacity is often thought to relate to a decrease in aggregate freeze-thaw durability (Barksdale, 1992); however, the results shown in Table 5.1 suggest this general trend does not hold true for the aggregates tested.

#### 5.1.2 MnDOT HFT Chamber Results

As previously noted three replicate samples from each aggregate source were tested in the MnDOT HFT chamber according to procedures described in Section 3.1.2, for a combined mass of approximately 24 lbs. (11 kg). The chamber and actuator pressures used were 1300 and 150 psi, respectively. After each 10 cycles, the samples were oven-dried, sieved over 3/4 in., 5/8 in., 1/2 in., 3/8 in., 5/16 in., 1/4 in., and #4 sieves, and the mass retained on each sieve was recorded to the nearest

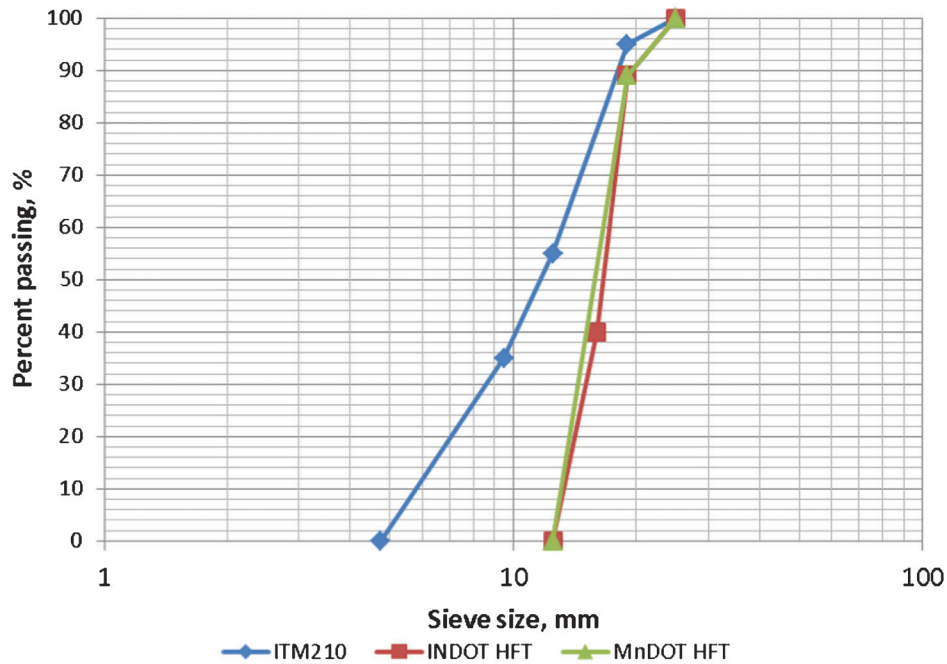


Figure 5.1 Aggregate gradation plots for HFT and ITM 210 tests.

0.1 g. The test results from the three replicates were combined for analysis. The HFT test report for source B3 is shown in Table 5.2 as an example of the recorded test result.

Figure 5.2 shows an example plot (source B3) of mass change on each sieve as a percentage of total initial mass after 50 cycles of HFT. This plot illustrates how the HFT mechanism breaks the larger particles into smaller ones. Generally the mass retained on the

larger sieves decreased while the mass retained on the smaller sieves increased due to an accumulation of fractured aggregate particles from the upper sieves. Typically the 3/4 in. and 5/8 in. sieves showed mass losses and the net mass on the 1/2 in. sieve sometimes showed a loss and sometimes showed a gain. Smaller sieves which contained no mass in the original test samples generally showed small mass gains.

As a check, the total mass retained on all sieves after 50 cycles of HFT testing was compared with the initial sample mass before testing. There was usually a small discrepancy amounting to less than 0.1% of the initial sample mass which was assumed to be a loss of fines due to the sieving and handling processes.

TABLE 5.1 Bulk specific gravity (BSG) and absorption (ABS) results of aggregates used in the study

Source #	BSG (SSD)	% ABS
A1	2.63	2.39
A2	2.62	1.69
A3	2.75	0.87
A4	2.68	0.88
A5	2.49	5.20
A6	2.69	1.10
<b>A Range</b>	<b>2.49–2.75</b>	<b>0.87–5.20</b>
B1	2.57	4.81
B2	2.66	2.33
B3	2.64	1.36
B4	2.67	2.66
B5	2.65	1.47
B6	2.62	1.08
<b>B Range</b>	<b>2.57–2.67</b>	<b>1.08–4.81</b>
C1	2.69	2.66
C3	2.67	1.47
C4	2.68	1.08
C5	2.48	5.13
C6	2.66	1.79
C7	2.65	1.36
<b>C Range</b>	<b>2.48–2.69</b>	<b>1.08–5.13</b>

### 5.1.3 INDOT HFT Chamber Results

The Hydraulic Fracture Test was performed on all aggregate sources using INDOT's HFT chamber and the procedure described in section 3.2.5. Similar to the data collection and processing steps presented for the MnDOT HFT chamber tests in section 5.1.2, mass retained on each sieve was collected after each 10 cycles of HFT testing and recorded, as shown in Table 5.3. The change in mass retained on each sieve was calculated as the difference in masses retained at 0 and 50 cycles. These mass changes were divided by the total initial mass and the values were plotted as mass gain/loss on each sieve due to the hydraulic fracturing process.

Figure 5.3 shows an example plot (source B3) of mass change on each sieve as a percentage of total initial mass after 50 cycles of HFT. This plot illustrates how the HFT mechanism breaks the larger particles into smaller ones as discussed in the previous section (Section 5.1.2).

TABLE 5.2  
MnDOT HFT result of a particular source (source B3)

	Mass (g)						Mass change after 50 cycles	
	0 cycles	10 cycles	20 cycles	30 cycles	40 cycles	50	(g)	%
3/4 in. sieve	1393.2	1103.4	1163.6	1133.9	1036.2	1048.6	-344.6	-3.3
5/8 in. sieve	3652.6	3590.1	3539.8	3629.2	3578.2	3522.7	-129.9	-1.2
1/2 in. sieve	5227.9	5438.7	5402.5	5291.3	5436.0	5476.0	248.1	2.4
3/8 in. sieve	218.1	284.5	294.4	330.6	325.7	321.3	103.2	1.0
5/16 in. sieve	0.0	0.8	3.1	2.3	3.7	3.6	3.6	0.0
1/4 in. sieve	0.0	0.0	0.0	1.5	2.8	4.9	4.9	0.0
#4 sieve	0.0	0.7	1.5	2.8	3.3	3.2	3.2	0.0
Pan	0.0	6.0	6.6	6.0	3.2	4.7	26.5	0.3
<b>Total mass</b>	<b>10491.8</b>					<b>10385.0</b>		

Note: All material that passed the #4 after each set of 10 test cycles was captured on the pan and not returned to the chamber for further testing. Therefore the total 'Pan' material after 50 cycles of testing is the sum of the 'Pan' material after each 10 cycles of testing.

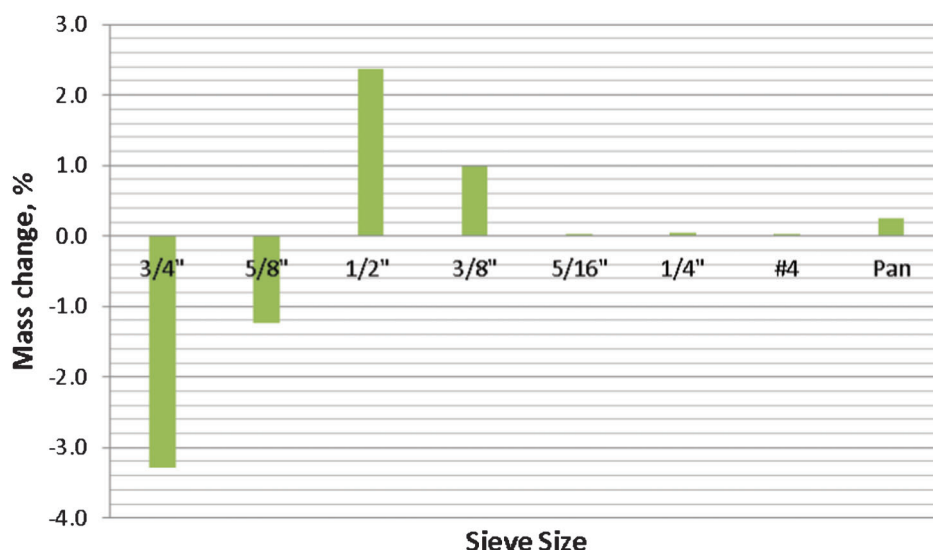


Figure 5.2 Mass changes of material retained on each sieve after 50 HFT cycles (source B3).

### 5.2 Concrete Freeze-Thaw Test Results

Concrete mixtures were designed for all aggregate sources, per ITM210 requirements. All of the coarse aggregates for each mixture came from the particular

source being tested and each source was sieved into component sizes and recombined to meet ITM 210 gradation requirements. The fine aggregate used for all mixtures was a natural sand from INDOT Source No. 2310 (as specified in ITM210-08). The mix designs

TABLE 5.3  
INDOT HFT result of a particular source (source B3)

	Mass (g)						Mass change after 50 cycles	
	0 cycles	10 cycles	20 cycles	30 cycles	40 cycles	50 cycles	(g)	%
3/4 in. sieve	1462.5	1462	1412.8	1363.6	1375.9	1263.8	-198.7	-1.5
5/8 in. sieve	6344.0	6338.4	6328.8	6270.2	6099.8	6266.7	-77.3	-0.6
1/2 in. sieve	5187.0	5180.5	5193.7	5281.2	5355.7	5243.8	56.8	0.4
3/8 in. sieve	0.0	0.0	13.7	9.4	44.7	78.9	78.9	0.6
5/16 in. sieve	0.0	0.0	0.0	0.0	1.3	4.0	4.0	0.0
1/4 in. sieve	0.0	0.0	0.5	0.0	0.0	0.0	0.0	0.0
#4 sieve	0.0	0.0	0.6	0.0	0.0	0.0	0.0	0.0
Pan	0.0	12.6	24.3	26.6	25.3	22.2	111.0	0.9
<b>Total mass</b>	<b>12993.5</b>					<b>12875.4</b>		

Note: All material that passed the #4 was captured on the pan and was not returned to the chamber for further testing. Therefore, the total 'Pan' material after 50 cycles of testing is the sum of the 'Pan' material retained after each 10 cycles of testing.

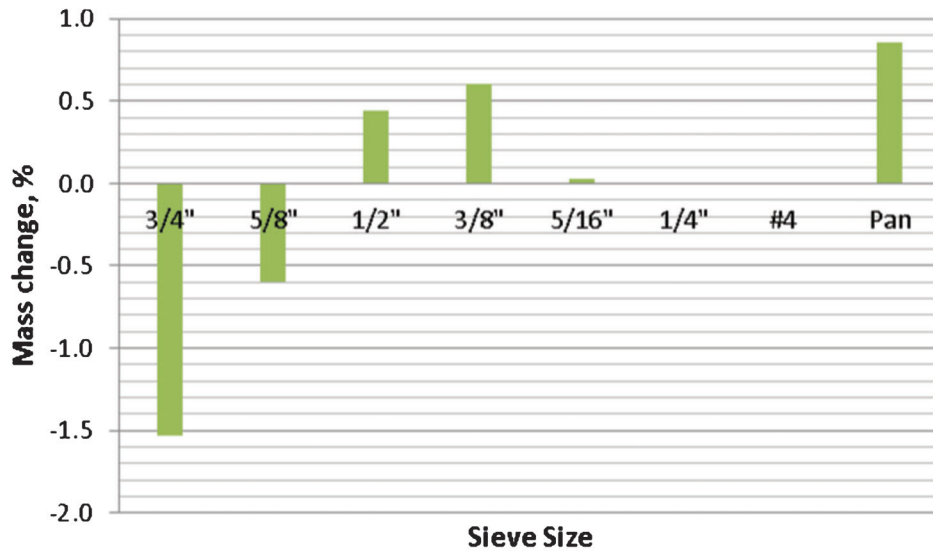


Figure 5.3 Mass changes on each sieve after 50 HFT cycles (source B3).

and other material requirements for ITM210, and fresh and hardened concrete properties for each mix are presented in Appendix-D.

#### 5.2.1 Fresh Concrete Test Result

Type I Portland cement and Catexol VR, a vinsol resin-based air-entraining admixture, were used for all mixtures, per ITM210. The air content of the fresh concrete was measured using the volumetric method (AASHTO T196) with a target of 6.5 ( $\pm 1.5$ ) percent air. Slump and unit weight of the concrete also were measured. If the mix did not meet the target air range, beams were not cast, the mix design was adjusted and rebatched until the air content fell within the target range.

#### 5.2.2 Hardened Concrete Test Results (ITM 210)

Six beams (3 in.  $\times$  4 in.  $\times$  15 in.) were fabricated from each concrete mixture batched. Three of the beams were tested for freeze-thaw durability following AASHTO T161 Procedure A (freeze and thaw in water) by the research team, and the remaining three beams were tested at INDOT Office of Materials following ITM 210, which is based on AASHTO T161 Procedure B (freeze in air, thaw in water).

INDOT's aggregate acceptance criteria for AP quality is that the average dilation (percent expansion) of at least 2 of the three test beams be less than 0.060% after 350 cycles of freezing and thawing. The durability factor (DF) for freeze-thaw specimens were based on measuring the relative dynamic modulus of elasticity (RDME) of each specimen and calculated per standard procedures described in ASTM C666. The ITM 210 test results are presented in Table 5.4.

As expected, all aggregate sources in Group A passed the freeze-thaw test while all sources in Group B tested as nondurable with expansions exceeding 0.060% and DF less than 75. Four of the six aggregate sources in Group C tested as nondurable and two passed (C5 and

C6) as shown in Figure 5.4. Of the 18 aggregate sources tested all the durable aggregate had dilations less than 0.024 and DF greater than 94, and all the nondurable aggregates had dilations greater than 0.080% and DF of less than 86.

There was a very good correlation between percent dilation and DF, as shown in Figure 5.5, with a trend line that had an  $R^2$  value of 0.91. If this trend line is accepted as a good representation of the data, then a 0.060% dilation correlates well with a DF of 86.

If a DF of greater than 86 is considered passing, then the DF successfully identified durable and nondurable aggregates for all 18 sources tested, as shown in Figure 5.6.

TABLE 5.4  
Summary of dilation and DF measured after 350 cycles

Source	Dilation	DF
A1	0.0035	96.6
A2	0.0028	98.2
A3	0.0071	98.5
A4	0.0115	99.0
A5	0.0047	96.2
A6	0.0198	94.3
<b>A Range</b>	<b>0.0028–0.0198</b>	<b>94.3–99.0</b>
B1	0.1631	69.3
B2	0.2700	36.2
B3	0.0849	75.9
B4	0.1794	61.9
B5	0.2435	36.4
B6	0.0835	74.8
<b>B Range</b>	<b>0.0849–0.2700</b>	<b>36.2–74.8</b>
C1	0.1440	85.9
C3	0.1458	60.8
C4	0.0922	77.3
C5	0.0044	96.3
C6	0.0232	94.1
C7	0.0809	78.3
<b>C Range</b>	<b>0.0044–0.1458</b>	<b>60.8–96.3</b>

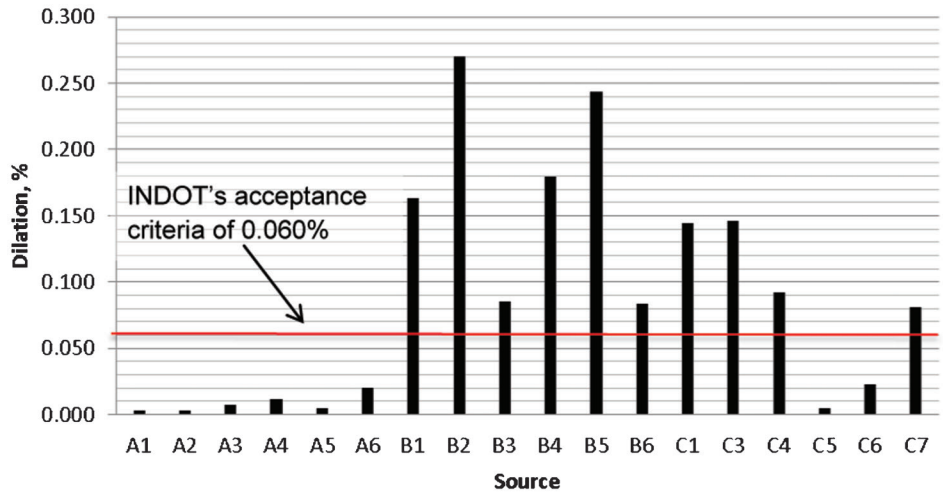


Figure 5.4 Plot of percent dilation compared against INDOT's acceptance criteria.

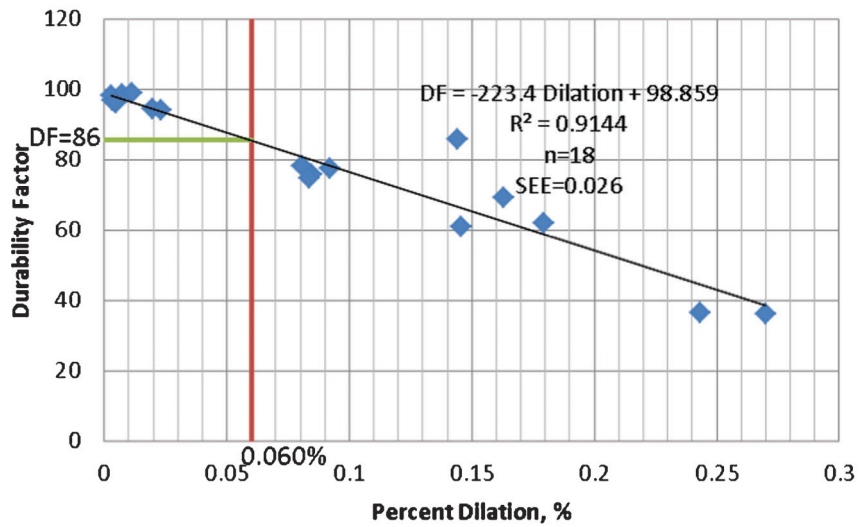


Figure 5.5 Percent dilation versus durability factor.

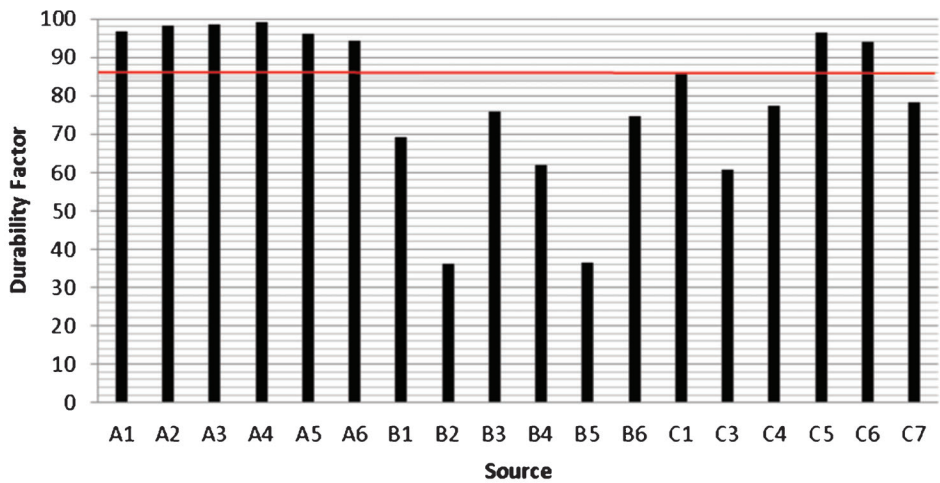


Figure 5.6 Plot of durability factor results compared with DF=86.

## 6. REGRESSION MODEL DEVELOPMENT

Linear regression models had been developed for MnDOT HFT data in previous studies (Embacher & Snyder, 2003; Hietpas, 1998); however, those previous models did not fit this project's data very well. The most likely reasons for the poor fit are because the aggregate size fractions tested and freeze-thaw test procedures used were different. The University of Minnesota study used a modification of AASHTO T161 ("Procedure C") in which the specimens were wrapped in saturated terry cloth and frozen in air and thawed in water, a method considered by AASHTO at that time but never adopted as a standard procedure. In addition, the MnDOT models were developed for specific particle size ranges (i.e., 1½ in. to ¾ in., ¾ in. to ½ in., and ½ in. to #4). In this study, the particle size range tested was 1 in. to ½ in. and proportioned based on ITM210 requirements (as described previously). Therefore, it is not surprising that the models developed in Minnesota did not accurately predict the dilation and DF of the aggregates tested in this study. Therefore it was necessary to develop new statistical models for the data generated in this study.

The purpose of the statistical analyses performed under this study was to develop linear regression models to predict average percent dilation and durability factor of freeze-thaw beam test results using variables obtained from HFT results. Separate predictive models were developed for percent dilation results and for durability factor results using the statistical analysis software package JMP®, Version 10 by SAS Institute Inc. This chapter presents statistical analyses of the test results obtained using the MnDOT HFT equipment (Section 6.1) and using the INDOT HFT equipment (Section 6.2).

### 6.1 Models Developed Using MnDOT HFT Results

Several models were developed to predict freeze-thaw test results (ITM210) using the data sets generated by testing each aggregate source using the MnDOT HFT equipment. Examples of some of these models are discussed in the following sections and are described in more detail in Appendix E.

#### 6.1.1 Selection of Predictor Variables

Initially, the test results were analyzed in a way that was similar to the techniques used in previous HFT studies (Embacher & Snyder, 2003; Hietpas, 1998) by developing the values of the "Cumulative Percentage of Mass Passing" (CPMP) each sieve size as predictor variables. These CPMP values were developed as a percentage of the total mass that passed through each sieve after 50 cycles of pressurization testing. The CPMP values as model predictors did not yield satisfactory models for this study, perhaps in part because of the particles size ranges used in this study

differed from that used in the previous studies. Hence, new predictor variables were developed and used as model inputs for this study.

Many potential predictor variables (generated from HFT results) were examined, and "percent change in mass retained" (PCMR) on each sieve was the most useful in developing freeze-thaw dilation models. The PCMR is defined here as the change in mass on each sieve from before any testing (0 cycles) to after 50 cycles of testing, divided by an initial mass value. For the ¾ in., ½ in. and ¼ in. sieves, the change in mass on each respective sieve is divided by the initial mass retained on that sieve. For the sieves smaller than ¼ in., which had little or no initial mass, the mass on each respective sieve after 50 cycles is divided by the entire sample's total initial mass. See Table E.1 for computational examples using source B3 data. Equations and additional computational details are presented in section E.1 of Appendix E.

Eight potential PCMR predictor variables were computed from the HFT test data for each aggregate source, and they were designated as follows: P34, P58, P12, P38, P516, P14, P4 and P0, where P stands for "Percent Change in Mass Retained" and the numbers stand for the various sieve sizes (i.e., ¾, ½, ¼, 3/8, 5/16, 1/4, #4 and minus #4 or pan respectively). These PCMR values were used as independent (or predictor) variables in the development of regression models for predicting the percent dilation and durability factor (which were the dependent, or response model variables).

Table 6.1 presents a summary of the HFT and freeze-thaw test results for all 18 aggregate sources; these values were used as regression model inputs. Details of the modeling process are given in Appendix E.

#### 6.1.2 Dilation Models Developed Using MnDOT HFT Results

The development of a regression model for dilation began with the adoption of a generalized linear model (GLM) with the form shown in Equation 6.1.

*Equation 6.1:*

$$\begin{aligned} \text{Dilation} = & \beta_0 + \beta_1 P34 + \beta_2 P58 + \beta_3 P12 \\ & + \beta_4 P38 + \beta_5 P516 + \beta_6 P14 + \beta_7 P4 + \beta_8 P0 \end{aligned} \quad (6.1)$$

Where:

Dilation = Percent dilation after 350 FT cycles as the response variable

$\beta_i$  = Regression coefficients

P34, P58, P12, P38, P516, P14, P4 and P0 are predictor variables.

The percent dilation measured was determined after 350 cycle of freeze-thaw testing. Although several specimens exceeded the failure criteria of 0.06% dilation prior to 350 cycles of freeze-thaw testing, dilation measurements continued for more than 350 cycles and the dilation values for 350 cycles were interpolated between the last two or more measurements.

The model development process is summarized in Appendix E, Section E.1.1. For each model developed.

TABLE 6.1  
Summary of freeze-thaw and MnDOT HFT results

Aggregate source	Response variables		Predictor variables							
	Freeze-thaw test result		HFT result (PCMR values)							
	Dilation	DF	P34	P58	P12	P38	P516	P14	P4	P0
A1	0.0035	96.6	-19.57	-6.01	0.81	2.23	0.31	0.2	0.16	0.41
A2	0.0028	98.2	-1.59	-10.70	1.62	2.51	0.32	0.3	0.15	0.47
A3	0.0071	98.5	-19.19	-8.42	6.32	1.74	0.02	0.01	0.01	0.13
A4	0.0115	99.0	-2.89	-2.97	0.75	0.93	0.01	0.01	0.03	0.10
A5	0.0047	96.2	-16.65	-5.39	1.63	1.99	0.22	0.18	0.11	0.52
A6	0.0198	94.3	-9.01	-2.67	-1.10	1.65	0.07	0.07	0.05	0.32
B1	0.1631	69.3	-26.46	-27.80	-1.00	7.92	2.33	1.88	1.21	2.33
B2	0.2700	36.2	-18.82	-8.28	7.32	1.81	0.08	0.05	0.05	0.28
B3	0.0849	75.9	-24.73	-3.56	4.75	0.98	0.03	0.05	0.03	0.25
B4	0.1794	61.9	-5.76	-1.88	0.15	0.72	0.02	0.04	0.03	0.25
B5	0.2435	36.4	3.71	-4.64	-1.85	1.34	0.07	0.05	0.04	0.22
B6	0.0835	74.8	-11.20	-3.08	1.46	1.11	0.02	0.02	0.02	0.23
C1	0.1440	85.9	-11.04	-12.76	13.21	1.62	0.17	0.19	0.08	0.33
C3	0.1458	60.8	-4.60	-0.19	-2.33	1.45	0.04	0.02	0.02	0.11
C4	0.0922	77.3	7.62	5.30	-11.28	0.2	0.01	0.01	0.01	0.15
C5	0.0044	96.3	-9.01	-2.67	-1.1	1.65	0.07	0.07	0.05	0.32
C6	0.0232	94.1	-6.79	-3.28	-1.93	1.69	0.19	0.19	0.09	0.20
C7	0.0809	78.3	-12.46	2.59	-2.46	0.6	0.01	0.06	0.00	0.16

Diagnostic tests were completed to determine whether the linear regression model assumptions were met. The assumptions which justify the use of linear regression models are linearity, independence, constant variance and normality. All models discussed in this chapter met those assumption criteria. Section E.2.2 of Appendix E presents more details concerning model diagnostics.

The model that provided the best fit between actual measured and predicted dilation values for the study data set generated by the MnDOT HFT equipment is presented in Equation 6.2. Figure 6.1 presents a plot of measured dilation versus predicted dilation for the 15 data points used to develop this model (n=15). The

solid line on the plot represents an ideal one-to-one relationship between the x and y axes. The trend line that best fits this data set is the red dashed line. As noted there is a good relationship between the measured and predicted dilation but it is slightly off from a perfect one-to-one relationship. The three outliers not considered in this model development were A4, B2 and B5, as shown in Figure 6.2. Further discussion of outliers and the development of this model can be found in Section E.1.2 (Appendix E).

The model presented as Equation 6.2 is recommended for use when testing aggregate samples using the gradations as described previously and the MnDOT HFT equipment to predict ITM 210 dilation measurements.

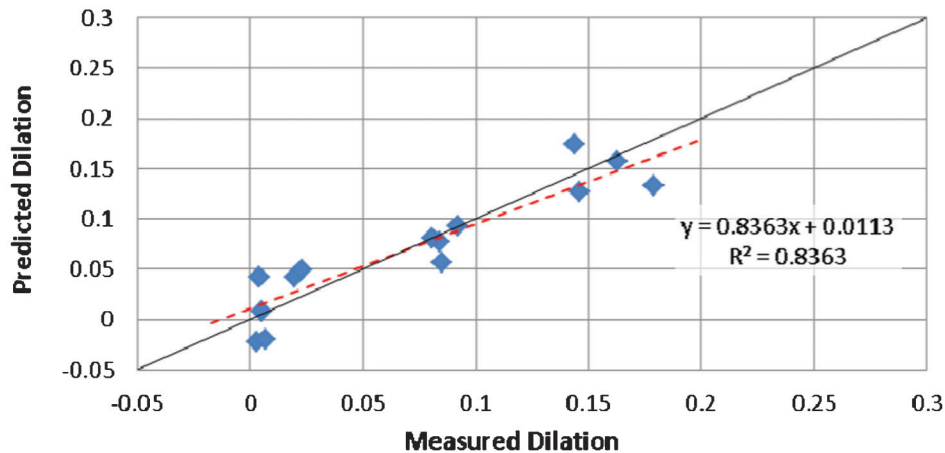
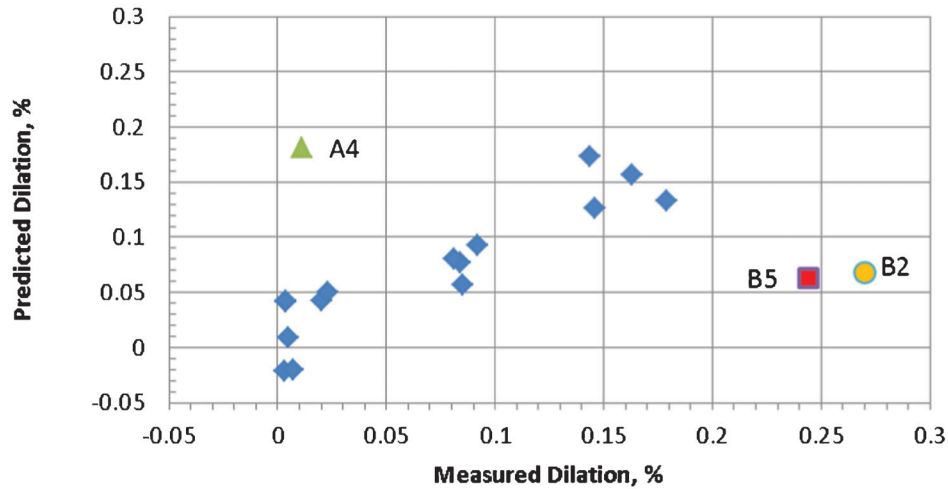


Figure 6.1 Measured versus predicted dilation by Equation 6.2. Dashed line is the trend line for this dataset. Solid line is where a perfect 1:1 trend would fall.



**Figure 6.2** Locations of the outliers (A4, B2 and B5) in reference to the measured and predicted dilation by the recommended model.

Equation 6.2:

$$\begin{aligned} \% \text{ Dilation} = & 2.49E-01 + 9.42E-03 * P34 + 3.80E \\ & -02 * P58 + 3.74E-02 * P125.36E-01 * P14 \quad (6.2) \\ & + 2.17E+00 * P4 - 1.56E-01 * P0 \end{aligned}$$

Model statistics:

$$\begin{aligned} R^2 &= 0.836 \\ R^2 \text{ (adj.)} &= 0.714 \\ SEE &= 0.0347 \\ N &= 15 \\ \text{Model P-value} &< 0.0081 \end{aligned}$$

### 6.1.3 Durability Factor Models Developed Using MnDOT HFT Results

The generalized linear model form presented in Equation 6.1 was used for developing a model of freeze-thaw durability factor (DF), except that durability factor after 350 freeze-thaw cycles, rather than percent dilation, was used as the response variable.

The best model developed to predict durability factor under this study was not very useful in accurately predicting durability factor from HFT results. The model as shown as Equation 6.3 has an adjusted  $R^2=0.53$  with  $n=18$ , Model P-value  $<0.9638$ , which is  $>0.05$  hence not significant and not recommended for further consideration. Additional details are provided in Appendix-E, Section E.1.3.

Equation 6.3:

$$\begin{aligned} DF = & 54.12 - 1.34E+00 * P34 - 3.25E \\ & + 00 * P58 - 4.08E+00 * P12 + 1.02E \\ & + 01 * P38 - 3.04E+02 * P516 + 3.40E \\ & + 02 * P14 - 2.50E+01 * P4 - 3.90E+01 * P0 \end{aligned} \quad (6.3)$$

Model statistics:

$$R^2 = 0.19$$

$$R^2 \text{ (adj.)} = -0.53$$

$$SEE = 25.04$$

$$n = 18$$

$$\text{Model P-value} < 0.9638 > 0.05$$

## 6.2 Models Developed Using INDOT HFT Results

The PCMR predictor variables were developed from INDOT HFT results for each source in a similar manner as described for the MnDOT HFT results in Section 6.1.1. A summary of the INDOT HFT chamber and ITM210 freeze-thaw test results for all 18 aggregate sources is presented in Table 6.2. Separate models were developed from this data set to predict ITM 210 average dilation and durability factor values.

### 6.2.1 Dilation Models Developed Using INDOT HFT Results

The same generalized linear regression model that was used for developing dilation models for the MnDOT HFT chamber (Equation 6.1) was also used for regression analysis of the INDOT HFT data. The model that best fit the data as shown in Table 6.3 is presented below in Equation 6.4.

Equation 6.4:

$$\begin{aligned} \% \text{ Dilation} = & 8.25E-2 + 6.33E-3 * P34 \\ & + 9.64E-2 * P38 - 3.12 * P14 + 4.3 * P4 \end{aligned} \quad (6.4)$$

Model statistics:

$$R^2 = 0.892$$

$$R^2 \text{ (adj.)} = 0.853$$

$$SEE = 0.029$$

$$n = 16$$

$$\text{Model P-value} < 0.0001$$

Sixteen sources were used to develop Equation 6.4. Two sources (A3 and B2) were outliers. Outliers and influential points are usually detected using studentized

TABLE 6.2  
Summary of freeze-thaw and INDOT HFT chamber results

Source	Response variables		Predictor variables							
	Freeze-thaw test result		HFT result (PCMR values)							
	Dilation	DF	P34	P58	P12	P38	P516	P14	P4	P0
A1	0.0035	96.6	-16.45	-10.27	9.75	1.19	0.01	0.02	0.00	1.57
A2	0.0028	98.2	-6.79	-3.28	-1.93	1.69	0.19	0.19	0.09	0.20
A3	0.0071	98.5	-5.37	-3.26	0.28	0.93	0.01	0.01	0.00	0.86
A4	0.0115	99.0	-9.78	-4.52	3.44	0.75	0.04	0.04	0.01	0.98
A5	0.0047	96.2	-13.75	-9.76	7.07	1.15	0.01	0.02	0.00	1.84
A6	0.0198	94.3	-14.78	-6.29	10.96	0.39	0.03	0.03	0.02	0.69
B1	0.1631	69.3	-20.21	-6.66	5.81	1.04	0.14	0.03	0.05	0.97
B2	0.2700	36.2	-7.41	-8.51	5.08	1.25	0.01	0.01	0.01	1.39
B3	0.0849	75.9	-13.59	-1.22	1.1	0.61	0.03	0.00	0.00	0.85
B4	0.1794	61.9	-12.87	-11.12	10.71	1.28	0.02	0.01	0.01	1.08
B5	0.2435	36.4	-8.89	-9.61	6.31	1.61	0.01	0.00	0.01	1.33
B6	0.0835	74.8	-17.96	-13.61	13.51	1.35	0.06	0.04	0.02	1.52
C1	0.1440	85.9	-8.9	-6.92	4.84	0.83	0.05	0.07	0.06	1.25
C3	0.1458	60.8	-11.63	-9.22	8.39	1.3	0.02	0.01	0.02	0.73
C4	0.0922	77.3	-11.81	-2.18	0.59	0.34	0.01	0.01	0.02	0.57
C5	0.0044	96.3	-33.16	-12.75	11.95	2.07	0.04	0.05	0.02	2.57
C6	0.0232	94.1	-7.33	-6.63	4.42	0.68	0.03	0.03	0.01	0.68
C7	0.0809	78.3	-9.96	-4.48	5.03	0.39	0.00	0.00	0.00	0.75

residual. As a rule of thumb, observations with a studentized residual of  $\pm 2$  are considered to be outliers. The absolute value of the studentized residual values for 16 sources ranged from 0.1 to 1.2 while both outlier sources A3 and B2 had studentized residual values of 2.0. Outlier observations can also be detected graphically from residual plots. The detailed outlier analysis presented in section E2.2.2 of appendix E, is part of a full range of diagnostic tests completed to determine whether the linear regression model assumptions were

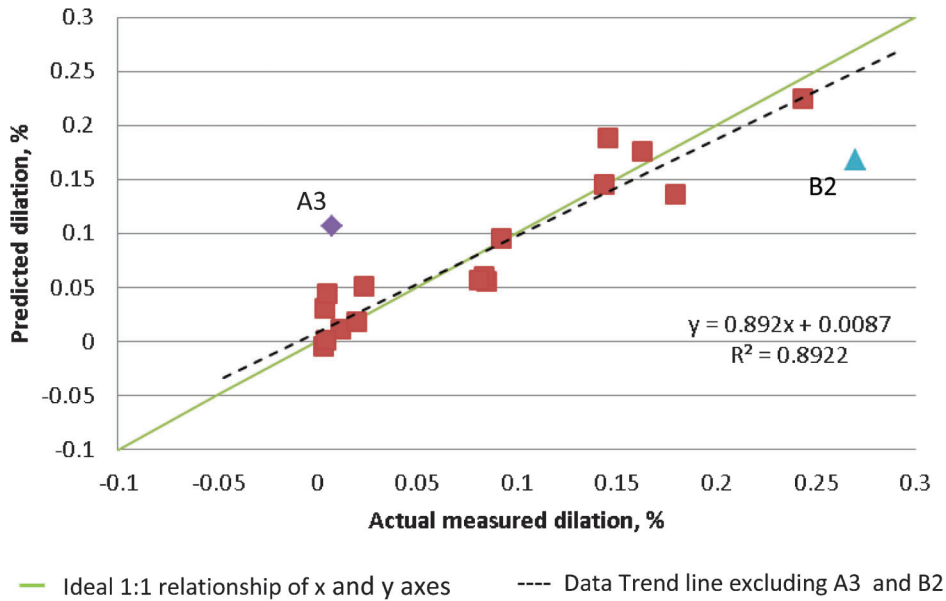
met for all models recommended in this report. All assumptions were met. Details of all those diagnostics used to develop the model presented in Equations 6.4 (also referred to as model I2) are given in Appendix E, Section E.2.2. Additional discussions on the development of the recommended dilation model are provided in Appendix E, Section E.2.3.

Figure 6.3 presents a plot of dilations predicted using the Equations 6.4 model versus measured dilation values for all 18 Sources; the data from the 16 sources used to develop the model and the two outlier sources (A3 and B2). Source B2 was identified as “nondurable” by the freeze-thaw test with an average dilation of 0.27%. In the HFT results for B2 many particles cracked but did not fracture completely, a distress that cannot be measured in the current HFT practice of measuring test results as a shift in particle size distribution. Additional cycles of testing or a higher pressure release rate might have completely fractured these particles and resulted in a better fit of the model for this source. Source A3 was identified as “durable” by the freeze-thaw test, with an average dilation of 0.0071%, but it experienced a more significant shift in particle size distribution during HFT testing for some reason. Source A3 is the only source described geologically as a Silurian Reefal Formation but further work is needed to understand if this phenomenon is associated with this rock type, or some other characteristic.

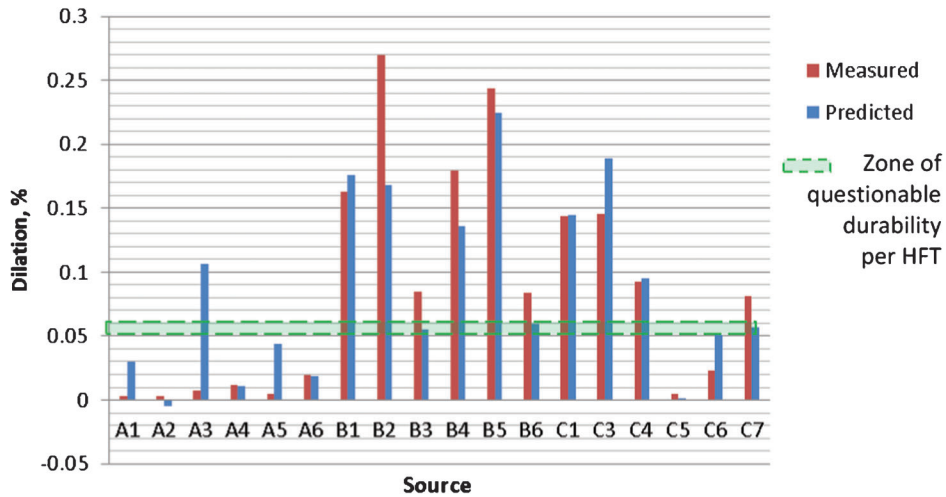
Figure 6.4 and Table 6.3 show that the selected model correctly predicts the durability or non-durability of 14 out of 18 sources correctly. Even though source B2 was not included in the model, the model correctly predicted this source as being nondurable. One of the four sources incorrectly identified by this model was freeze-thaw-durable source A3, which had a

TABLE 6.3  
Measured and predicted dilation by Equation 6.4

Source	Measured dilation, %	Predicted dilation, %
A1	0.0035	0.0304
A2	0.0028	-0.0048
A3	0.0071	0.1068
A4	0.0115	0.0107
A5	0.0047	0.0437
A6	0.0198	0.0185
B1	0.1631	0.1756
B2	0.2700	0.1677
B3	0.0849	0.0551
B4	0.1794	0.1360
B5	0.2435	0.2242
B6	0.0835	0.0597
C1	0.1440	0.1450
C3	0.1458	0.1887
C4	0.0922	0.0950
C5	0.0044	0.0015
C6	0.0232	0.0508
C7	0.0809	0.0569



**Figure 6.3** Measured versus predicted dilation with outliers A3 and B2.



**Figure 6.4** Comparing measured and predicted dilation values with acceptance criteria.

measured dilation of 0.0071% and a model-predicted dilation of 0.1068%. In addition, three sources that are considered nondurable (B3, B6 and C7, with measured dilations of 0.0849%, 0.0835% and 0.0809%, respectively) were identified as being marginally durable with model-predicted dilation values of 0.055%, 0.0597% and 0.057%, respectively, just below the INDOT 0.060% acceptance criterion. The model appears to lose some sensitivity in predicting the performance of

sources in the mid-range values that marginally failed with measured dilations at or below 0.085%. Although this model accurately predicts durability for most sources additional testing using ITM210 is recommended to determine the freeze-thaw durability of that source if the HFT results predict dilations between 0.050% and 0.060%.

The general linear model was considered for regression analysis using DF as a response variable. The

model which best fit the available data and is recommended for use is presented in Equation 6.5.

Equation 6.5:

$$DF = 78.13 - 0.92 * P34 - 33.1 * P38 + 654.7 * P14 - 613.96 * P4 + 13.95 * P0 \quad (6.5)$$

Model statistics:

$$R^2 = 0.875$$

$$R^2 \text{ (adj.)} = 0.812$$

$$SEE = 7.66$$

$$n = 16$$

$$\text{Model P-value} < 0.0003$$

Table 6.4 and Figure 6.5 show measured versus predicted durability factor using the recommended model (Equation 6.5). It is apparent that there is a very good correlation between the measured and predicted durability factor with  $R^2=0.875$ , Adjusted  $R^2=0.812$  and  $n=16$ , Model P-value  $<0.0003$  ( $<0.05$  hence highly significant). It is recommended that INDOT HFT results be modeled using Equation 6.5 to predict the DF of ITM 210 freeze-thaw specimens at 350 cycles. Details on the development of this model (also referred to as model I5) are given in Appendix E, Section E.2.4.

As in discussed in section 5.2.2, a measured DF of 86 correctly delineated durable and nondurable aggregate for the 18 sources tested. Using this criterion, the model represented by Equation 6.5 accurately identifies all nondurable sources but two durable sources, A3 and C6 were incorrectly identified (i.e., measured DF of 98.5 and 94.1 and a model-predicted DF of 70.8 and 85.4 respectively). Although this model accurately predicts durability for most sources additional testing using ITM210 is recommended as an option if the HFT results predict failure.

TABLE 6.4  
Measured and predicted DF by Equation 6.5

Source	Measured DF	Predicted DF	Pass/fail ITM210
A1	96.6	88.9	Pass
A2	98.2	100.4	Pass
A3	98.5	70.8	Pass
A4	99.0	96.0	Pass
A5	96.2	91.5	Pass
A6	94.3	95.8	Pass
B1	69.3	64.8	Fail
B2	36.2	63.4	Fail
B3	75.9	82.3	Fail
B4	61.9	63.1	Fail
B5	36.4	45.4	Fail
B6	74.8	85.1	Fail
C1	85.9	85.3	Fail
C3	60.8	50.2	Fail
C4	77.3	80.0	Fail
C5	96.3	96.4	Pass
C6	94.1	85.4	Pass
C7	78.3	84.8	Fail

### 6.3 Summary of Model Development

The purpose of the statistical analyses was to develop linear regression models to predict average percent dilation and durability factor of ITM210 freeze-thaw test results using variables obtained from HFT results. Separate predictive models were developed from test data from each chamber, for predicting both percent dilation and durability factor (as shown in Table 6.5). The dilation models provided higher  $R^2$  values as opposed to durability factor models for both HFT chamber results. Based on the discussions presented in this chapter and based on the model statistics, the

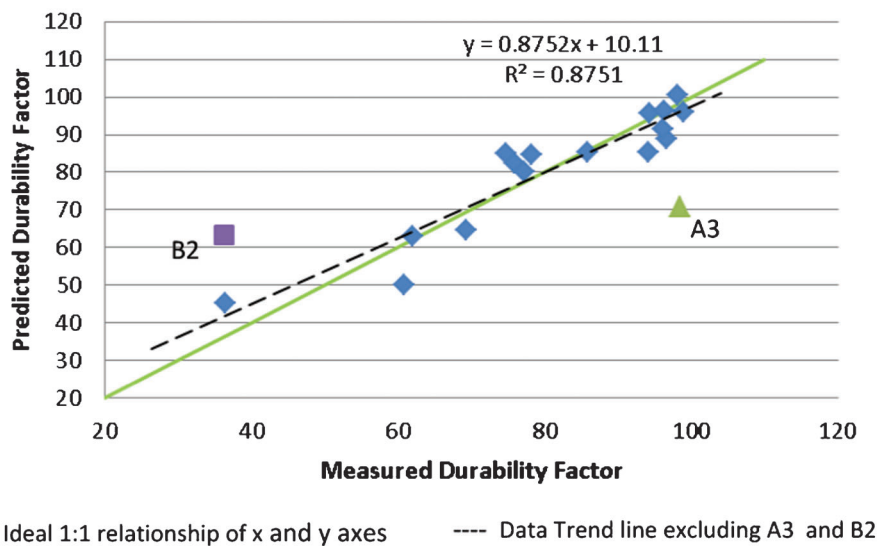


Figure 6.5 Predicted DF using Equation 6.5 versus measured values.

TABLE 6.5  
Summary of regression analysis models

HFT chamber	Model	Equation	R <sup>2</sup>	Adj.R <sup>2</sup>	SEE	n	Eqn.
MnDOT	% Dilation	% Dilation=2.49E-01+9.42E-03*P34+3.80E-02*P58+3.74E-02*P12-5.36E-01*P14+2.17E+00*P4-1.56E-01*P0	0.836	0.714	0.0347	15	Eqn. 6.2
	DF	DF=54.12-1.34E+00*P34-3.25E+00*P58-4.08E+00*P12+1.02E+01*P38-3.04E+02*P516+3.40E+02*P14-2.50E+01*P4-3.90E+01*P0	0.190	0.530	25.04	18	Eqn. 6.3
INDOT	% Dilation	% Dilation=8.25E-2+6.33E-3*P34+9.64E-2*P38-3.12*P14+4.3*P4	0.892	0.853	0.029	16	Eqn. 6.4
	DF	DF=78.13-0.92*P34-33.1*P38+654.7*P14-613.96*P4+13.95*P0	0.875	0.812	7.660	16	Eqn. 6.5

dilation model and DF model developed for INDOT HFT chamber are recommended for further development and use. From the models developed for MnDOT chamber the dilation model only is recommended for further development and use.

## 7. SUMMARY AND DISCUSSIONS

The main objective of this study was to develop a reliable, quick test method for determining the freeze-thaw resistance of carbonate quarried aggregates in Indiana using Hydraulic Fracture Test (HFT) equipment and procedures. Initially existing equipment from MnDOT were used for testing. After extensive modifications to existing INDOT equipment, an INDOT HFT chamber was developed for use. The testing procedures were modified and the analysis procedures refined.

Aggregate samples were identified and collected from 18 quarried carbonate sources from across Indiana that represented a range of freeze-thaw performance: durable (designated as Group A), nondurable (designated as Group B) and of variable or unknown performance (designated as Group C). Representative aggregates from each source were tested for specific gravity and absorption capacity using standard AASHTO procedures, and subjected to HFT testing using both the MnDOT chamber and refined INDOT HFT chamber. In addition, concrete beams prepared from each aggregate source were tested in accordance with ITM 210-Class AP Coarse Aggregate for freeze-thaw resistance. Regression analyses were performed to develop models that used HFT results to predict ITM 210 performance.

The aggregate sources tested represented a range of specific gravity values (2.48 to 2.75) and absorption capacity values (0.87% to 5.20%). As expected, there was a general trend between increased absorption with decreased specific gravity. However, there was no correlation between the ITM 210 FT results and these aggregate characteristics. Aggregates with both the highest and lowest absorptions and specific gravities

tested as freeze-thaw durable, and the mid-range values tested as both durable and nondurable, with no distinct trend detected.

Based on the ITM 210 freeze-thaw test results and INDOT's acceptance criteria of less than 0.060% expansion, all Group A aggregate sources tested as durable while all Group B sources tested as nondurable (as expected). Four of the six aggregate sources in Group C tested as nondurable and two tested as durable (C5 and C6). The aggregate sources tested in this study represented a wide range of freeze-thaw performance, with dilations ranging from 0.003% to 0.270%.

There was a strong correlation between percent dilation and the freeze-thaw durability factor (R<sup>2</sup> value of 0.91). Based on test data from these 18 aggregate sources, a DF of 80 or above for acceptance would properly identify all sources that failed INDOT's freeze-thaw dilation criterion except for one failing source that had a DF of 85.9. An acceptance criterion of DF greater than 86 would properly identify all aggregates that were tested in this study as durable and nondurable according to the INDOT dilation criterion. See Table 7.1 for a summary of ITM210 results. Statistical analyses were performed on the data generated in this study to develop linear regression models to predict average percent dilation and durability factor of ITM210 concrete beam freeze-thaw test results using variables derived from HFT results.

Models developed in previous studies using data from the MnDOT HFT chamber were reviewed (Embacher & Snyder, 2003; Hietpas, 1998), but those models did not fit this project's data very well, most likely because the aggregate size fractions tested and freeze-thaw test procedures used were different. The percent dilation model developed using the MnDOT HFT results and ITM 210 showed a good correlation with an R<sup>2</sup> value of 0.836 and adjusted R<sup>2</sup> value of 0.71, but the DF models exhibited poor fit with the data (R<sup>2</sup> value of 0.19 and adjusted R<sup>2</sup> value was even lower).

The model presented as Equation 6.4 that was developed using the INDOT HFT results provided a

TABLE 7.1  
Summary of measured versus predicted values (INDOT HFT)

Source	Measured dilation, %	Predicted dilation, %	Measured DF	Predicted DF
A1	0.0035	0.0304	96.6	88.9
A2	0.0028	-0.0048	98.2	100.4
A3	0.0071	<b>0.1068</b>	98.5	<b>70.8</b>
A4	0.0115	0.0107	99.0	96.0
A5	0.0047	0.0437	96.2	91.5
A6	0.0198	0.0185	94.3	95.8
B1	0.1631	0.1756	69.3	64.8
B2	0.2700	0.1677	36.2	63.4
B3	0.0849	<b>0.0551</b>	75.9	82.3
B4	0.1794	0.1360	61.9	63.1
B5	0.2435	0.2242	36.4	45.4
B6	0.0835	<b>0.0597</b>	74.8	85.1
C1	0.1440	0.1450	85.9	85.3
C3	0.1458	0.1887	60.8	50.2
C4	0.0922	0.0950	77.3	80.0
C5	0.0044	0.0015	96.3	96.4
C6	0.0232	0.0508	94.1	<b>85.4</b>
C7	0.0809	<b>0.0569</b>	78.3	84.8

Note: **Boldface values** indicate an inaccurate durability prediction if acceptance criteria of 0.060% percent dilation and DF greater than 86 is assumed.

good correlation between the measured dilation and predicted dilation, with  $R^2=0.892$  and adjusted  $R^2$  value of 0.853. This model predicts the freeze-thaw durability of 14 out of 18 sources correctly. Even though test results from source B2 were not included in the model development, the model correctly predicted this source as being nondurable. One of the four sources incorrectly identified by this model was freeze-thaw-durable source A3, which had a measured dilation of 0.0071% and a model-predicted dilation of 0.1068%. In addition, three sources that are considered nondurable (B3, B6 and C7, with measured dilations of 0.0849%, 0.0835% and 0.0809%, respectively) were identified as being marginally durable with model-predicted dilation values of 0.055%, 0.0597% and 0.057%, respectively, just below the INDOT 0.060% acceptance criterion. The model appears to lose some sensitivity in predicting the performance of sources in the mid-range values that marginally failed with measured dilations at or below 0.085%. All measured and predicted values are shown in Table 7.1.

The DF model presented as Equation 6.5 that was developed using INDOT HFT results and ITM 210 had a good correlation between the measured and predicted durability factor with  $R^2=0.875$ , adjusted  $R^2=0.812$ . The number of accurate durability predictions depends on what DF value is used as an acceptance criterion. If DF greater than 86 is considered durable, then two durable sources were predicted to fail using this equation (A3 and C6 at predicted DF=70.8 and 85.4 respectively), and all nondurable sources were predicted accurately.

## 8. CONCLUSIONS AND RECOMMENDATIONS

The objectives of this project were met. The 18 aggregate sources identified and tested were a good

representation of both the geological and geographic distribution of carbonates quarried aggregates available to INDOT for concrete pavement construction. The variability in durability was also well represented, with eight sources that tested as freeze-thaw durable and 10 sources that tested as nondurable. There were some gaps in the range of dilations measured with all durable sources tested having dilations less than 0.024%; and all nondurable sources having dilations between 0.081% and 0.270%. There were no aggregates that tested as marginally durable (i.e., between 0.05% and 0.07% dilation) and overall, no test results between 0.024% and 0.081%.

All eight durable aggregate sources tested in this study had  $DF>90$  and all but one of the ten nondurable aggregates had  $DF<80$ . One source (C1) failed with dilation =0.144% but had a  $DF=85.9\%$ . Based on this data, it is difficult to propose a reliable DF to use as an acceptance criterion. Until additional sources are tested especially on sources that have dilations between 0.030% and 0.080%, it is recommended that both dilation and DF be measured. A possible interim criteria could be that a  $DF\geq 90$  be considered durable and  $DF<80$  be considered nondurable but DF between 80 and 90 should rely on the dilation measurements for acceptance, until a larger database of sources are tested and these criteria refined.

Considering other aggregate characteristics, aggregates with a fairly wide range of specific gravities and percent absorptions were tested. However results from these simple aggregate tests did not provide any indication as to its freeze-thaw performance.

The models previously developed to analyze the MnDOT HFT equipment test results were not appropriate for this study. They did not accurately predict the FT test results. This is not surprising

considering that different initial aggregate sizes were used and a different FT testing procedure was used than in previous studies.

Of the 18 aggregate sources tested, both the MnDOT and INDOT HFT equipment gave good test results in 8 days. Because of the smaller size of the MnDOT chamber, three replicates needed to be tested from one source in order to test a sufficiently large sample to be considered representative of the source material. Because of its larger size, the modified INDOT HFT equipment can accommodate an entire representative sample, eliminating the need for replicate samples and reducing the time and labor for testing an aggregate source. The dilation models developed using the modified INDOT HFT apparatus accurately predicted the freeze-thaw durability, as determined by the 90-day ITM 210 test, approximately 80% of the time. Based on these results, Equation 6.3 can be used with the INDOT HFT results to predict the ITM 210 dilation results of most carbonate quarried aggregate sources. To increase reliability, additional testing using ITM 210 is recommended if the predicted dilations are between 0.050% and 0.060% in order to more confidently determine the freeze-thaw durability of such sources. Using this process, all nondurable sources would have been properly identified and only one durable source (A3) would have been improperly identified as nondurable.

The one durable aggregate source (A3) that repeatedly failed to fit the predictive models was different geologically than the other sources, being the only source identified geologically as a Silurian Reefal formation. Additional petrographic work is needed to identify the rock characteristics that may have contributed to its singular response to the HFT test.

The DF predictive models developed under this study (Equation 6.4) showed reasonably good correlation with measured DF. However, until additional testing is completed from which a reliable acceptance criterion for DF is developed, it is recommended that the DF model be used for research and development only. After additional testing is completed, especially of marginally acceptable sources, and a suitable DF criterion is established, this DF model should be reevaluated and possibly be refined or redeveloped.

The INDOT HFT equipment can be used to test carbonate quarried aggregates in Indiana for freeze-thaw durability. At this time it is recommended that the HFT be used for research and as a screening tool. Additional sources should be tested in both the HFT and ITM 210, and the test results used to check and, if necessary, refine the predictive model.

The tentative acceptance criteria recommended at this time are:

- If the dilation is predicted to be less than 0.050% then the aggregate is expected to be durable.
- If the dilation is predicted to be greater than 0.060%, then the aggregate is probably nondurable. Actual freeze-thaw durability testing can be performed to confirm.

- If predicted dilations are between 0.050% and 0.060%, or if the aggregate is mined from a Reefal formation, then ITM210 testing is necessary to determine acceptance.

Using the above criteria the freeze-thaw durability of all 18 sources tested in this study would have been correctly identified. These criteria would have correctly identified the durability of 14 sources using the 8-day HFT and would have indicated that the ITM 210 test was required for proper identification of the four remaining sources. The number of 90-day ITM210 tests needed and the time needed to determine aggregate source acceptability would be greatly reduced.

## 9. IMPLEMENTATION STRATEGIES AND RECOMMENDATIONS FOR FUTURE RESEARCH

### 9.1 Implementation Strategies

As discussed in Chapter 8, the percent dilation model developed using INDOT HFT and ITM 210 results (presented in Equation 6.3) is recommended to predict the ITM 210 freeze-thaw behavior of carbonate aggregates quarried in Indiana in eight working days. However, this model appears to lose some sensitivity in predicting the freeze-thaw performance of sources in the mid-range values. Three sources failed with measured dilations at or below 0.085% but the model predicted them to be marginally passing with dilations between 0.050% and 0.060%. Plus two sources were not included in the model development process because their predicted versus measured values fell far off the trend line and were statistically identified as outliers.

At this time the following is recommended as part of the implementation strategies:

- The INDOT HFT equipment and procedures outlined in this report be used for any HFT testing.
- Aggregate sources continue to be tested in ITM 210 for acceptance and companion samples be tested in the HFT.
- The HFT be used as a screening tool using the INDOT equipment using the following tentative acceptance criteria:
  - If the dilation is predicted to be less than 0.050% then the aggregate is expected to be durable.
  - If the dilation is predicted to be greater than 0.060%, then the aggregate is probably nondurable. Actual freeze-thaw durability testing can be performed to confirm.
  - If predicted dilations are between 0.050% and 0.060%, or if the aggregate is mined from a Reefal formation, then aggregate ITM210 testing is necessary to determine acceptance.
- HFT testing of additional aggregate sources that have ITM 210 test results between 0.03% and 0.08% dilation are important to further refine and validate the models
- With continued HFT and ITM 210 testing of additional aggregate sources, the model(s) may be refined such that the HFT with the INDOT chamber may eventually replace some, if not all of the long and expensive ITM 210 test.

## 9.2 Recommendations for Future Research

The following are recommended for future study:

- Investigate the effect the sieving process has on the overall mass loss measurement, especially for softer, weaker aggregate with the intention of possibly eliminating the need for sieving every 10 cycles.
- Examine the microstructure of the aggregates to determine if there are unique characteristics that the outlier aggregate sources possess that explain why they behave differently in the HFT. This may lead to refinement of the HFT procedures, or a prescreening of aggregate type that increases the accuracy and reliability of the HFT.
- Test non-INDOT aggregate sources to further validate or refine the model to give the HFT wider applicability and acceptance as a standardized test procedure.
- Examine the characteristics of chert particles to help explain why chert particles that fail in freezing and thawing do not fail in HFT.
- The INDOT chamber is capable of higher release rates than used in this study. Examine whether a more optimum combination of release rate and number of cycles needed may further reduce the test duration and/or increase accuracy.

## REFERENCES

- Alford, T. E., & Janssen, D. J. (1995). Calibrating Washington hydraulic fracture apparatus. *Transportation Research Record*, 1486, 142–148.
- Barksdale, R. D. (1991). *Aggregate Handbook*. Washington, DC: National Stone Association.
- Embacher, R. A., & Snyder, M. B. (2003). Refinement and validation of the hydraulic fracture test. *Transportation Research Record*, 1837, 80–88.
- Hietpas, J. J. (1998). *Refinement and validation of the Washington hydraulic fracture test* (Master's thesis). Minneapolis, MN: University of Minnesota.
- Indiana Geological Survey. (n.d.). Bedrock Geology of Indiana. Retrieved May 5, 2014, from <http://igs.indiana.edu/Bedrock/>.
- INDOT. (n.d.). INDOT—Approved Materials List. Retrieved May 5, 2014, from <http://www.in.gov/indot/div/mt/appmat/appmat.htm>.
- Issa, M., & Bendok, M. (2000). Modified Washington hydraulic fracture test to determine D-cracking susceptible aggregate. *Cement Concrete Aggregates*, 22(2), 116–127.
- Janssen, D. J., & Snyder, M. B. (1994). Resistance of Concrete to Freezing and Thawing (Strategic Highway Research Program Publication No. SHRP-C-391). Washington, D.C.: National Research Council.
- Hasenmueller, N. R., & Hasenmueller, W. A. (n.d.). Bedrock Geology of Marion County. Retrieved May 5, 2014, from <http://igs.indiana.edu/MarionCounty/BedrockGeology.cfm>.
- Neville, A. M. (2012). *Properties of concrete* (5th ed.). Upper Saddle River, NJ: Prentice Hall.
- NYDOT. (n.d.). *Hydraulic-fracture test apparatus and procedure for then determination of aggregate durability* (Research Project R225-01-881 Final Report). New York Department of Transportation unpublished report.
- Powers, T. C. (1975). *Freezing effects in concrete*. ACI Special Publication SP-46, pp. 1–11. Detroit, MI: American Concrete Institute.
- Rettner, D. L., & Embacher, R. A. (2009). *Implementation of hydraulic fracture test*. St. Paul, MN: Minnesota Department of Transportation.
- Schuster, R. L. (1957). *A review of research on deleterious substances in concrete aggregates* (Joint Transportation Research Program Publication No. FHWA/IN/JHRP-57/37). West Lafayette, IN: Purdue University. <http://dx.doi.org/10.5703/1288284313540>.
- Shaffer, A., & Wenning, N. (2009). *Carbonate rocks for concrete aggregate: Mineralogical and geophysical approaches*. Unpublished report prepared for the Indiana Department of Transportation.
- Smith, N. M., Brookley, A. C., Jr., & McGregor, D. J. (1954). *Common rocks, minerals, and fossils found in Indiana*. Geological Survey, Circular No. 3. Bloomington, IN: Indiana Department of Conservation.
- Snyder, M. (2005). *Implementation of the hydraulic fracture test at MnDOT*. St. Paul, MN: Minnesota Department of Transportation.
- Snyder, M. B. (2009). *Recycling concrete pavements*. Engineering Bulletin 043P. Skokie, IL: American Concrete Pavement Association.
- Snyder, M. B., Janssen, D. J., Hansen, W., Hietpas, J., Alford, T., & Holt, E. (1996). *Adoption of a rapid test for determining aggregate durability in Portland cement concrete* (Report No. RC 1345). Lansing, MI: Michigan Department of Transportation.
- Stark, D. (1976). Characteristics and utilization of coarse aggregates associated with D-cracking. Washington, D.C.: Transportation Research Board.
- Stark, P., & Klieger, D. (1973). Effects of maximum size of coarse aggregate on D-cracking in concrete pavements. *Highway Research Record*, 441, 33–43.
- U.S. Geological Survey. (2009). *USGS minerals information: Indiana*. Retrieved May 5, 2014, from <http://minerals.usgs.gov/minerals/pubs/state/in.html>.
- United States Department of Transportation. (1998). *Interlaboratory evaluation of AASHTO TP12 hydraulic fracture of concrete aggregates*. Washington, DC: Federal Highway Administration.
- Verian, K. P., Whiting, N. M., Olek, J., Jain, J., & Snyder, M. B. (2013). *Using recycled concrete as aggregate in concrete pavements to reduce materials cost* (Joint Transportation Research Program Publication No. FHWA/IN/JTRP-2013/18). West Lafayette, IN: Purdue University. <http://dx.doi.org/10.5703/1288284315220>.
- Zubery, M. H., Hossain, M., & Clowers, K. C. (1997). Kansas experience with Strategic Highway Research Program Washington Hydraulic. *Transportation Research Record*, 1577, 45–52.

## APPENDICES

### APPENDIX A: LITERATURE REVIEW

#### A.1 HISTORY OF HYDRAULIC FRACTURE TEST (HFT)

ASTM C666, *Standard Test Method for Resistance of Concrete to Rapid Freezing and Thawing*, is the most widely accepted method of assessing freeze-thaw (freeze-thaw) durability of aggregates intended for use in Portland Cement Concrete. This test procedure is time taking (sometimes takes up to six months from sampling to completion) and requires the use of expensive test equipment and skilled operators. The Hydraulic Fracture Test was developed in 1994 under the Strategic Highway Research Program (SHRP) by Dr. Donald J. Janssen and Dr. Mark B. Snyder in an effort to replace ASTM C666 with a more rapid test. The HFT was relatively inexpensive and capable of identifying the freeze-thaw durability of several aggregate samples in seven days (Stark, 1976). This test has been standardized as AASHTO TP12-93, Method for Determining the Hydraulic Fracture of Coarse Aggregate (Janssen & Snyder, 1994).

The HFT simulates the hydraulic pressure exerted in critically saturated aggregate particles in concrete due to freezing and thawing cycles by forcing water into and out of the pore structure of oven dried aggregate particles in a water-filled HFT chamber. The water is forced into the aggregate pores using a pressurized nitrogen gas. Then the pressure is rapidly released to allow compressed air trapped within the aggregate pores to expand, expel water from the aggregate pores creating hydraulic pressure. Aggregate particles fracture when their pore structure does not allow rapid dissipation of the pore pressures and/or the aggregate particles are weak. The amount of fracturing that result from this test is used to indicate freeze-thaw durability of aggregates (Stark, 1976).

Several studies have been performed by several agencies to validate and refine test procedure and/or equipment. This chapter describes the most significant findings and recommendations of these studies. Section 2.2 describes the original SHRP study. Studies done by several states based on the original SHRP study are discussed in Section 2.3. Recent developments in HFT are discussed in section 2.4.

#### A.2 ORIGINAL SHRP STUDY (JANSSEN & SNYDER, 1994)

The main goal of the original study was to use HFT as a rapid and reliable test method for identifying freeze-thaw durability of aggregates. In this study, 13 aggregate sources were selected from five different states. Seven of these aggregates were reported as freeze-thaw susceptible by the agencies that provided them while six of the aggregates were reported as non-susceptible to freezing and thawing. The freeze-thaw durability of the aggregates was determined from their field performance histories.

Before testing, each aggregate sample was separated by sieving into two size ranges: 1/2 to 3/4 in. (12.5 to 19.0 mm) and 3/4 to 1.25 in. (19.0 to 31.5 mm). Each aggregate was then washed, oven dried and treated with Silane solution and again oven dried before placing them in HFT chamber. The HFT chamber utilized in this study can hold a sample size of approximately 7.0 lb (3200 g) which is about 450 pieces in the 1/2 to 3/4 in. (12.5 to 19 mm) range and 150–225 pieces in the 19.0 to 31.5 mm (3/4 to 1 1/4 in.) range. To ensure that there are no pre-existing fractures in the aggregates prior to testing, each sample was initially tumbled in a rock tumbler for one minute and then all pieces passing the 3/8 in. (9.5 mm) are removed. The initial weight and number of particles of the sample were recorded and then placed in HFT chamber for testing. Then the chamber was bolted, flooded with water and pressurized with compressed nitrogen. The pressure then is rapidly released. This cycle of pressurizing and decompressing is repeated for a total of 23 minutes over 10 cycles.

At the end of the 10 cycles, the HFT chamber pressure is rapidly released, water drained and aggregate samples removed and oven dried. The following day, the oven dried sample was tumbled in a rock tumbler for one minute and then separated using 3/8 in. (9.5 mm) and No. 4 sieves. All aggregate particles retained on both sieves were weighed and counted. The material retained on the 3/8 in. (9.5 mm) sieve is subjected to an additional 10 pressurization cycles. The pressurization and depressurization was repeated for a total of 50 cycles for each aggregate sample.

Analysis of HFT results included calculation of three parameters namely percent fracture (PF), Hydraulic Fracture Index (HFI) and percent mass loss (ML). These parameters were calculated from the number of aggregate particles tested, number of aggregate particles retained on the 3/8 in. (9.5 mm) sieve and number of particles passing the 3/8 in. (9.5 mm) sieve but retained on the No. 4 (4.75 mm) sieve after each 10 pressurization cycles. Details of the HFT chamber, test procedures, and analysis of results and validation of the test are described in Stark (1976).

Analysis of the HFT result showed that all of the freeze-thaw susceptible aggregates, except one, had HFI values below 60 and all of the freeze-thaw durable aggregates, with the exception of one (which was inexplicable), had a HFI values above 100. If HFI were used to distinguish freeze-thaw durable aggregates from nondurable ones, 11 out of 13 aggregates tested were identified correctly. Further study showed that the amount of fracturing produced depended on the magnitude of the pressure used to pressurize the HFT chamber; an increase in pressure increased the percentage of fracture. Also, the percentage of fractures decreased as the size of the material tested is reduced. Inter-laboratory variability of HFI showed a “good” agreement between two of the three laboratories running the HFT test while the third laboratory provided consistently higher HFI values due to a pressure gauge calibration problem.

The results also showed that as the number of particles tested increased the coefficient of variation of HFI decreased. The study proposed that the minimum sample size should be in the range of 600–800 particles to bring the coefficient of variation below 10. This finding led to the development of a large HFT chamber as big as five times the volume of the original (small) HFT chamber. The study emphasized that the large HFT chamber should be calibrated to have a similar pressure release rate with original (small) HFT chamber to ensure similar amounts of aggregate fracture are produced.

#### A.3 STUDIES BASED ON ORIGINAL SHRP STUDY

##### A.3.1 Michigan Department of Transportation Study (Snyder et al., 1996)

There were two main purposes to this study; to determine whether the Michigan Department of Transportation (MDOT) could implement the HFT as acceptance testing to evaluate freeze-thaw susceptibility of aggregates and to further develop the HFT apparatus, test procedures and acceptance criteria that would make the HFT a more reliable test method.

Thirteen natural and manufactured aggregates with a range of freeze-thaw performances were selected for the study. Freeze-thaw testing was performed on all of the aggregate samples collected according to MDOT test procedure which is a variation of ASTM C666 Procedure B. HFT was performed on nine of these sources to correlate the data with the freeze-thaw testing. The HFT tests were performed using different chamber pressures, chamber sizes, pressure release systems, actuator pressures and with/without chamber linings.

The analysis of the results led to modification of the large HFT equipment which included increasing the pressure release valve diameter to achieve a higher release rate. However, the pressure release rate achieved by the small HFT chamber could not be reproduced due to turbulence in the pressure release valve. Also the small HFT chamber plug pressure release valve system was replaced by an electro pneumatically operated ball valve. Another modification to the small HFT chamber was lining the inside of

chamber with a thin neoprene pad to minimize the friction between the aggregate and the steel chamber which led to mechanical crushing of the aggregate not induced by the Hydraulic Fracture mechanism.

The main change in the analysis procedure was in the calculation of Hydraulic Fracture Index (HFI), the number of HFT cycles necessary to produce 10% fracturing. The decrease in percent fracture due to chamber lining with neoprene pad led to modification of HFI to represent the number of cycles necessary to produce 5% fracturing.

The research indicated that it was not possible to correlate HFI with dilation and durability factor results due to the fact that freeze-thaw durable aggregates produced a HFI of anything greater than 100. Also the open ended nature of the HFI equation could give an undefined or very large value for aggregates with zero or a small percent fracture. In addition to this the HFT was unable to fracture chert particles, which are strongly associated with the freezing and thawing problem.

Despite the refinements to the HFT chamber and analysis procedure, the study concluded that the HFT in its current form is not a reliable and consistent method to predict the results of freeze-thaw durability testing according to MDOT test procedures (MTM115).

### **A.3.2 Kansas State University Study (Zubery et al., 1997)**

The objective of this study was to assess the freeze-thaw durability of Kansas aggregates using the HFT procedure and comparing the results with ASTM C666 test results.

Aggregate samples from 32 different sources were tested in the study. A correlation study was performed for durability factor, percentage expansion, freeze-thaw soundness value, pavement vulnerability factor, percentage acid insoluble, percentage absorption, percentage fracture, percentage mass loss, and Hydraulic Fracture Index (HFI). Four types of relationships (linear, exponential, logarithmic, and power) were investigated.

The study concluded that the HFT results are found to be poorly correlated with ASTM C666 test results. However, the HFT results are "correlated significantly" with the results of the KDOT-modified freeze-thaw tests on unconfined aggregates. The study further concluded that the HFT test method, in its current form, does not appear to be a feasible choice to replace the existing ASTM C666 test procedure.

### **A.3.3 Interlaboratory Evaluation of AASHTO TP12 Hydraulic Fracture of Concrete Aggregates (UDOT, 1998)**

The main purpose of this study was to determine within-lab and between-lab evaluation of the precision of the HFT. Ten testing labs participated in the testing of four aggregate sources selected for the study. Nine of the labs used the small HFT chamber and the tenth lab used the larger version of HFT chamber. For each aggregate source, five replicate samples were tested at each testing lab. HFT and ASTM C666 tests were conducted on the aggregates selected by the participating labs. However, no attempt was made to fully standardized the freeze-thaw test because each testing lab has different sample conditioning and test variables.

Despite these differences the study attempted to correlate HFT values, Hydraulic Fracture Index (HFI) and total mass loss, with durability factor (DF) of the freeze-thaw test. The data analysis showed that there was no linear relationship between HFT results and DF.

The statistical data analyses of the experimental results showed that there is a wide range of variability associated with HFT method. However, the majority of the coefficient of variation for percent mass loss in this study fell below 40% which is comparable with ASTM C666. The variance for HFI was not determined because for some sources it was not possible to determine the HFI.

The variance of the large chamber, which can accommodate slightly more than twice the number of particles than the small chamber, was less than the variance of most of the smaller chambers used for the study. The study recommended that AASHTO TP12 should not be used as an acceptance test or as an alternate test to AASHTO T161.

### **A.3.4 Modified WHFT to Determine D-Cracking Susceptible Aggregates (Issa & Bendok, 2000)**

The purpose of this study was to address the variability of test results between replicate samples associated with testing of small quantity of samples in the small HFT chamber. The study tried to address this issue by developing a larger HFT chamber (WHFT97) which would allow testing of a larger sample size. Unlike the original SHRP's HFT chamber the large chamber is fully automated in terms of utilized air to drive the water into aggregate voids instead of nitrogen.

Aggregate samples from twenty-one different sources with a range of freeze-thaw performance were tested using the small and WHFT97 chambers and ASTM C666. The analysis of the results showed that there was no direct correlation between HFT result and ASTM C666 results. However, the pass/fail criteria (percent fracture (2%) for WHFT97 and 0.06% percent expansion for ASTM C666) established the WHFT97 identified correctly 76% of the aggregates sources tested. The study concluded that the modified WHFT97 chamber has the potential to be used as a screening test prior to ASTM C666 test.

### **A.3.5 New York State Department of Transportation Study (NYDOT, n.d.)**

The purpose of the study was to develop a simplified HFT chamber and determine the relationship between HFT and magnesium-sulfate and freeze-thaw test to determine if the HFT can be used as a prescreening test for an aggregate. Comparison of the stress induced on aggregate particles in HFT and FT test were made analytically using Finite Element models. The numerical experiment showed that the HFT creates a stress state in the stone that is dissimilar to the stress state produced by the freeze-thaw test. The experimental tests also showed that the percent mass fracture (HFT result) was much smaller in the HFT than the freeze-thaw test and magnesium-sulfate test. The study was terminated due to the fact that numerical and experimental test results did not support the hypothesis of the study, "The HFT Machine must produce a similar stress state with comparable or greater magnitude to the stress induced in the freeze thaw test, if it is going to fracture a similar or greater mass of aggregate."

## **A.4 FURTHER DEVELOPMENT OF HYDRAULIC FRACTURE TEST**

### **A.4.1 University of Minnesota Study: Phase I (Hietpass, 1998)**

The main purpose of this study was to further refine and validate the HFT. In this study, a calibration procedure was developed to determine the combinations of chamber pressure and actuator pressure to ensure similar pressure release rate curves. After calibration is done seven aggregate sources with particle sizes in the 3/4 to 1.25 in. (19 to 32 mm) ranges were tested according to the procedure developed under the SHRP program except that several sieves were added to the screening operation.

The study completed by developing models to correlate the data obtained from the HFT to dilation data obtained using ASTM C666 (Procedure C). The cumulative percent masses retained on different sieves were used to predict the dilation per 100 cycles. The resulting model had a very high R<sup>2</sup> value of 0.95. Due to the small number of aggregate sources tested, it was necessary to further refine and validate the models. Results of the modified large HFT chamber suggested that the large chamber

has the potential to eliminate the replicate testing needed with the small chamber.

#### **A.4.2 University of Minnesota Study: Phase II (Embacher & Snyder, 2003)**

The study was conducted in two phases. The purpose of the first phase was to validate the modification of HFT procedure proposed in the Michigan Department of Transportation Study (Snyder et al., 1996). The main focus of this phase was to use additional sieves to better characterize the nature of the fracturing taking place during Hydraulic Fracture testing. Aggregate particle counts and masses retained on the various sieves were used to develop models to predict freeze-thaw dilation. Aggregate size fractions, 3/4 to 1.5 in. (19.0 to 37.5 mm), 1/2 to 3/4 in. (12.5 to 19.0 mm), and No. 4 to 1/2 in. (4.75 to 12.5 mm) were tested to determine the effects of rapid freezing and thawing on aggregate particle sizes less than 3/4 in. (19.0 mm).

Freeze-thaw testing was performed on concrete beams prepared from each of the twenty aggregate sources and dilation and durability factor values were determined. Regression models were developed to determine these values from the HFT results. The second phase of the study involved the development of large HFT chamber to accommodate larger samples of aggregate.

The results of regression analyses performed on the HFT data show strong correlations between HFT outputs and concrete test specimen dilation data obtained from rapid freezing and thawing tests.

#### **A.4.3 Minnesota Department of Transportation Study (Rettner & Embacher, 2009)**

The study was conducted to determine whether the large HFT chamber could replace the small HFT chamber to reduce the

number of replicate tests necessary due to the larger sample size and to utilize the same mathematical model developed under the earlier research projects.

A total of twelve quarried and gravel sources were selected to represent a broad range of aggregate freeze-thaw performance characteristics. Freeze-thaw beams were cast for each source for use in freeze thaw testing in accordance with ASTM C666 procedure A. The HFT was completed for all aggregate sources using both small and large chambers. The small chamber was pressurized to 1300 psi and the large chamber was pressurized to 1350 psi, with both chambers having 150 psi release pressure.

A review of the existing model for the small chamber showed that the model generated from the previous University of Minnesota study did not fit the data that was produced by this study very well. Combining the previous study's data with the new data reduced the coefficient of determination ( $R^2$ ) from 0.978 (U of M study) data to 0.2323. This reduction in the coefficient of determination could be due to the difference in the freeze-thaw testing procedure changing from ASTM C666 Procedure C (a modification of the standard test) to ASTM C666 Procedure A. A review of the new small chamber data alone resulted in a coefficient of determination of only 0.0132, meaning that there is essentially no relationship between the predicted and the measured dilation using ASTM C666 Procedure A.

A review of the data for the large chamber data generated from the original University of Minnesota study and this project shows that the combined data has a coefficient of determination of 0.0451, showing no relationship exists between the predicted dilation and the actual measured dilation suggesting that new mathematical model will need to be developed for the use of the large chamber. However, the study failed to develop a model because the number of aggregate sources tested was not large enough to develop a new model.

## APPENDIX B: HFT EQUIPMENT CALIBRATION AND STANDARD TEST PROCEDURES

### B.1 CALIBRATION OF THE HFT EQUIPMENT (ADOPTED FROM SNYDER, 2005)

**1.1.** The Hydraulic Fracture Test (HFT) apparatus must be operated in a manner that produces aggregate fracture rates that are consistent with those that were used in the development of the dilation prediction model. Previous research (Hietpas, 1998; Rettner & Embacher, 2009; Stark, 1976) has found that aggregate fracture rates useful in durability prediction can be obtained consistently by controlling the rate of release of pressure from the test chamber. Higher pressure release rates correspond with higher fracture rates. Therefore, the parameter used to calibrate the HFT apparatus is the maximum pressure release rate, computed over and plotted against various time intervals.

**1.2.** Generation of a maximum pressure release rate versus time interval graph or profile begins with measurement of chamber pressure versus time during the pressure release event. Pressure release rates can be monitored using an appropriate chamber-mounted pressure transducer with a dynamic signal analyzer.

**1.3.** Chamber pressure during the release event should be sampled at a rate of approximately 500 Hz (i.e., one pressure measurement every 0.002 seconds). The data are then used to compute the average pressure release rate (psi/sec) during each 0.002 second time interval and the highest rate is selected and recorded as the maximum pressure release rate over a 0.002 second time interval. This analysis process is repeated for successively larger time intervals (e.g., 0.004 seconds, 0.006 seconds, etc.), and the maximum pressure release rate for each time interval is plotted against the respective time intervals.

**1.4.** Figure B.1 presents the plot of maximum pressure release rate versus time interval that was used to calibrate the test apparatus used in developing the current dilation prediction model. Table B.1 summarizes the data used to create Figure B.1. Previous research (Hietpas, 1998; Rettner & Embacher, 2009; Stark, 1976) indicates that it is most important to match the target maximum pressure release rate profile at 0.01 seconds, although the overall maximum pressure release profile should closely resemble that of the target.

**1.5.** Release rates can be varied most easily by modifying the pressure used to operate the actuator that opens the pressure

release valve, with higher actuator pressure corresponding to faster release rates. Release rates can also be accomplished by modifying the test chamber plumbing (i.e., modifying pressure release port sizes, pipe and valve sizes, etc.) and/or chamber operating pressure (although pressures less than 1150 psi may not produce aggregate fractures, and pressures significantly higher than 1150 psi may produce too much aggregate fracture).

**1.6.** Maximum pressure release rate profiles for each actuator pressure setting (or chamber modification) can then be compared with the target curve (as shown in Figure B.2 and Figure B.3). The pressure settings and/or chamber configurations that produce the maximum release rate profile closest to the target profile should be selected for test operation as long as it does not significantly exceed the developed operating pressure of 1150 psi.

**1.7.** Repeatability of the chosen release rates is important and several release rate curves should be captured at the selected chamber and actuator pressures. The exact release rate profile may vary slightly, as shown Figure B.2.

### B.2 DRAFT STANDARD HFT TEST PROCEDURES

#### Class AP Coarse Aggregate Using Hydraulic Fracture Test ITM No. XXX-14

##### 1. Scope

**1.1.** This method sets forth standard testing procedures for classification of an aggregate as Class AP using the Hydraulic Fracture Test (HFT) equipment.

**1.2.** Aggregate is sieved to a specified gradation, the initial mass on each sieve size determined then recombined and placed in the HFT chamber. The chamber is flooded with water and pressurized. The pressure is held for a prescribed time then released quickly. The pressurization-release cycle is repeated for a total of 10 cycles. Aggregate is oven dried, sieved and mass loss on each sieve recorded. This process is repeated until a total of 50 cycles have been completed.

**1.3.** This ITM may involve hazardous materials, operations, and equipment and may not address all of the safety problems associated with the use of the test method. The user of the ITM is responsible for establishing appropriate safety and health practices and determining the applicability of regulatory limitations prior to use.

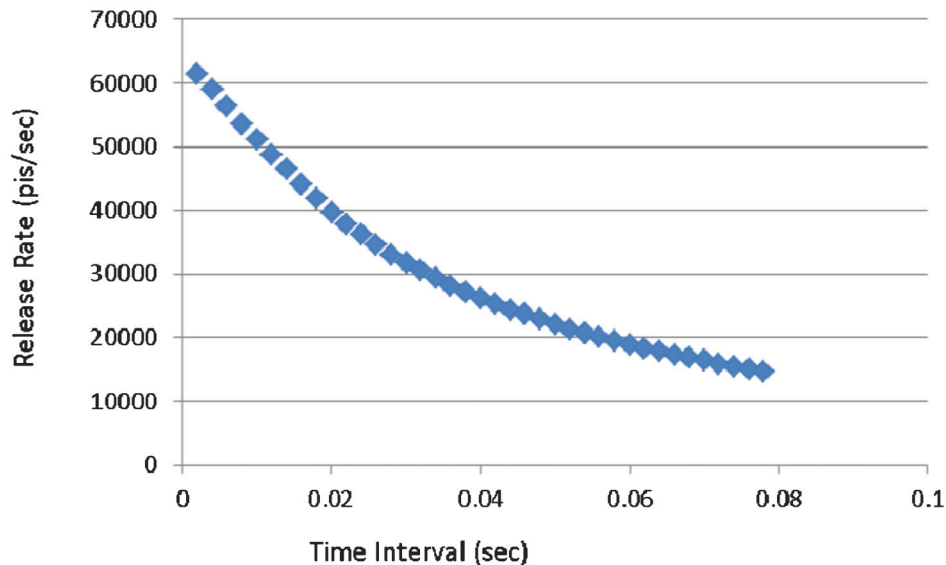


**Figure B.1** Target release rate calibration curve developed for original SHRP equipment (Snyder, 2005).

TABLE B.1  
Target release rate calibration data

Time interval (sec)	Max pressure release rate (psi/sec)	Time interval (sec)	Max pressure release rate (psi/sec)	Time interval (sec)	Max pressure release rate (psi/sec)
0.00203	61467	0.02804	33027	0.05402	20694
0.00402	58950	0.03004	31697	0.05601	20054
0.00602	56343	0.03203	30469	0.05805	19441
0.00801	53615	0.03402	29301	0.06003	18868
0.01004	51159	0.03601	28214	0.06203	18322
0.01203	48706	0.03804	27156	0.06403	17796
0.01402	46387	0.04004	26195	0.06601	17298
0.01602	44035	0.04203	25288	0.06805	16821
0.01801	41759	0.04402	24416	0.07004	16365
0.02004	39675	0.04602	23614	0.07203	15916
0.02203	37802	0.04805	22811	0.07403	15492
0.02402	36119	0.05004	22072	0.07602	15086
0.02601	34521	0.05203	21362	0.07801	14691

2. General Requirements (Taken from ITM210)

2.1. No testing of the aggregate will be made until the material is rated Class A aggregate; however, the material may be tested for class A and AP concurrently if so directed by the Department. Blending or combining of a ledge that does not meet quality or deleterious requirements will be permitted only by the approval of the Department.

2.2. The coarse aggregate Producer shall provide a written description of the production control in the Source Quality Control

Plan in accordance with ITM 211. This plan shall specify the ledges to be incorporated into the production for crushed stone, the relative production zone within the pit for gravel, general handling and crushing procedures used in the production, the final production gradation obtained, and any other pertinent information relative to the coarse aggregate production, such as stockpile signage. Any unauthorized change in the approved Quality Control Plan will be cause for the suspension of shipment of this material.

2.3. Tests will be conducted by the Office of Materials Management or a Department approved AASHTO Accredited

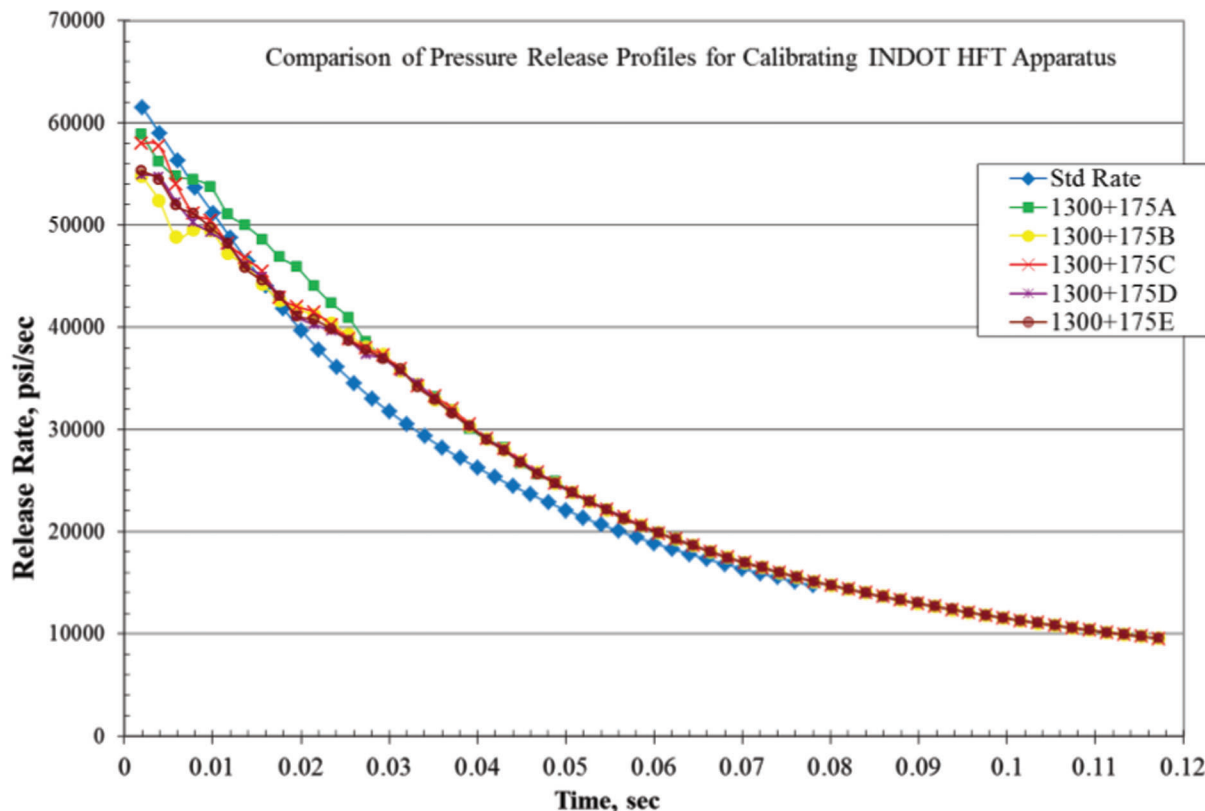
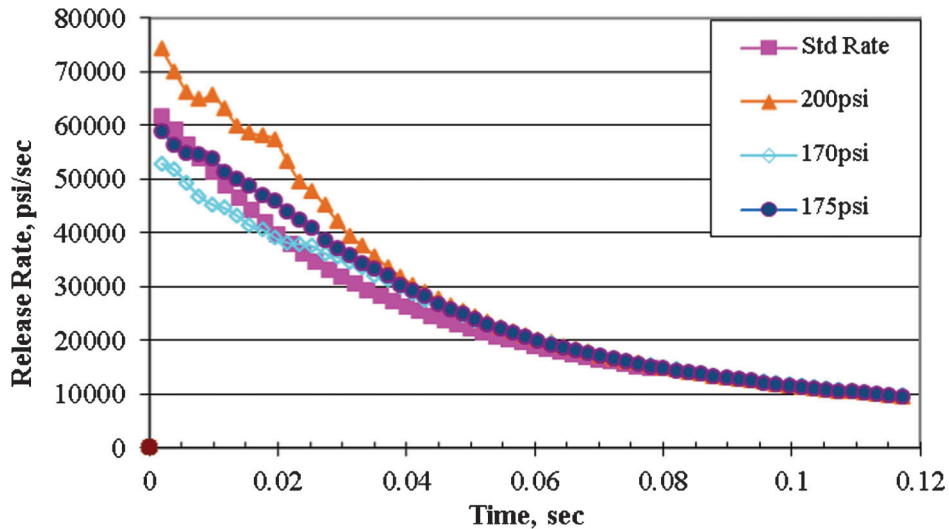


Figure B.2 Example of variability of pressure release rates with constant chamber and actuator pressure, INDOT chamber.



**Figure B.3** Pressure release profiles for chamber pressure of 1300 psi using three different pressure settings to trigger the release valve.

Laboratory until Department tests are available. Department tests results will control the re-sampling schedule.

### 3. References

#### 3.1. AASHTO Standards

- M 92 Wire Cloth and Sieves for Testing Purposes
- M 231 Weighing Devices Used in the Testing of Materials
- T 27 Sieve Analyses of Fine and Course Aggregate

#### 3.2. ASTM Standards

#### 3.3. ITM Standards

- 203 Control Procedures for Classification of Aggregates
- 207 Sampling Stockpiled Aggregates
- 210 Class AP Coarse Aggregate
- 211 Certified Aggregate Producer Program

### 4. Terminology

Definitions for terms and abbreviations shall be in accordance with the Department's Standard Specifications, Section 101.

### 5. Significance and Use

This ITM shall be used for preliminary classification of aggregates as Class AP for use as designated in the Standard Specifications only by the approval of the Department.

### 6. Apparatus

- Balance, G2, in accordance with AASHTO M 231
- Mechanical Sieve Shaker, in accordance with AASHTO T 27
- Oven, appropriate size capable of maintaining a uniform temperature of  $230 \pm 9^\circ\text{F}$
- Sieves, in accordance with AASHTO M 92
- Hydraulic Fracture Equipment
- Rock tumbler
- Pressurized nitrogen and other miscellaneous equipment such as hoses, gages, pans, etc.

### 7. Sampling

An approximate 100 lbs. coarse aggregate sample of the material to be tested will be obtained in accordance with ITM 207.

### 8. Preparation of Aggregate Test Specimen

**8.1. Sizing aggregate** Separate the sample into the required sieve sizes in accordance with AASHTO T 27. Recombine the quantity from each sieve size according to the gradation shown in Table B.2. Approximately 28 lb. (13 kg) of aggregate is required to fill the INDOT HFT chamber. (Note: This gradation is recommended for HFT results that are comparable to ITM 210. If results are to be compared to different freeze-thaw tests procedures then the gradation should match the proportions of the 1/2-in.-plus fractions of the coarse aggregate used to fabricate the FT concrete prisms.)

**8.2. Wash** Wash the test sample thoroughly until clear water runs from the aggregate. Dry the test sample to a constant mass in an oven at a temperature  $110 \pm 5^\circ\text{C}$  a minimum of 12 hours. Cool to room temperature.

**8.3. Silane coating** Submerge the test sample in a water-based penetrating silane solution for 60 seconds in a well-ventilated room. A double boiler pan, similar to that shown in Figure B.4 is suitable. (Note: Enviroseal® 40 silane penetrating sealer is an example of acceptable product.)

**8.4. Drain** Drain the aggregate sample. If using a double-boiler lift the inner perforated pot containing the aggregate to drain. The silane solution can be reused but should be stored in a sealed container between uses and not be reused if it begins to thicken.

**TABLE B.2**  
Aggregate gradation used for HFT test using INDOT's HFT chamber

Sieve size	Percentage passing	Quantity needed, lbs. (kg)
1 in. (25 mm)	100	0
3/4 in. (19 mm)	89	3.08 (1.43)
5/8 in. (16 mm)	40	13.72 (6.37)
1/2 in. (12.5 mm)	0	11.20 (5.20)



**Figure B.4** Double boiler used to soak aggregate sample.

**8.5. Dry** Dry the aggregate sample to a constant mass in an oven at a temperature  $110^{\circ} \pm 5^{\circ}\text{C}$  for a minimum of 12 hours and cool to room temperature.

**8.6. Tumble** Tumble the aggregate sample in a rock tumbler (similar to example shown in Figure B.5). Fill tumbler approximately half full and tumble for  $30 \pm 5$  revolutions of the tumbler. Remove aggregate from the tumbler. Repeat this process until the entire aggregate sample has been tumbled.

**8.7.** Sieve the aggregate sample over the 1/2 in. sieves and discard any piece passing the 1/2 in. sieve.

**8.8. Check final aggregate quantity** Place the mesh basket in the HFT chamber and place only enough aggregate to fill the chamber. Do not overfill as to avoid any aggregate particle fracturing due to closure of the chamber lid. Remove the aggregate from the test chamber. To remove the aggregate from the chamber, it can be scooped out or the basket containing the aggregate as a whole can be removed from the chamber as shown in Figure B.6.

**8.9. Final sieving** Sieve the aggregate sample over the 3/4 in., 5/8 in. and 1/2 in. sieves. Use a scale with the appropriate precision and record the mass retained on each sieve  $\pm 0.1$  gram. This is the initial mass of the specimen (mass at zero HFT cycles). The HFT sample is now ready for testing. The specimen must be handled with care not to lose any aggregate particles.



**Figure B.5** Example of a suitable rock tumbler.



**Figure B.6** Basket containing the aggregate as removed from the chamber.

## 9. HFT Testing Procedures (INDOT Chamber)

**9.1. Nitrogen tanks** Two pressurized nitrogen tanks are needed to run the test. The higher pressure tank should be a minimum of 1500 psi and the lower pressure tank should be a minimum of 175 psi. With Valve E closed (Figure B.7), open the tank valve to gage 1 on higher pressure cylinder attached to the HFT chamber to check the available pressure in that cylinder. If the pressure is less than or equal to 1500 psi close the gauge and replace the cylinder. Do the same for low pressure cylinder (2) used to trigger the actuator, and if the pressure valve 2 is 175 psi or lower then replace that cylinder.

**9.2. Close inlet valves** The water and pressure inlet valves should be closed.

**9.3. Place aggregate in chamber** Insure that the 200-mesh screen is in place in the bottom of the chamber. Place the basket in the chamber and place the prepared aggregate sample in the basket in the chamber. Cover the top of the chamber with the basket top (an open mesh) as shown in Figure B.8.

**9.4. Close chamber** Place the cover assembly on top of the pressure chamber and bolt them together with the 12 high strength bolts.

**9.5. Warm up the pressure release valve** Warm up the pressure release valve by turning the actuator switch on and off at least 20 times. This process should be repeated if the apparatus has not been used in the past 1 hour. End with the switch in the off position.

**9.6. Fill chamber with water** With drain Valve C closed, open Valve A and Valve B to fill the chamber with water, and open Valve D to the top drain line (see Figures B.7 and B.9). When the chamber is full excess water will drain out through the Valve D and top drain line. Allow water to continue to flow through the chamber and out the top drain line until clear water with no bubbles are visible flowing through the drain line. Note: before opening water inlet valves make sure that the ball valve is closed (the actuator switch is in off position) otherwise water will rise into the exhaust pipe once the chamber is filled.

**9.7. Close valves** Close the drain Valve D first then close valve A and Valve B after 20 seconds.

**9.8. Adjust pressure regulators** With the actuator switch in off position and Valve E closed, open the pressure tank valve on the high pressure cylinder and adjust the pressure regulator until Gage 1 reads 1300 psi. Open the tank valve on the low pressure cylinder and adjust pressure regulator until Gage 2 reads 175 psi (see Figure B.7). Note: If the calibration process indicates that the chamber or actuator pressure should be something other than

1300 psi or 175 psi respectively, then adjust the pressure regulator(s) to the proper setting at this time.

**9.9. Pressurize chamber** Pressurize the chamber by opening Valve E and leave it open for 5 minutes for the first cycle, and open for 2 minutes for each of the remaining nine cycles.

**9.10. Depressurizing chamber** After the pressurization is completed and the proper time has lapsed (5 minutes for the first cycle and 2 minutes for cycles 2–10) quickly close Valve E and switch the actuator on to open ball valve and depressurize the chamber. Then turn the actuator switch off. Note: Wearing proper hearing protection during the chamber depressurization is important.

**9.11. Repeat steps** Repeat steps 9.6 to 9.10 above for nine more cycles with the pressurization time at 2 minutes in step 9.9, for a total of 10 pressurization-depressurization cycles.

**9.12. Drain chamber** After completing ten cycles of pressurization, close both nitrogen tank valves then open Valve A and C. Water will drain out from the chamber at a slow rate. To drain the water completely, add a small amount of pressure to the chamber by slowly open Valve E. When the water is completely drained out of the chamber close Valve E.

**9.13. Remove sample from chamber** Remove the bolts and lid, place the chamber lid on the side table and remove the aggregate sample from the chamber and basket. Oven dry aggregate to a constant mass at a temperature  $110^{\circ} \pm 5^{\circ}\text{C}$  for at least 12 hours and cool to room temperature.

**9.14. Tumble the specimen** Tumble the specimen according to the procedure described in step 8.6.

**9.15. Sieve** Divide the specimen into equal parts so as not to overload the sieves, and sieve through 3/4 in., 5/8 in., 1/2 in., 3/8 in., 5/16 in., 1/4 in., and #4 sieves, catching the minus #4 material in the pan. Note: Dividing the sample into 4 equal parts is appropriate for 12 in. diameter sieves.

**9.16. Weigh aggregate** Measure the mass of the aggregate retained on each sieve and the pan using a scale with the precision of  $\pm 0.1$  gram. Record mass retained on each sieve to within a gram. Sample worksheet for recording test data is given in Figure B.10. Note: Continue to handle the specimen with care so as not to lose any aggregate particles.

**9.17. Repeat** Repeat the procedures 9.1 to 9.16 four more times until the specimen has been tested for a total of 50 cycles of pressurization and depressurization.

## 10. Calculations

**10.1** First calculate the percent change in mass retained (PCMR) for each sieve size as follows:

$$P34 = \left( \frac{M50 - M0}{M0} \right) 100$$

$$P38 = \left( \frac{M50 - M0}{MT} \right) 100$$

$$P14 = \left( \frac{M50 - M0}{MT} \right) 100$$

$$P4 = \left( \frac{M50 - M0}{MT} \right) 100$$

Where:

P34 refers to the PCMR for the 3/4 in. sieve

P38 refers to the PCMR for the 3/8 in. sieve

P14 refers to the PCMR for the 1/4 in. sieve

P4 refers to the PCMR for the #4 sieve

M50 is mass retained at 50 cycles for that particular sieve

M0 is initial mass retained at zero cycle on a particular sieve

MT is total initial mass at zero cycle

**10.2** Calculate the comparable dilation values using the P-values obtained in Section 10.1 and the following equation:

$$\begin{aligned} \% \text{ Dilation} = & 0.0825 + 0.00633(P34) \\ & + 0.0964(P38)3.12(P14) + 4.3(P4) \end{aligned}$$

## 11. Report

**11.1. Test report data will include the following items:**

- Coarse aggregate source identification
- Type of material
- Gradation of production material
- Ledges of aggregate, if applicable
- Date sampled
- Individual(s) obtaining sample
- Date of test completion

**11.2. A table of the calculated PMCR values**

**11.3. The calculated comparable dilation value**

## 12. Aggregate Acceptance or Rejection Criteria

**12.1. Aggregate acceptance criteria** Department acceptance criteria: The calculated comparable dilation value shall be less than 0.060 percent expansion. However, when the calculated dilation is less than 0.060 percent expansion and greater than 0.050 percent expansion then ITM 210 testing is required for acceptance.

- If calculated dilation is 0.060 percent or greater than the producer has the option of submitting the sample for ITM 210 testing. In all cases if companion samples are tested in both the ITM 210 and the HFT then results from the ITM 210 will prevail.

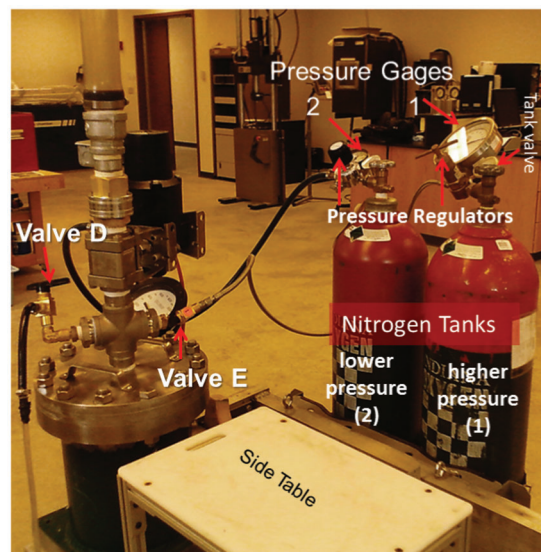


**Figure B.7** INDOT HFT equipment set up.

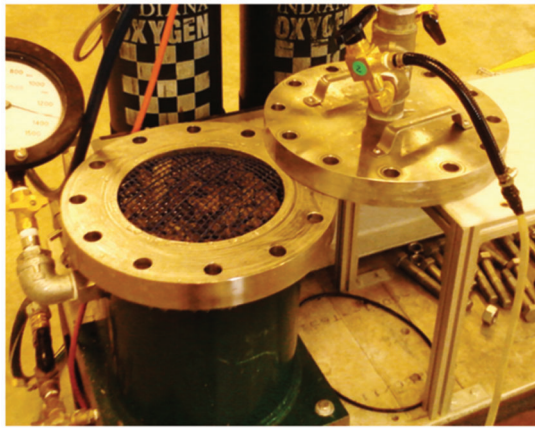


**Figure B.8** Aggregate specimen in HFT chamber with open mesh basket lid in place.

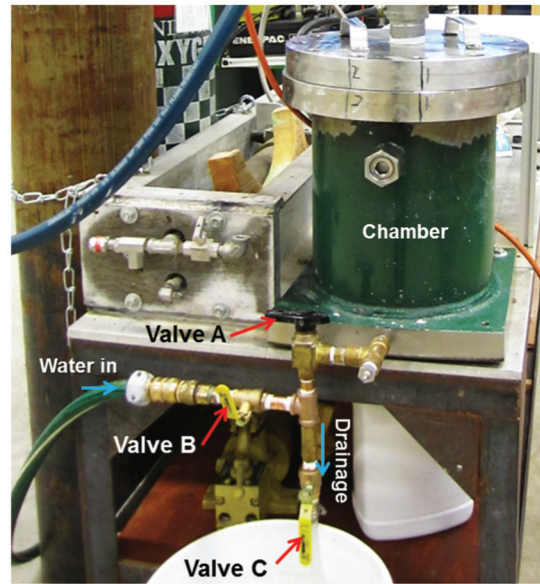


**Figure B.9** INDOT HFT chamber with water fill and drain valves A, B and C.

<b>Source:</b>					
<b>Date Received:</b>			<b>Date Testing Started:</b>		
<b>Initial Mass, Kg</b>			<b>Date Testing Completed:</b>		
<b>Initial Mass, Kg</b>	M3/4 (ret), kg		<b>30 cycles</b>	M3/4 (ret), kg	
	M5/8 (ret), kg			M5/8 (ret), kg	
	M1/2 (ret), kg			M1/2 (ret), kg	
	M3/8 (ret), kg			M3/8 (ret), kg	
	M5/16 (ret), kg			M5/16 (ret), kg	
	M1/4 (ret), kg			M1/4 (ret), kg	
	M#4 (ret), kg			M#4 (ret), kg	
	Mpan, kg			Mpan, kg	
	Mass Check:			Mass Check:	
<b>10 Cycles</b>	M3/4 (ret), kg		<b>40 cycles</b>	M3/4 (ret), kg	
	M5/8 (ret), kg			M5/8 (ret), kg	
	M1/2 (ret), kg			M1/2 (ret), kg	
	M3/8 (ret), kg			M3/8 (ret), kg	
	M5/16 (ret), kg			M5/16 (ret), kg	
	M1/4 (ret), kg			M1/4 (ret), kg	
	M#4 (ret), kg			M#4 (ret), kg	
	Mpan, kg			Mpan, kg	
	Mass Check:			Mass Check:	
<b>20 cycles</b>	M3/4 (ret), kg		<b>50 cycles</b>	M3/4 (ret), kg	
	M5/8 (ret), kg			M5/8 (ret), kg	
	M1/2 (ret), kg			M1/2 (ret), kg	
	M3/8 (ret), kg			M3/8 (ret), kg	
	M5/16 (ret), kg			M5/16 (ret), kg	
	M1/4 (ret), kg			M1/4 (ret), kg	
	M#4 (ret), kg			M#4 (ret), kg	
	Mpan, kg			Mpan, kg	
	Mass Check:			Mass Check:	
<b>Date recorded:</b>			<b>Chamber Pressure:</b>		
<b>Test Technician:</b>			<b>Soloid Pressure:</b>		
<b>Comments</b>					

Figure B.10 Hydraulic Fracture data sheet.

## APPENDIX C: HFT RESULTS

### C.1 MNDOT HFT CHAMBER TEST RESULTS

TABLE C.1  
MnDOT HFT result of aggregate source A1

	Mass (g)						Mass change after 50 cycles	
	0 cycles	10 cycles	20 cycles	30 cycles	40 cycles	50 cycles	(g)	%
3/4 in. sieve	1091.9	1027.8	1072.5	922.1	896.5	878.2	-213.7	-2.0
5/8 in. sieve	4006.7	3752.7	3669.9	3865.2	3736.1	3766.0	-240.7	-2.2
1/2 in. sieve	5535.3	5690.7	5641.7	5513.8	5629.5	5580.4	45.1	0.4
3/8 in. sieve	224.3	332.8	412.5	440.8	434.3	466.8	242.5	2.2
5/16 in. sieve	0.0	9.7	17.3	23.7	24.9	34.0	34.0	0.3
1/4 in. sieve	0.0	7.1	11.0	15.9	21.8	22.2	22.2	0.2
#4 sieve	0.0	6.1	6.8	13.4	17.2	17.5	17.5	0.2
Pan	0.0	7.0	7.1	13.4	9.1	7.9	44.5	0.4
<b>Total mass</b>	<b>10858.2</b>					<b>10773.0</b>		

TABLE C.2  
MnDOT HFT result of aggregate source A2

	Mass (g)						Mass change after 50 cycles	
	0 cycles	10 cycles	20 cycles	30 cycles	40 cycles	50 cycles	(g)	%
3/4 in. sieve	1276.0	1199.5	1190.2	1186.8	1199.5	1255.7	-20.3	-0.2
5/8 in. sieve	4576.7	4222.0	4175.5	4197.5	4071.9	4087.0	-489.7	-4.7
1/2 in. sieve	4487.2	4748.9	4684.7	4725.4	4711.5	4560.1	72.9	0.7
3/8 in. sieve	119.8	248.6	324.7	268.9	344.6	382.8	263.0	2.5
5/16 in. sieve	0.0	6.5	17.2	18.3	28.0	33.7	33.7	0.3
1/4 in. sieve	0.0	5.3	14.6	6.8	22.1	31.3	31.3	0.3
#4 sieve	0.0	4.6	7.5	2.1	12.1	16.0	16.0	0.2
Pan	0.0	10.2	12.7	4.8	10.9	10.6	49.2	0.5
<b>Total mass</b>	<b>10459.7</b>					<b>10377.2</b>		

TABLE C.3  
MnDOT HFT result of aggregate source A3

	Mass (g)						Mass change after 50 cycles	
	0 cycles	10 cycles	20 cycles	30 cycles	40 cycles	50 cycles	(g)	%
3/4 in. sieve	1368.0	1244.3	1255.7	1202.0	1165.7	1105.5	-262.5	-2.4
5/8 in. sieve	3863.2	3577.2	3553.3	3578.4	3523.8	3537.8	-325.4	-3.0
1/2 in. sieve	5463.9	5799.9	5744.5	5739.8	5828.9	5809.1	345.2	3.2
3/8 in. sieve	172.7	289.8	291.0	307.8	302.1	361.3	188.6	1.7
5/16 in. sieve	0.0	2.3	2.2	2.1	1.9	1.9	1.9	0.0
1/4 in. sieve	0.3	0.0	0.0	0.7	1.3	1.3	1.0	0.0
#4 sieve	0.7	1.8	1.7	1.7	2.0	1.9	1.2	0.0
Pan	0.0	2.7	2.9	2.9	2.8	2.6	13.9	0.1
<b>Total mass</b>	<b>10868.8</b>					<b>10821.4</b>		

TABLE C.4  
MnDOT HFT result of aggregate source A4

	Mass (g)						Mass change after 50 cycles	
	0 cycles	10 cycles	20 cycles	30 cycles	40 cycles	50 cycles	(g)	%
3/4 in. sieve	1230.8	1288.1	1292.5	1299.9	1240.8	1195.2	-35.6	-0.3
5/8 in. sieve	4598.2	4494.5	4458.6	4638.0	4676.8	4461.5	-136.7	-1.3
1/2 in. sieve	4784.7	4733.4	4750.2	4561.7	4129.8	4820.4	35.7	0.3
3/8 in. sieve	0.0	79.9	90.6	86.8	75.9	99.1	99.1	0.9
5/16 in. sieve	0.0	0.0	0.0	0.0	457.4	1.0	1.0	0.0
1/4 in. sieve	0.0	0.7	0.7	0.6	0.3	0.7	0.7	0.0
#4 sieve	0.0	0.4	0.1	0.4	0.2	3.1	3.1	0.0
Pan	0.0	2.8	2.6	2.0	1.7	1.6	10.7	0.1
<b>Total mass</b>	<b>10613.7</b>					<b>10582.6</b>		

TABLE C.5  
MnDOT HFT result of aggregate source A5

	Mass (g)						Mass change after 50 cycles	
	0 cycles	10 cycles	20 cycles	30 cycles	40 cycles	50 cycles	(g)	%
3/4 in. sieve	1139.4	1044.4	1034.2	973.1	911.8	949.7	-189.7	-1.9
5/8 in. sieve	4142.6	4100.3	4108.0	3998.1	3916.1	3919.5	-223.1	-2.2
1/2 in. sieve	4817.7	4862.2	4828.3	4904.8	4938.6	4896.1	78.4	0.8
3/8 in. sieve	0.0	72.8	80.8	139.8	206.6	200.6	200.6	2.0
5/16 in. sieve	0.0	0.0	7.1	20.7	23.9	22.1	22.1	0.2
1/4 in. sieve	0.0	0.5	4.7	11.7	17.2	18.2	18.2	0.2
#4 sieve	0.0	1.3	3.2	7.5	12.1	10.9	10.9	0.1
Pan	0.0	11.7	7.0	12.2	13.3	8.4	52.6	0.5
<b>Total mass</b>	<b>10099.7</b>					<b>10025.5</b>		

TABLE C.6  
MnDOT HFT result of aggregate source A6

	Mass (g)						Mass change after 50 cycles	
	0 cycles	10 cycles	20 cycles	30 cycles	40 cycles	50 cycles	(g)	%
3/4 in. sieve	1219.0	1225.7	1276.5	1227.0	1174.9	1109.2	-109.8	-1.0
5/8 in. sieve	3509.2	3552.3	3640.7	3383.4	3432.5	3415.5	-93.7	-0.9
1/2 in. sieve	5845.1	5664.6	5489.9	5756.9	5711.1	5780.7	-64.4	-0.6
3/8 in. sieve	0.0	96.9	128.5	151.6	178.5	174.9	174.9	1.7
5/16 in. sieve	0.0	4.0	2.2	3.0	8.5	6.9	6.9	0.1
1/4 in. sieve	0.0	5.8	4.8	3.7	6.4	7.5	7.5	0.1
#4 sieve	0.0	0.5	0.4	0.8	3.6	5.7	5.7	0.1
Pan	0.0	12.5	5.1	3.6	6.7	6.0	33.9	0.3
<b>Total mass</b>	<b>10573.3</b>					<b>10506.4</b>		

TABLE C.7  
MnDOT HFT result of aggregate source B1

	Mass (g)						Mass change after 50 cycles	
	0 cycles	10 cycles	20 cycles	30 cycles	40 cycles	50 cycles	(g)	%
3/4 in. sieve	1178.6	975.8	907.2	882.9	792.4	866.7	-311.9	-2.9
5/8 in. sieve	4935.2	4358.2	4108.9	3954.9	3747.7	3563.1	-1372.1	-13.0
1/2 in. sieve	4319.9	4635.4	4509.4	4354.2	4325.7	4276.9	-43.0	-0.4
3/8 in. sieve	149.3	381.7	666.9	800.2	958.1	988.0	838.7	7.9
5/16 in. sieve	0.0	106.0	123.5	165.6	209.1	246.3	246.3	2.3
1/4 in. sieve	0.0	30.2	88.8	129.0	171.0	198.9	198.9	1.9
#4 sieve	0.0	25.4	56.7	85.8	114.1	128.2	128.2	1.2
Pan	0.0	47.2	61.3	45.7	53.5	39.1	246.8	2.3
<b>Total mass</b>	<b>10583.0</b>					<b>10307.2</b>		

TABLE C.8  
MnDOT HFT result of aggregate source B2

Cycles	Mass (g)						Mass change after 50 cycles	
	0 cycles	10 cycles	20 cycles	30 cycles	40 cycles	50 cycles	(g)	%
3/4 in. sieve	1323.9	1062.9	1102.4	1086.0	1085.9	1074.7	-249.2	-2.3
5/8 in. sieve	4554.5	4200.7	4189.6	4261.5	4275.2	4177.2	-377.3	-3.5
1/2 in. sieve	4828.6	5278.9	5217.8	5127.5	5079.1	5182.0	353.4	3.3
3/8 in. sieve	110.3	259.9	281.3	299.5	321.1	306.3	196.0	1.8
5/16 in. sieve	1.0	1.2	3.8	3.8	6.5	9.2	8.2	0.1
1/4 in. sieve	0.0	0.0	2.3	2.0	3.3	5.5	5.5	0.1
#4 sieve	0.1	0.3	1.9	2.9	4.2	5.2	5.1	0.0
Pan	0.0	6.6	6.8	5.4	6.3	5.5	30.6	0.3
<b>Total mass</b>	<b>10818.4</b>					<b>10765.6</b>		

TABLE C.9  
MnDOT HFT result of aggregate source B3

Cycles	Mass (g)						Mass change after 50 cycles	
	0 cycles	10 cycles	20 cycles	30 cycles	40 cycles	50 cycles	(g)	%
3/4 in. sieve	1393.2	1103.4	1163.6	1133.9	1036.2	1048.6	-344.6	-3.3
5/8 in. sieve	3652.6	3590.1	3539.8	3629.2	3578.2	3522.7	-129.9	-1.2
1/2 in. sieve	5227.9	5438.7	5402.5	5291.3	5436.0	5476.0	248.1	2.4
3/8 in. sieve	218.1	284.5	294.4	330.6	325.7	321.3	103.2	1.0
5/16 in. sieve	0.0	0.8	3.1	2.3	3.7	3.6	3.6	0.0
1/4 in. sieve	0.0	0.0	0.0	1.5	2.8	4.9	4.9	0.0
#4 sieve	0.0	0.7	1.5	2.8	3.3	3.2	3.2	0.0
Pan	0.0	6.0	6.6	6.0	3.2	4.7	26.5	0.3
<b>Total mass</b>	<b>10491.8</b>					<b>10385.0</b>		

TABLE C.10  
MnDOT HFT result of aggregate source B4

Cycles	Mass (g)						Mass change after 50 cycles	
	0 cycles	10 cycles	20 cycles	30 cycles	40 cycles	50 cycles	(g)	%
3/4 in. sieve	1150.9	1227.2	1153.7	1048.6	1019.6	1084.6	-66.3	-0.6
5/8 in. sieve	4221.3	4140.5	4014.6	4112.5	4150.9	4142.0	-79.3	-0.7
1/2 in. sieve	5237.7	5181.6	5369.2	5345.4	5303.0	5245.6	7.9	0.1
3/8 in. sieve	184.6	221.1	228.8	243.1	266.9	262.5	77.9	0.7
5/16 in. sieve	0.0	2.4	1.7	1.7	1.7	1.7	1.7	0.0
1/4 in. sieve	0.0	1.2	1.8	3.7	3.7	4.5	4.5	0.0
#4 sieve	0.0	3.1	3.1	2.7	2.9	2.8	2.8	0.0
Pan	0.0	11.3	4.9	5.0	2.9	3.4	27.5	0.3
<b>Total mass</b>	<b>10794.5</b>					<b>10747.1</b>		

TABLE C.11  
MnDOT HFT result of aggregate source B5

Cycles	Mass (g)						Mass change after 50 cycles	
	0 cycles	10 cycles	20 cycles	30 cycles	40 cycles	50 cycles	(g)	%
3/4 in. sieve	1097.1	1139.3	1104.2	1190.2	1156.2	1137.8	40.7	0.4
5/8 in. sieve	3669.7	3551.4	3585.9	3488.4	3733.6	3499.5	-170.2	-1.6
1/2 in. sieve	5551.2	5537.8	5519.1	5450.6	5309.7	5448.4	-102.8	-1.0
3/8 in. sieve	352.1	424.0	417.8	478.1	399.0	495.3	143.2	1.3
5/16 in. sieve	0.0	3.1	1.1	6.1	8.0	7.2	7.2	0.1
1/4 in. sieve	0.0	1.0	1.9	3.9	4.0	5.5	5.5	0.1
#4 sieve	0.0	0.7	1.6	1.9	6.4	3.8	3.8	0.0
Pan	0.0	6.8	5.6	4.5	2.0	4.5	23.4	0.2
<b>Total mass</b>	<b>10670.1</b>					<b>10602.0</b>		

TABLE C.12  
MnDOT HFT result of aggregate source B6

	Mass (g)						Mass change after 50 cycles	
	0 cycles	10 cycles	20 cycles	30 cycles	40 cycles	50 cycles	(g)	%
3/4 in. sieve	1060.6	1191.3	1027.2	1028.9	1009.8	941.8	-118.8	-1.1
5/8 in. sieve	4204.4	4441.9	4147.0	4143.7	4182.7	4075.0	-129.4	-1.2
1/2 in. sieve	5299.8	4899.7	5277.1	5256.5	5224.5	5377.2	77.4	0.7
3/8 in. sieve	0.0	22.1	80.2	92.1	101.9	117.5	117.5	1.1
5/16 in. sieve	0.0	0.0	0.0	0.0	1.5	1.8	1.8	0.0
1/4 in. sieve	0.0	0.0	1.8	0.0	0.8	2.4	2.4	0.0
#4 sieve	0.0	1.1	1.2	3.7	2.8	1.7	1.7	0.0
Pan	0.0	2.5	5.2	6.2	5.1	4.8	23.8	0.2
<b>Total mass</b>	<b>10564.8</b>					<b>10522.2</b>		

TABLE C.13  
MnDOT HFT result of aggregate source C1

	Mass (g)						Mass change after 50 cycles	
	0 cycles	10 cycles	20 cycles	30 cycles	40 cycles	50 cycles	(g)	%
3/4 in. sieve	1288.2	1109.8	1126.3	1251.0	1210.8	1146.0	-142.2	-1.3
5/8 in. sieve	5387.0	4847.4	4820.8	4735.5	4703.9	4699.8	-687.2	-6.3
1/2 in. sieve	4095.2	4683.4	4637.8	4547.0	4570.1	4636.0	540.8	5.0
3/8 in. sieve	89.6	184.7	222.4	248.1	275.1	266.0	176.4	1.6
5/16 in. sieve	0.0	6.6	8.5	14.1	16.8	18.2	18.2	0.2
1/4 in. sieve	0.0	5.4	8.8	13.2	18.7	20.1	20.1	0.2
#4 sieve	0.0	2.1	4.1	7.0	7.2	8.9	8.9	0.1
Pan	0.0	9.0	8.5	7.8	7.3	3.5	36.1	0.3
<b>Total mass</b>	<b>10860.0</b>					<b>10798.5</b>		

TABLE C.14  
MnDOT HFT result of aggregate source C3

	Mass (g)						Mass change after 50 cycles	
	0 cycles	10 cycles	20 cycles	30 cycles	40 cycles	50 cycles	(g)	%
3/4 in. sieve	1132.5	1079.2	1129.8	1205.5	1161.8	1080.4	-52.1	-0.5
5/8 in. sieve	3618.2	3623.2	3612.4	3811.7	3473.8	3611.5	-6.7	-0.1
1/2 in. sieve	5879.8	5799.3	5760.2	5460.2	5835.7	5742.8	-137.0	-1.3
3/8 in. sieve	0.0	112.0	103.5	119.9	123.8	154.2	154.2	1.5
5/16 in. sieve	0.0	4.9	4.6	4.4	4.7	4.6	4.6	0.0
1/4 in. sieve	0.0	0.4	1.4	2.7	2.4	2.3	2.3	0.0
#4 sieve	0.0	0.2	0.8	2.3	1.7	2.3	2.3	0.0
Pan	0.0	3.3	3.4	1.8	1.9	1.8	12.2	0.1
<b>Total mass</b>	<b>10630.5</b>					<b>10599.9</b>		

TABLE C.15  
MnDOT HFT result of aggregate source C4

	Mass (g)						Mass change after 50 cycles	
	0 cycles	10 cycles	20 cycles	30 cycles	40 cycles	50 cycles	(g)	%
3/4 in. sieve	1302.8	1237.2	1365.6	1315.3	1482.7	1402.1	99.3	0.9
5/8 in. sieve	5410.7	5495.4	5433.8	5634.1	5737.3	5697.2	286.5	2.7
1/2 in. sieve	4049.5	3990.3	3924.8	3751.9	3475.2	3592.7	-456.8	-4.2
3/8 in. sieve	0.0	27.8	20.1	25.4	11.3	21.4	21.4	0.2
5/16 in. sieve	0.0	0.0	1.3	1.8	1.5	1.5	1.5	0.0
1/4 in. sieve	0.0	0.4	0.6	1.2	1.2	1.1	1.1	0.0
#4 sieve	0.0	0.0	0.0	0.0	0.8	0.7	0.7	0.0
Pan	0.0	3.0	2.5	2.5	8.2	0.1	16.3	0.2
<b>Total mass</b>	<b>10763.0</b>					<b>10716.8</b>		

TABLE C.16  
MnDOT HFT result of aggregate source C5

	Mass (g)						Mass change after 50 cycles	
	0 cycles	10 cycles	20 cycles	30 cycles	40 cycles	50 cycles	(g)	%
3/4 in. sieve	1219.0	1225.7	1276.5	1227.0	1174.9	1109.2	-109.8	-1.0
5/8 in. sieve	3509.2	3552.3	3640.7	3383.4	3432.5	3415.5	-93.7	-0.9
1/2 in. sieve	5845.1	5664.6	5489.9	5756.9	5711.1	5780.7	-64.4	-0.6
3/8 in. sieve	0.0	96.9	128.5	151.6	178.5	174.9	174.9	1.7
5/16 in. sieve	0.0	4.0	2.2	3.0	8.5	6.9	6.9	0.1
1/4 in. sieve	0.0	5.8	4.8	3.7	6.4	7.5	7.5	0.1
#4 sieve	0.0	0.5	0.4	0.8	3.6	5.7	5.7	0.1
Pan	0.0	12.5	5.1	3.6	6.7	6.0	33.9	0.3
<b>Total mass</b>	<b>10573.3</b>					<b>10506.4</b>		

TABLE C.17  
MnDOT HFT result of aggregate source C6

	Mass (g)						Mass change after 50 cycles	
	0 cycles	10 cycles	20 cycles	30 cycles	40 cycles	50 cycles	(g)	%
3/4 in. sieve	1225.7	1268.8	1219.5	1281.2	1228.7	1142.5	-83.2	-0.8
5/8 in. sieve	4900.7	4951.5	5061.1	4923.0	4791.7	4740.1	-160.6	-1.5
1/2 in. sieve	4559.0	4367.6	4287.1	4301.6	4419.4	4471.1	-87.9	-0.8
3/8 in. sieve	0.0	41.2	67.2	108.5	139.8	181.0	181.0	1.7
5/16 in. sieve	0.0	0.0	3.1	3.7	8.0	20.6	20.6	0.2
1/4 in. sieve	0.0	2.9	6.6	11.5	17.5	20.1	20.1	0.2
#4 sieve	0.0	0.0	0.6	1.0	6.3	9.4	9.4	0.1
Pan	0.0	2.6	3.6	6.0	4.4	4.7	21.3	0.2
<b>Total mass</b>	<b>10685.4</b>					<b>10589.5</b>		

TABLE C.18  
MnDOT HFT result of aggregate source C7

	Mass (g)						Mass change after 50 cycles	
	0 cycles	10 cycles	20 cycles	30 cycles	40 cycles	50 cycles	(g)	%
3/4 in. sieve	1274.6	1182.5	1181.2	1112.7	1205.3	1115.8	-158.8	-1.5
5/8 in. sieve	4303.8	4381.6	4299.1	4391.3	4369.8	4415.3	111.5	1.1
1/2 in. sieve	4987.9	4924.7	5006.7	4947.6	4826.7	4865.1	-122.8	-1.2
3/8 in. sieve	0.0	43.6	44.1	47.5	68.0	63.9	63.9	0.6
5/16 in. sieve	0.0	0.0	1.8	2.0	1.3	1.5	1.5	0.0
1/4 in. sieve	0.0	5.0	2.9	3.0	4.0	6.0	6.0	0.1
#4 sieve	0.0	0.0	0.0	1.6	2.6	0.0	0.0	0.0
Pan	0.0	8.4	3.2	2.2	1.8	1.4	17.0	0.2
<b>Total mass</b>	<b>10566.3</b>					<b>10469.0</b>		

## C.2 INDOT HFT CHAMBER TEST RESULTS

TABLE C.19  
INDOT HFT result of aggregate source A1

	Mass (g)						Mass change after 50 cycles	
	0 cycles	10 cycles	20 cycles	30 cycles	40 cycles	50 cycles	(g)	%
3/4 in. sieve	1466.5	1368.8	1380.6	1211.5	1280.1	1225.3	-241.2	-1.9
5/8 in. sieve	6351.7	6056.3	5969.5	5921.7	5813.5	5699.2	-652.5	-5.0
1/2 in. sieve	5191.7	5480.0	5483.0	5606.8	5607.7	5698.1	506.4	3.9
3/8 in. sieve	0.0	55.4	87.0	131.8	122.6	155.1	155.1	1.2
5/16 in. sieve	0.0	1.1	0.9	0.7	0.9	1.0	1.0	0.0
1/4 in. sieve	0.0	0.0	0.0	0.3	1.0	2.2	2.2	0.0
#4 sieve	0.0	0.0	0.0	0.5	0.8	0.3	0.3	0.0
Pan	0.0	45.1	33.0	43.8	41.2	40.6	203.7	
<b>Total mass</b>	<b>13009.9</b>					<b>12781.2</b>		

TABLE C.20  
INDOT HFT result of aggregate source A2

	Mass (g)						Mass change after 50 cycles	
	0 cycles	10 cycles	20 cycles	30 cycles	40 cycles	50 cycles	(g)	%
3/4 in. sieve	1225.7	1268.8	1219.5	1281.2	1228.7	1142.5	-83.2	-0.8
5/8 in. sieve	4900.7	4951.5	5061.1	4923.0	4791.7	4740.1	-160.6	-1.5
1/2 in. sieve	4559.0	4367.6	4287.1	4301.6	4419.4	4471.1	-87.9	-0.8
3/8 in. sieve	0.0	41.2	67.2	108.5	139.8	181.0	181.0	1.7
5/16 in. sieve	0.0	0.0	3.1	3.7	8.0	20.6	20.6	0.2
1/4 in. sieve	0.0	2.9	6.6	11.5	17.5	20.1	20.1	0.2
#4 sieve	0.0	0.0	0.6	1.0	6.3	9.4	9.4	0.1
Pan	0.0	2.6	3.6	6.0	4.4	4.7	21.3	0.2
<b>Total mass</b>	<b>10685.4</b>					<b>10589.5</b>		

TABLE C.21  
INDOT HFT result of aggregate source A3

	Mass (g)						Mass change after 50 cycles	
	0 cycles	10 cycles	20 cycles	30 cycles	40 cycles	50 cycles	(g)	%
3/4 in. sieve	1464.5	1462.5	1456.8	1433.4	1406.4	1385.9	-78.6	-0.6
5/8 in. sieve	6350.1	6344.0	6237.3	6169.2	6190.1	6143.0	-207.1	-1.6
1/2 in. sieve	5190.0	5131.0	5239.5	5279.6	5189.8	5204.4	14.4	0.1
3/8 in. sieve	0.0	60.5	30.3	40.7	98.2	120.3	120.3	0.9
5/16 in. sieve	0.0	0.0	0.0	0.0	0.8	0.8	0.8	0.0
1/4 in. sieve	0.0	0.0	1.9	2.0	2.2	1.9	1.9	0.0
#4 sieve	0.0	0.0	0.8	2.9	0.0	0.3	0.3	0.0
Pan	0.0	0.0	27.5	29.5	24.3	30.4	111.7	0.9
<b>Total mass</b>	<b>13004.6</b>					<b>12887.0</b>		

TABLE C.22  
INDOT HFT result of aggregate source A4

	Mass (g)						Mass change after 50 cycles	
	0 cycles	10 cycles	20 cycles	30 cycles	40 cycles	50 cycles	(g)	%
3/4 in. sieve	1471.8	1580.0	1498.4	1466.6	1492.1	1327.9	-143.9	-1.1
5/8 in. sieve	6345.0	6063.8	5983.5	6000.3	5968.3	6058.4	-286.6	-2.2
1/2 in. sieve	5186.0	5271.1	5389.1	5392.4	5325.2	5364.3	178.3	1.4
3/8 in. sieve	0.0	47.4	55.5	40.9	83.4	97.4	97.4	0.7
5/16 in. sieve	0.0	0.6	1.8	2.8	4.9	4.9	4.9	0.0
1/4 in. sieve	0.0	0.3	1.7	2.5	3.1	5.0	5.0	0.0
#4 sieve	0.0	0.0	0.4	0.5	1.1	0.7	0.7	0.0
Pan	0.0	32.7	27.5	23.4	27.5	16.6	127.7	1.0
<b>Total mass</b>	<b>13002.8</b>					<b>12875.2</b>		

TABLE C.23  
INDOT HFT result of aggregate source A5

	Mass (g)						Mass change after 50 cycles	
	0 cycles	10 cycles	20 cycles	30 cycles	40 cycles	50 cycles	(g)	%
3/4 in. sieve	1225.1	1337.8	1243.3	1175.7	1156.1	1056.6	-168.5	-1.5
5/8 in. sieve	5397.0	5061.5	5053.3	4964.1	4895.8	4870.0	-527.0	-4.8
1/2 in. sieve	4418.8	4543.7	4559.2	4650.8	4638.4	4731.2	312.4	2.8
3/8 in. sieve	0.0	58.3	89.6	103.5	147.3	126.8	126.8	1.1
5/16 in. sieve	0.0	0.0	0.0	0.9	0.0	1.0	1.0	0.0
1/4 in. sieve	0.0	0.9	0.9	0.8	2.2	2.3	2.3	0.0
#4 sieve	0.0	0.0	0.1	0.1	0.0	0.0	0.0	0.0
Pan	0.0	28.8	46.7	38.8	44.8	43.6	202.7	1.8
<b>Total mass</b>	<b>11040.9</b>					<b>10831.5</b>		

TABLE C.24  
INDOT HFT result of aggregate source A6

	Mass (g)						Mass change after 50 cycles	
	0 cycles	10 cycles	20 cycles	30 cycles	40 cycles	50 cycles	(g)	%
3/4 in. sieve	2150.3	2118.1	1952.1	1859.3	1934.3	1832.4	-14.8	-1.5
5/8 in. sieve	5564.5	5461.3	5354.0	5346.3	5272.6	5214.7	-6.3	-4.8
1/2 in. sieve	4464.1	4538.8	4757.6	4833.2	4836.7	4953.4	11.0	2.8
3/8 in. sieve	0.0	27.6	56.4	57.9	29.2	47.7	0.4	1.1
5/16 in. sieve	0.0	1.1	2.3	2.6	1.7	3.6	0.0	0.0
1/4 in. sieve	0.0	0.0	2.5	2.9	2.5	4.0	0.0	0.0
#4 sieve	0.0	1.6	0.4	1.5	1.8	2.1	0.0	0.0
Pan	0.0	15.2	15.4	14.5	21.4	17.7	0.7	1.8
<b>Total mass</b>	<b>12178.9</b>					<b>12075.6</b>		

TABLE C.25  
INDOT HFT result of aggregate source B1

	Mass (g)						Mass change after 50 cycles	
	0 cycles	10 cycles	20 cycles	30 cycles	40 cycles	50 cycles	(g)	%
3/4 in. sieve	1749.5	1675.3	1559.0	1494.2	1510.7	1395.9	-353.6	-2.4
5/8 in. sieve	6982.5	6755.3	6891.4	6724.7	6687.1	6517.7	-464.8	-3.2
1/2 in. sieve	5961.0	6079.4	5944.1	6155.6	6054.7	6307.3	346.3	2.4
3/8 in. sieve	0.0	66.0	89.1	96.3	36.3	153.4	153.4	1.0
5/16 in. sieve	0.0	3.5	1.8	13.7	73.4	21.0	21.0	0.1
1/4 in. sieve	0.0	0.8	4.7	6.3	16.4	4.4	4.4	0.0
#4 sieve	0.0	26.9	0.3	7.1	3.4	7.2	7.2	0.0
Pan	0.0	23.3	29.7	36.5	24.6	27.9	142.0	1.0
<b>Total mass</b>	<b>14693.0</b>					<b>14434.8</b>		

TABLE C.26  
INDOT HFT result of aggregate source B2

	Mass (g)						Mass change after 50 cycles	
	0 cycles	10 cycles	20 cycles	30 cycles	40 cycles	50 cycles	(g)	%
3/4 in. sieve	1463.2	1605.0	1458.7	1388.3	1385.7	1354.8	-108.4	-0.8
5/8 in. sieve	6345.0	5935.7	5979.6	6036.6	5944.1	5804.9	-540.1	-4.2
1/2 in. sieve	5190.8	5329.4	5376.2	5320.7	5376.9	5454.4	263.6	2.0
3/8 in. sieve	0.0	75.1	83.5	111.5	116.0	162.2	162.2	1.2
5/16 in. sieve	0.0	0.5	1.0	1.4	2.4	1.9	1.9	0.0
1/4 in. sieve	0.0	0.0	0.5	0.4	1.2	0.9	0.9	0.0
#4 sieve	0.0	0.2	0.8	0.9	1.2	1.4	1.4	0.0
Pan	0.0	39.6	40.2	37.1	23.2	40.4	180.5	1.4
<b>Total mass</b>	<b>12999.0</b>					<b>12820.9</b>		

TABLE C.27  
INDOT HFT result of aggregate source B3

	Mass (g)						Mass change after 50 cycles	
	0 cycles	10 cycles	20 cycles	30 cycles	40 cycles	50 cycles	(g)	%
3/4 in. sieve	1462.5	1462.0	1412.8	1363.6	1375.9	1263.8	-198.7	-1.5
5/8 in. sieve	6344.0	6338.4	6328.8	6270.2	6099.8	6266.7	-77.3	-0.6
1/2 in. sieve	5187.0	5180.5	5193.7	5281.2	5355.7	5243.8	56.8	0.4
3/8 in. sieve	0.0	0.0	13.7	9.4	44.7	78.9	78.9	0.6
5/16 in. sieve	0.0	0.0	0.0	0.0	1.3	4.0	4.0	0.0
1/4 in. sieve	0.0	0.0	0.5	0.0	0.0	0.0	0.0	0.0
#4 sieve	0.0	0.0	0.6	0.0	0.0	0.0	0.0	0.0
Pan	0.0	12.6	24.3	26.6	25.3	22.2	111.0	0.9
<b>Total mass</b>	<b>12993.5</b>					<b>12879.4</b>		

TABLE C.28  
INDOT HFT result of aggregate source B4

	Mass (g)						Mass change after 50 cycles	
	0 cycles	10 cycles	20 cycles	30 cycles	40 cycles	50 cycles	(g)	%
3/4 in. sieve	1471.4	1447.8	1408.9	1378.7	1338.2	1282.1	-189.3	-1.5
5/8 in. sieve	6347.4	5923.5	5824.5	5798.8	5747.9	5641.4	-706.0	-5.4
1/2 in. sieve	5189.1	5527.4	5628.9	5593.3	5647.8	5744.6	555.5	4.3
3/8 in. sieve	0.0	79.0	80.0	131.1	134.3	166.6	166.6	1.3
5/16 in. sieve	0.0	0.0	0.0	0.0	0.0	2.4	2.4	0.0
1/4 in. sieve	0.0	0.0	0.6	0.5	0.7	0.9	0.9	0.0
#4 sieve	0.0	0.0	0.5	1.2	1.0	1.2	1.2	0.0
Pan	0.0	28.0	31.7	28.6	26.0	26.1	140.4	1.1
<b>Total mass</b>	<b>13007.9</b>					<b>12865.3</b>		

TABLE C.29  
INDOT HFT result of aggregate source B5

	Mass (g)						Mass change after 50 cycles	
	0 cycles	10 cycles	20 cycles	30 cycles	40 cycles	50 cycles	(g)	%
3/4 in. sieve	1467.4	1537.0	1497.4	1388.3	1402.5	1337.0	-130.4	-1.0
5/8 in. sieve	6349.8	6054.3	5925.7	5957.6	5815.6	5739.9	-609.9	-4.7
1/2 in. sieve	5194.8	5251.5	5362.9	5348.1	5443.4	5522.8	328.0	2.5
3/8 in. sieve	0.0	121.4	128.4	179.7	179.5	209.4	209.4	1.6
5/16 in. sieve	0.0	0.0	0.0	0.0	1.1	1.0	1.0	0.0
1/4 in. sieve	0.0	0.0	0.0	0.0	0.0	0.3	0.3	0.0
#4 sieve	0.0	0.4	0.4	0.4	0.4	0.9	0.9	0.0
Pan	0.0	46.1	36.0	33.9	28.0	29.6	173.6	1.3
<b>Total mass</b>	<b>13012.0</b>					<b>12840.9</b>		

TABLE C.30  
INDOT HFT result of aggregate source B6

	Mass (g)						Mass change after 50 cycles	
	0 cycles	10 cycles	20 cycles	30 cycles	40 cycles	50 cycles	(g)	%
3/4 in. sieve	1464.0	1518.0	1406.0	1327.3	1342.9	1201.1	-262.9	-2.0
5/8 in. sieve	6352.2	5848.7	5795.8	5802.5	5672.2	5487.5	-864.7	-6.6
1/2 in. sieve	5198.5	5496.0	5606.5	5614.8	5640.8	5900.8	702.3	5.4
3/8 in. sieve	0.0	90.9	95.1	116.7	164.4	175.3	175.3	1.3
5/16 in. sieve	0.0	1.3	1.5	3.7	3.9	7.2	7.2	0.1
1/4 in. sieve	0.0	1.7	1.6	2.7	4.0	4.6	4.6	0.0
#4 sieve	0.0	1.6	1.6	1.9	1.7	2.1	2.1	0.0
Pan	0.0	48.2	41.5	38.2	30.1	40.3	198.3	1.5
<b>Total mass</b>	<b>13014.7</b>					<b>12818.9</b>		

TABLE C.31  
INDOT HFT result of aggregate source C1

	Mass (g)						Mass change after 50 cycles	
	0 cycles	10 cycles	20 cycles	30 cycles	40 cycles	50 cycles	(g)	%
3/4 in. sieve	1410.2	1417.0	1388.4	1316.1	1316.2	1284.7	-125.5	-1.0
5/8 in. sieve	6108.0	5902.0	5814.2	5820.5	5648.0	5685.1	-422.9	-3.4
1/2 in. sieve	4988.8	5107.5	5169.3	5179.3	5278.0	5230.5	241.7	1.9
3/8 in. sieve	0.0	35.8	48.2	66.5	96.4	103.2	103.2	0.8
5/16 in. sieve	0.0	1.8	3.4	4.5	7.0	6.7	6.7	0.1
1/4 in. sieve	0.0	4.9	4.5	7.1	7.2	8.7	8.7	0.1
#4 sieve	0.0	2.6	4.1	5.5	6.3	7.3	7.3	0.1
Pan	0.0	29.8	35.6	26.9	35.4	29.2	156.9	1.3
<b>Total mass</b>	<b>12507.0</b>					<b>12355.4</b>		

TABLE C.32  
INDOT HFT result of aggregate source C3

	Mass (g)						Mass change after 50 cycles	
	0 cycles	10 cycles	20 cycles	30 cycles	40 cycles	50 cycles	(g)	%
3/4 in. sieve	1478.9	1520.4	1423.1	1503.5	1290.4	1306.9	-172.0	-1.3
5/8 in. sieve	6347.9	5904.6	5852.5	5713.3	5880.2	5762.7	-585.2	-4.5
1/2 in. sieve	5188.7	5490.9	5611.2	5570.3	5591.3	5623.8	435.1	3.3
3/8 in. sieve	0.0	64.6	68.2	131.4	127.9	169.7	169.7	1.3
5/16 in. sieve	0.0	0.3	0.0	0.0	2.1	2.1	2.1	0.0
1/4 in. sieve	0.0	0.0	0.2	0.4	1.1	1.3	1.3	0.0
#4 sieve	0.0	28.9	0.6	1.9	1.8	2.4	2.4	0.0
Pan	0.0	0.0	22.6	26.4	23.2	22.5	94.7	0.7
<b>Total mass</b>	<b>13015.5</b>					<b>12891.4</b>		

TABLE C.33  
INDOT HFT result of aggregate source C4

	Mass (g)						Mass change after 50 cycles	
	0 cycles	10 cycles	20 cycles	30 cycles	40 cycles	50 cycles	(g)	%
3/4 in. sieve	2173.4	2075.3	2081.8	1903.3	1867.2	1916.8	-256.6	-1.6
5/8 in. sieve	7222.9	7149.8	7055.6	7024.1	7220.1	7065.1	-157.8	-1.0
1/2 in. sieve	6170.1	6268.8	6157.5	6327.2	6141.9	6206.2	36.1	0.2
3/8 in. sieve	0.0	29.6	36.1	55.0	49.2	52.2	52.2	0.3
5/16 in. sieve	0.0	0.0	1.1	1.0	0.6	1.2	1.2	0.0
1/4 in. sieve	0.0	1.3	0.9	1.0	0.8	1.3	1.3	0.0
#4 sieve	0.0	0.4	0.0	0.0	0.0	2.4	2.4	0.0
Pan	0.0	23.3	15.6	18.3	15.8	15.4	88.4	0.6
<b>Total mass</b>	<b>15566.4</b>					<b>15260.6</b>		

TABLE C.34  
INDOT HFT result of aggregate source C5

	Mass (g)						Mass change after 50 cycles	
	0 cycles	10 cycles	20 cycles	30 cycles	40 cycles	50 cycles	(g)	%
3/4 in. sieve	1341.6	1293.9	1177.5	1049.6	925.7	896.7	-444.9	-3.7
5/8 in. sieve	5862.0	5498.4	5335.9	5328.8	5232.8	5114.7	-747.3	-6.2
1/2 in. sieve	4790.4	4980.5	5116.7	5165.8	5286.7	5363.0	572.6	4.8
3/8 in. sieve	0.0	136.6	189.4	195.9	242.0	248.2	248.2	2.1
5/16 in. sieve	0.0	0.8	1.7	3.2	3.5	4.2	4.2	0.0
1/4 in. sieve	0.0	2.0	2.1	3.5	4.7	6.1	6.1	0.1
#4 sieve	0.0	0.8	1.0	1.9	2.7	2.7	2.7	0.0
Pan	0.0	78.1	79.7	67.6	39.0	44.2	308.6	2.6
<b>Total mass</b>	<b>11994.0</b>					<b>11679.8</b>		

TABLE C.35  
INDOT HFT result of aggregate source C6

	Mass (g)						Mass change after 50 cycles	
	0 cycles	10 cycles	20 cycles	30 cycles	40 cycles	50 cycles	(g)	%
3/4 in. sieve	2126.8	2036.3	2014.8	1981.4	2014.0	1970.8	-156.0	-1.2
5/8 in. sieve	6025.2	5942.8	5896.8	5717.5	5636.8	5625.8	-399.4	-3.1
1/2 in. sieve	4883.9	4883.6	4920.1	5070.2	5071.8	5100.0	216.1	1.7
3/8 in. sieve	0.0	37.7	36.3	5070.2	92.8	88.3	88.3	0.7
5/16 in. sieve	0.0	9.7	8.0	78.0	5.4	3.9	3.9	0.0
1/4 in. sieve	0.0	1.1	1.0	3.6	1.2	3.5	3.5	0.0
#4 sieve	0.0	0.9	0.7	2.8	2.8	1.8	1.8	0.0
Pan	0.0	26.9	20.5	1.6	25.3	23.7	98.0	0.8
<b>Total mass</b>	<b>13035.9</b>					<b>12817.8</b>		

TABLE C.36  
INDOT HFT result of aggregate source C7

	Mass (g)						Mass change after 50 cycles	
	0 cycles	10 cycles	20 cycles	30 cycles	40 cycles	50 cycles	(g)	%
3/4 in. sieve	1462.5	1461.4	1438.4	1368.2	1334.7	1316.9	-145.6	-1.1
5/8 in. sieve	6344.0	6330.2	6235.3	6322.9	6149.3	6059.5	-284.5	-2.2
1/2 in. sieve	5189.1	5181.7	5268.7	5223.4	5367.4	5450.2	261.1	2.0
3/8 in. sieve	0.0	7.4	12.6	16.1	42.1	50.7	50.7	0.4
5/16 in. sieve	0.0	0.0	0.0	1.9	1.9	0.0	0.0	0.0
1/4 in. sieve	0.0	0.0	0.0	0.0	0.0	0.0	0.0	0.0
#4 sieve	0.0	0.0	0.4	0.5	0.0	0.0	0.0	0.0
Pan	0.0	14.0	16.8	19.3	20.0	18.4	88.5	0.7
<b>Total mass</b>	<b>12995.6</b>					<b>12895.7</b>		

### C.3 RCA HFT RESULTS

TABLE C.37  
HFT result of RCA source R-1

	Mass (g)						Mass change after 50 cycles	
	0 cycles	10 cycles	20 cycles	30 cycles	40 cycles	50 cycles	(g)	%
3/4 in. sieve	1319.0	1286.3	1254.9	1186.0	1142.2	1129.2	-189.8	-1.6
5/8 in. sieve	5967.3	5830.0	5785.8	5642.9	5528.8	5473.6	-493.7	-4.1
1/2 in. sieve	4889.4	4923.6	4902.7	5083.5	5139.6	5163.1	273.7	2.2
3/8 in. sieve	0.0	66.2	104.1	115.5	155.1	169.5	169.5	1.4
5/16 in. sieve	0.0	3.4	4.5	4.4	9.1	8.4	8.4	0.1
1/4 in. sieve	0.0	3.2	5.0	6.2	8.7	10.1	10.1	0.1
#4 sieve	0.0	2.5	5.1	6.3	6.7	7.7	7.7	0.1
Pan	0.0	53.2	52.1	39.1	6.7	32.2	183.3	1.5
<b>Total mass</b>	<b>12175.7</b>					<b>11993.8</b>		

TABLE C.38  
HFT result of RCA source R-2

	Mass (g)						Mass change after 50 cycles	
	0 cycles	10 cycles	20 cycles	30 cycles	40 cycles	50 cycles	(g)	%
3/4 in. sieve	1476.4	1360.6	1241.3	1125.3	1093.7	1071.0	-405.4	-3.4
5/8 in. sieve	5411.0	5333.0	5286.8	5167.7	5059.2	4988.0	-423.0	-3.6
1/2 in. sieve	5000.8	5023.7	5117.6	5282.1	5304.7	5384.7	383.9	3.2
3/8 in. sieve	0.0	66.8	81.9	116.3	162.7	147.6	147.6	1.2
5/16 in. sieve	0.0	5.1	5.6	5.1	5.2	11.2	11.2	0.1
1/4 in. sieve	0.0	6.2	7.4	13.6	13.6	16.7	16.7	0.1
#4 sieve	0.0	2.3	3.0	3.9	6.8	7.0	7.0	0.1
Pan	0.0	69.8	89.0	56.9	44.2	35.8	295.7	2.5
<b>Total mass</b>	<b>11888.2</b>					<b>11662.0</b>		

TABLE C.39  
HFT result of RCA source R-3

	Mass (g)						Mass change after 50 cycles	
	0 cycles	10 cycles	20 cycles	30 cycles	40 cycles	50 cycles	(g)	%
3/4 in. sieve	1409.1	1445.8	1368.3	1325.2	1285.2	1262.4	-146.7	-1.2
5/8 in. sieve	5520.8	5168.5	5131.1	5076.5	5045.6	4952.7	-568.1	-4.7
1/2 in. sieve	5049.1	5260.6	5251.2	5306.6	5302.8	5371.2	322.1	2.7
3/8 in. sieve	0.0	30.9	110.3	113.3	142.5	144.5	144.5	1.2
5/16 in. sieve	0.0	1.9	8.1	10.6	13.5	17.5	17.5	0.1
1/4 in. sieve	0.0	2.6	5.6	8.5	7.2	11.0	11.0	0.1
#4 sieve	0.0	3.6	5.5	6.0	6.8	7.5	7.5	0.1
Pan	0.0	64.6	51.5	35.3	35.4	28.3	215.1	1.8
<b>Total mass</b>	<b>11979.0</b>					<b>11795.1</b>		

TABLE C.40  
HFT result of RCA source R-4

	Mass (g)						Mass change after 50 cycles	
	0 cycles	10 cycles	20 cycles	30 cycles	40 cycles	50 cycles	(g)	%
3/4 in. sieve	1477.5	1306.8	1272.4	1269.8	1184.8	1193.2	-284.3	-2.3
5/8 in. sieve	5781.0	5345.2	5208.6	5090.2	5016.3	4882.1	-898.9	-7.4
1/2 in. sieve	4951.2	5091.3	5093.6	5131.5	5203.9	5249.0	297.8	2.4
3/8 in. sieve	0.0	91.7	179.0	218.9	243.5	298.1	298.1	2.4
5/16 in. sieve	0.0	1.1	4.0	4.6	7.3	10.2	10.2	0.1
1/4 in. sieve	0.0	1.2	3.6	6.4	8.0	12.2	12.2	0.1
#4 sieve	0.0	1.4	3.3	5.8	7.0	8.4	8.4	0.1
Pan	0.0	78.5	57.7	55.4	42.3	43.8	277.7	2.3
<b>Total mass</b>	<b>12209.7</b>					<b>11697.0</b>		

TABLE C.41  
HFT result of RCA source R-5

	Mass (g)						Mass change after 50 cycles	
	0 cycles	10 cycles	20 cycles	30 cycles	40 cycles	50 cycles	(g)	%
3/4 in. sieve	1447.3	1334.2	1230.5	1196.7	1171.3	1192.6	-254.7	-2.2
5/8 in. sieve	5781.0	5766.9	5742.8	5625.4	5533.0	5463.1	-317.9	-2.7
1/2 in. sieve	4583.5	4606.0	4723.2	4783.3	4836.4	4859.7	276.2	2.3
3/8 in. sieve	0.0	66.2	69.1	98.5	117.2	122.0	122.0	1.0
5/16 in. sieve	0.0	1.7	3.0	2.8	5.8	5.8	5.8	0.0
1/4 in. sieve	0.0	1.0	2.4	3.8	4.2	3.7	3.7	0.0
#4 sieve	0.0	0.3	1.5	2.8	3.6	4.8	4.8	0.0
Pan	0.0	57.8	37.3	37.7	33.2	31.1	197.1	1.7
<b>Total mass</b>	<b>11811.8</b>					<b>11682.8</b>		

TABLE C.42  
HFT result of RCA source R-6

	Mass (g)						Mass change after 50 cycles	
	0 cycles	10 cycles	20 cycles	30 cycles	40 cycles	50 cycles	(g)	%
3/4 in. sieve	1466.7	1407.3	1277.7	1231.5	1261.8	1150.5	-316.2	-2.6
5/8 in. sieve	6038.9	5788.8	5823.3	5640.8	5359.9	5338.1	-700.8	-5.8
1/2 in. sieve	4587.9	4717.6	4705.8	4826.7	4972.5	4988.8	400.9	3.3
3/8 in. sieve	0.0	64.9	92.3	130.8	148.7	211.8	211.8	1.8
5/16 in. sieve	0.0	4.5	16.3	19.7	22.0	22.0	22.0	0.2
1/4 in. sieve	0.0	4.1	4.9	10.5	16.8	20.4	20.4	0.2
#4 sieve	0.0	3.2	4.8	7.7	10.7	14.1	14.1	0.1
Pan	0.0	91.3	76.5	61.5	58.4	52.8	340.5	2.8
<b>Total mass</b>	<b>12093.5</b>					<b>11798.5</b>		

## APPENDIX D: MATERIALS USED FOR BATCHING CONCRETE AND FRESH CONCRETE PROPERTIES

The materials and general mix design parameters used to batch the concrete test specimens for freeze-thaw testing met the ITM210 specifications, and are shown in Table D.1.

All concrete mixtures were batched in 1 ft<sup>3</sup> sized batches from which six beams were fabricated. The concrete was consolidated using a vibrating table, cured in the mold for one day under plastic-lined wet burlap, de-molded within 24 hrs ( $\pm 1$  hr) and placed in a lime-saturated bath. Between ages 12–14 days three of the beams were placed in a covered bucket with water, and/or wrapped in plastic and carefully transported approximately 70 miles to the INDOT Office of Materials where they continued to wet cure until 14 days of age. At an age of 14 days the beams were placed in the testing chamber and freeze-thaw cycling began. The beams at INDOT Research were tested using Procedure A, freeze and thaw in water. Beams tested at INDOT Office of Materials

were tested using Procedure B, freeze in air and thaw in water (per ITM 210 specifications).

All concrete used to fabricate ITM 210 concrete beams met the required percent air (as shown in Tables D.2 and D.3). If the concrete did not meet the percent air requirement the amount of air entraining admixture was adjusted and the mixture was batched again until the required percent air was met. Most concrete batches successfully met the air requirement in the first attempt. One mixture, using R-6 had to be batched several times before adequate air content was obtained.

The aggregate from source R-6 was made from recycled concrete (RCA) crushed from miscellaneous structures from Indianapolis Department of Public Works. It contained more fines and other waste products than any of the other RCA tested. Even after washing over a #200 sieve several times the amount of fines clinging to the aggregate particles was high and interfered with batching a mixture with acceptable air. Adequate air content was achieved once the air entraining agent was switched to a synthetic (Micro Air).

**TABLE D.1**  
**Mix Design Parameters and concrete materials**

Material	Proportion	Source
Cement	564 lb/yd <sup>3</sup> (335 kg/m <sup>3</sup> )	Type I Source 0002
Water/cement ratio	0.43	
Air content	6.5 $\pm$ 1.5%	Catexol VR air entraining admixture, Source No. 8273*
Coarse Aggregates (SSD)	Absolute volume of 0.40	
Fine aggregate	Specified gradation	No. 23 natural sand from Source 2310

\*Micro Air was used in the mixture with R-1 source as discussed in the text of this appendix.

**TABLE D.2**  
**Plastic concrete properties for ITM210 mixtures using quarried aggregate**

Aggregate source	Slump (in)	Air %	Aggregate source	Slump (in)	Air %	Aggregate source	Slump (in)	Air %
A1	2.5	6.25	B1	*	*	C1	1.75	6.5
A2	2.25	7.0	B2	2.5	7.5	C3	2.25	5.25
A3	1.25	6.25	B3	1.75	6.25	C4	1.5	4.5
A4	2.0	6.75	B4	2.5	6.25	C5	1.5	6.5
A5	1.25	6.25	B5	*	*	C6	2.25	6.25
A6	1.5	5.0	B6	2.25	5.75	C7	1.25	5.25

\*Mixtures passed ITM 210 requirements but specific values were not available.

**TABLE D.3**  
**Plastic concrete properties for ITM210 mixtures using RCA**

Aggregate source	Slump (in)	%Air
R-1	1.25	6.25
R-2	1	5.25
R-3	0.875	5.5
R-4	2	6.25
R-5	1.25	6.25
R-6	1.25	5.5

## APPENDIX E: REGRESSION MODEL DEVELOPMENT

Statistical analysis of all the test data included the development of regression models to predict the ITM210 results of percent dilation and durability factor from variables obtained from HFT results. Separate predictive models were developed for percent dilation and durability factors. The predictor variables (a.k.a. independent variables) were developed from the HFT results and the response variables (a.k.a. dependent variables) were the measured dilations and durability factors of the concrete test beams after 350 freeze-thaw cycles. The test results were analyzed and regression models developed using the statistical analysis software package JMP, developed by SAS.

This Appendix presents results of regression analysis of MnDOT HFT chamber results in Section E.1 and INDOT HFT chamber results in Section E.2.

### E.1 REGRESSION MODEL DEVELOPMENT FOR MNDOT HFT CHAMBER

A number of predictors were generated from the HFT results. From the different predictor variables considered the percent mass change (PCMR) on each sieve were developed as successful predictor variables. Eight predictor variables were obtained for each source designated as PCMR values (P34, P58, P12, P38, P516, P14, P4 and P0). Table E.1 shows an example of the HFT results and related PCMR values developed using the data from source B3 as an example. Equations E.1 through E.8 show the equations used to develop the PCMR values. A summary of the PCMR values developed from the MnDOT HFT results and freeze-thaw test results for all 18 aggregate sources are presented in Table 6.1. These values were used as model inputs. (All the HFT results are given in Appendix C.)

For example:

$$P34 = 100 * \frac{1048.6 - 1393.2}{1393.2} = -24.73$$

$$P14 = \frac{4.9 - 0}{10491.8} = 0.05$$

The following equations were used to develop the PCMR predictor variables:

$$P34 = 100 * (M50 - M0) / M0 \quad (E.1)$$

$$P58 = 100 * (M50 - M0) / M0 \quad (E.2)$$

$$P12 = 100 * (M50 - M0) / M0 \quad (E.3)$$

$$P38 = 100 * (M50 - M0) / MT \quad (E.4)$$

$$P516 = 100 * (M50 - M0) / MT \quad (E.5)$$

$$P14 = 100 * (M50 - M0) / MT \quad (E.6)$$

$$P4 = 100 * (M50 - M0) / MT \quad (E.7)$$

$$P0 = 100 * (M10 + M20 + M30 + M40 + M50) / MT \quad (E.8)$$

Where:

M50 is mass retained at 50 cycles on a particular sieve

M0 is initial mass retained at zero cycle on a particular sieve

MT is total mass at zero cycle

P0 is the sum of mass retained on pan from zero to 50 cycles

The data sets for all 18 sources were presented in Table 6.1. Separate models were developed for percent dilation and durability factors and are discussed under Sections 6.1.2 and 6.1.3.

#### E.1.1 Dilation Models Developed Using MnDOT HFT Results

The general linear regression model shown as Equation E.9 was used for all model development.

$$\begin{aligned} \text{Dilation} = & \beta_0 + \beta_1 P34 + \beta_2 P58 + \beta_3 P12 \\ & + \beta_4 P38 + \beta_5 P516 + \beta_6 P14 + \beta_7 P4 + \beta_8 P0 \end{aligned} \quad (E.9)$$

Where:

Dilation = Response variable = Percent dilation at 350 cycles

$\beta_i$  = Regression coefficients

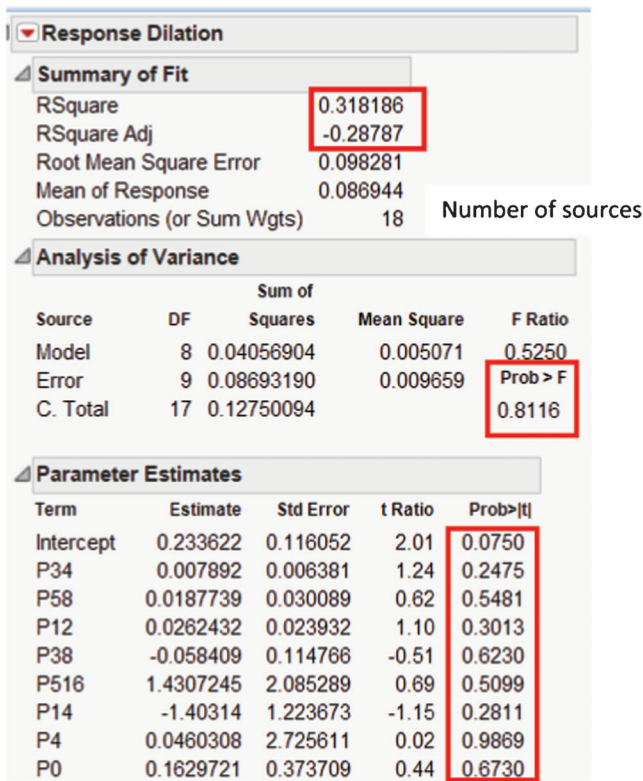
P34, P58, P12, P38, P516, P14, P4 and P0 are predictor variables.

**Model M1** All the eight predictors and corresponding data points (PCMR values) for all 18 sources (observations) were considered for analysis. The analysis of this model is summarized in Figure E.1.

If the P-value is <0.05 then there is a significant relationship between the predictor variables (PCMR values) and the response variable (in this case dilation). JMP puts an asterisks (\*) by the value if it is considered significant. The P-value for the model is

TABLE E.1  
Table shows an example of HFT results and related PCMR values (source B3)

	Mass (g)						Mass change after 50 cycles (g)	% Mass change (PCMR)	PCMR designation
	0 cycles (M0)	10 cycles (M10)	20 cycles (M20)	30 cycles (M30)	40 cycles (M40)	50 cycles (M50)			
3/4 in. sieve	1393.2	1103.4	1163.6	1133.9	1036.2	1048.6	-344.6	-24.73	P34
5/8 in. sieve	3652.6	3590.1	3539.8	3629.2	3578.2	3522.7	-129.9	-3.56	P58
1/2 in. sieve	5227.9	5438.7	5402.5	5291.3	5436	5476	248.1	4.75	P12
3/8 in. sieve	218.1	284.5	294.4	330.6	325.7	321.3	103.2	0.98	P38
5/16 in. sieve	0	0.8	3.1	2.3	3.7	3.6	3.6	0.03	P516
1/4 in. sieve	0	0	0	1.5	2.8	4.9	4.9	0.05	P14
#4 sieve	0	0.7	1.5	2.8	3.3	3.2	3.2	0.03	P4
Pan	0	6	6.6	6	3.2	4.7	26.5	0.25	P0
<b>Total mass</b>	<b>10491.8 (MT)</b>					<b>10385.0</b>			



**β values**

**Figure E.1** JMP output of Model M1.

listed under the Analysis of Variance section as Prob>F and the P-value corresponding to each predictor is listed in the last column under Parameter Estimates in JMP output. Model M1 has a P-value of 0.8116 which is >0.05 and an adjusted R<sup>2</sup> value of -0.2878 indicating Model M1 is not significant, the predictor variables and the dependent variable are less correlated, and none of the predictors are significant.

It appears from Figure E.2 and Table E.2 that sources B2, B5 and A4 are influential observations having studentized residual values close to 2 which is a conventional cut-off value used to detect influential observations.

**Model M2** Model M2 was developed by excluding the influential or outlying observations B2, B5 and A4 identified by the Model M1 analysis and re-analyzing the data. The resulting model M2 is summarized in Figure E.3. Unlike M1, M2 has a higher Adjusted R<sup>2</sup> (0.67), the model is significant (P value =0.0379, which is <0.05) and three predictors are significant (P34, P58 and P12).

**Model M3** Dropping the data input from the two most highly insignificant predictors (P516 and P38) from Model M2

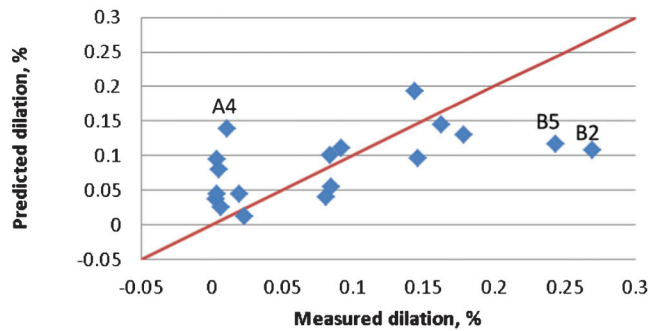


**Figure E.2** Predicted dilation versus measured dilation plot of Model M1.

resulted in an improved model (Model M3). Figure E.4 shows that Model M3 has a slightly improved adjusted R<sup>2</sup> value of 0.7135, it is a highly significant model (P-value =0.0081<0.05) with four predictors being significant, P34, P58, P12 and P4. It was observed that further removal of insignificant variables reduced the R-squared value so model M3 was considered as the best model that could be developed for this data set.

**E.1.2 Comparison of Dilation Models**

Ideally a perfect model will accurately predict the freeze-thaw behavior of an aggregate source. If a model predicts passing when the source actually fails freeze-thaw testing that model is considered unacceptable in this study because it puts the user at risk of building with concrete that fails prematurely. Such a model is not recommended. A model that predicts a source will fail when it actually passes freeze-thaw testing is considered a conservative model and may be considered with the caveat that the source should not be rejected until further testing is completed.

The predicted dilation for all aggregate sources using the three models developed in section E.1.1 are presented in Table E.3 and Figure E.5. Model M1 did not correctly predict five sources and predicted two of the 10 failing sources would pass. Because of the poor performance of M1 plus that fact that analysis indicates it is not a significant this model was not considered further. Both models M2 and M3 are significant with several significant predictor variables. Models M2 and M3 predicted the dilations accurately enough to predict pass/fail per INDOT’s specification of 0.060% dilation failure criteria, for all but one source for M2 (A4) and two sources for M3 (A4 and B3). Model M3 was considered highly significant, had a higher adjusted R<sup>2</sup> (suggesting a more stable model) and had more significant predictor variables than M2. Further testing of additional sources may delineate which model is better, but because of the relatively good predictive capabilities, higher stability and more significant predictors, M3 is the favored model at this time.

The recommended Model M3 is presented in Equation E.10 as follows:

**TABLE E.2**  
**Studentized residual values for all sources**

Source	Studentized residual	Source	Studentized residual	Source	Studentized residual
A1	-1.3	B1	1.5	C1	-1.2
A2	-0.5	B2	1.9	C3	0.9
A3	-0.3	B3	0.4	C4	-0.3
A4	-1.9	B4	0.6	C5	-0.5
A5	-1.1	B5	1.6	C6	0.2
A6	-0.3	B6	-0.2	C7	0.6

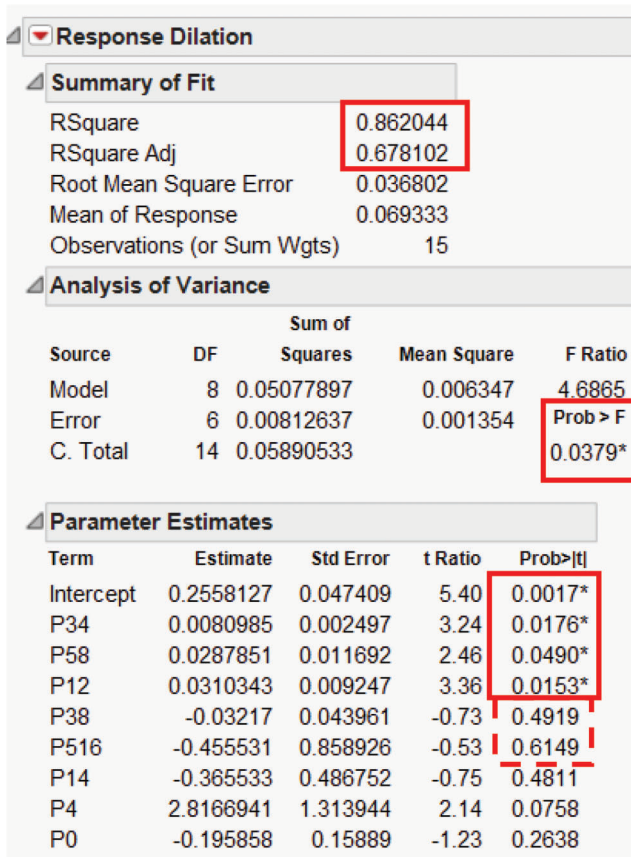


Figure E.3 JMP output of Model M2.

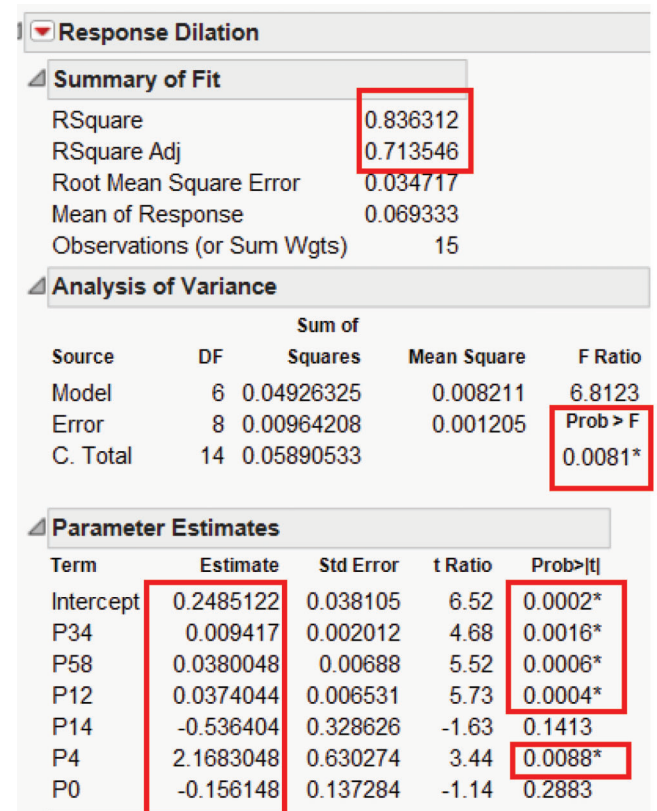


Figure E.4 JMP output of Model M3.

TABLE E.3  
Comparison of measured and predicted dilation

Source	Measured dilation	Predicted dilation by Model M1	Predicted dilation by Model M2	Predicted dilation by Model M3
A1	0.004	0.094*	0.034	0.042
A2	0.003	0.036	-0.021	-0.022
A3	0.007	0.025	-0.012	-0.020
A4	0.011	0.138*	0.197*	0.181*
A5	0.005	0.080*	-0.006	0.009
A6	0.020	0.044	0.039	0.042
B1	0.163	0.145	0.159	0.157
B2	0.270	0.108	0.065	0.068
B3	0.085	0.054*	0.073	0.057*
B4	0.179	0.129	0.148	0.133
B5	0.244	0.117	0.071	0.063
B6	0.084	0.100	0.081	0.077
C1	0.144	0.193	0.171	0.174
C3	0.146	0.096	0.103	0.126
C4	0.092	0.111	0.104	0.093
C5	0.004	0.044	0.039	0.042
C6	0.023	0.011	0.050	0.050
C7	0.081	0.041*	0.076	0.080

\*Incorrect prediction by the model per INDOT's pass/fail specification of 0.060% dilation.

$$\begin{aligned} \% \text{ Dilation} = & 2.49E-01 + 9.42E-03 * P34 \\ & + 3.80E-02 * P58 + 3.74E-02 * P125.36E \\ & - 01 * P14 + 2.17E+00 * P4 - 1.56E-01 * P0 \end{aligned} \quad (E.10)$$

With  $R^2=0.836$ ,  $R^2$  (adj.)= $0.714$ ,  $SEE=0.0347$ ,  $n=15$ , and Model P-value  $<0.0081$

### E.1.3 Durability Factor Models Developed Using MnDOT HFT Results

To predict the DF for the data presented in Table E.2, the general linear regression model presented in Equation E.11 was considered:

$$\begin{aligned} DF = & \beta_0 + \beta_1 P34 + \beta_2 P58 + \beta_3 P12 \\ & + \beta_4 P38 + \beta_5 P516 + \beta_6 P14 + \beta_7 P4 + \beta_8 P0 \end{aligned} \quad (E.11)$$

Where:

DF= Response variable = Durability Factor after 350 FT cycles

$\beta_i$ = Regression coefficients

P34, P58, P12, P38, P516, P14, P4 and P0 are predictor variables as previously described.

**Model M4** In this model all the predictors and data points and all 18 sources were considered for analysis. The JMP output is presented in Figure E.6. From this table it can be observed that the model had extremely low R squared value indicating that the DF was not correlated with HFT.

Other models were considered but had similar or worse correlations than M4. Therefore M4 is further analyzed as the best option.

$$\begin{aligned} DF = & 54.12 - 1.34E+00 * P34 - 3.25E \\ & + 00 * P58 - 4.08E+00 * P12 + 1.02E \\ & + 01 * P38 - 3.04E+02 * P516 + 3.40E \\ & + 02 * P14 - 2.50E+01 * P4 - 3.90E+01 * P0 \end{aligned} \quad (E.12)$$

Model statistics:  $R^2=0.19$ ,  $R^2$  (adj.)= $-0.53$ ,  $SEE=25.04$ ,  $n=18$  and Model P-value  $<0.9638>0.05$

The predicted DF for all sources using Model M4 are presented in Table E.4 and Figure E.7. If DF of 80%, 86% or 90% were used as acceptance criteria, Model M4 predicted the DF accurately

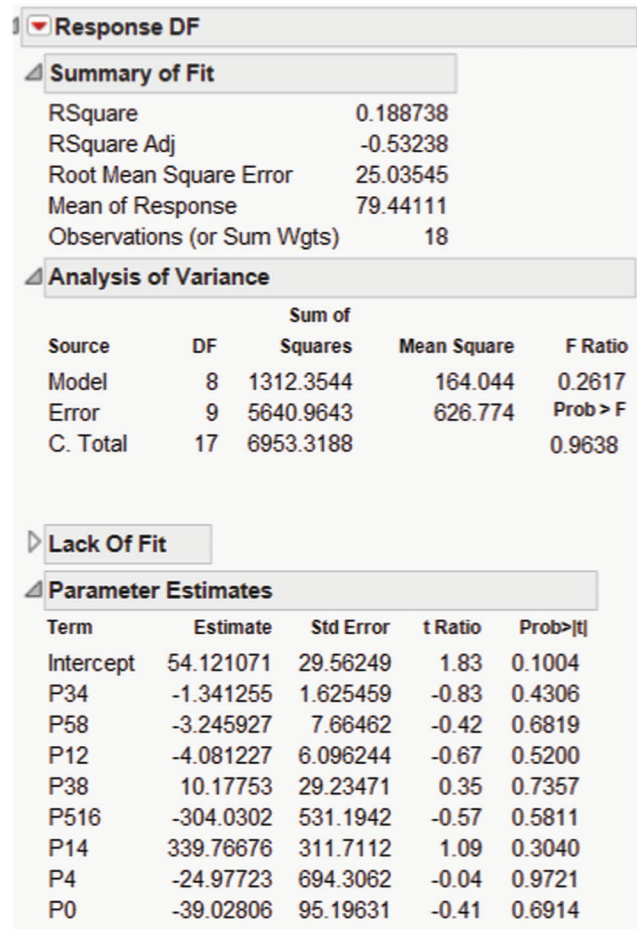


Figure E.6 JMP output of Model M4.

approximately 60% of the time, for all but five or six sources. An acceptance criterion of  $DF \geq 90\%$  would be needed with M4 in order to accurately predict all failing sources, however such a high acceptance criterion would exclude the use of about 30% of the good sources as well. This is a very conservative model, and the

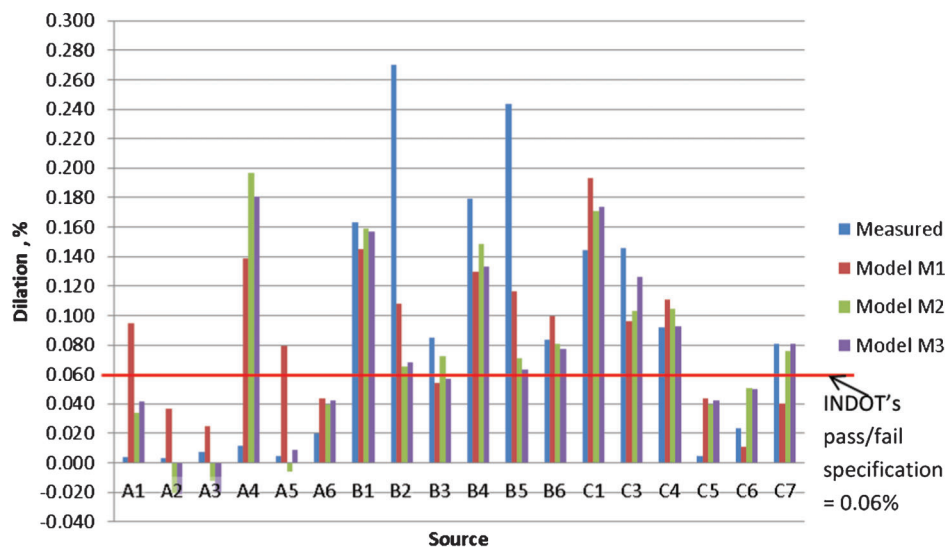


Figure E.5 Comparison of dilation models.

TABLE E.4  
Measured and predicted DF values for Model M4

Source	Measured DF	Predicted DF by Model M4	Accurate if acceptable DF $\geq 90$
A1	96.62	72.97	
A2	98.21	92.47	✓
A3	98.50	91.10	✓
A4	99.00	69.75	
A5	96.20	78.78	✓
A6	94.33	84.92	
B1	69.28	73.75	✓
B2	36.19	75.28	✓
B3	75.90	86.80	✓
B4	61.94	71.67	✓
B5	36.44	71.52	✓
B6	74.75	75.72	✓
C1	85.85	70.91	✓
C3	60.79	75.02	✓
C4	77.25	69.02	✓
C5	96.28	84.92	
C6	94.11	95.69	✓
C7	78.30	89.67	✓

JMP analysis indicates it is not a stable model (high P-value with non-significant predictors) and therefore is not recommended for use.

## E.2 MODELS DEVELOPED USING INDOT HFT RESULTS

HFT and freeze-thaw tests were completed for all aggregate samples selected from 18 sources and the summary of the data is presented in Table 6.3 (Chapter 6, Section 6.2). The net percent mass change (NMC) (i.e., mass change after 50 HFT cycles divided by the total sample mass on different sieves was calculated after 50 cycles. Initially a simple model was developed based on NMC on each sieve and compared to dilation. The trend line for the first 10 of 11 sources tested provided a good correlation between net mass change and dilation with an  $R^2$  value of 0.78. However, after testing all 18 sources and plotting the NMC versus

dilation for all 18 sources a trend was no longer apparent and a more sophisticated regression model with different predictors was needed. New predictor variables were developed from INDOT HFT results for each source and designated as PCMR values (P34, P58, P12, P38, P516, P14, P4 and P0) in the same way as described above in Section E.1 and Equations E.1–E.8 for the MnDOT HFT results. The PCMR values were used as predictors or independent variables and percent dilation and DF as response or dependent variables. The inputs were modeled with the aid of the statistical software package JMP. Separate models were developed for percent dilation and durability factors.

### E.2.1 Dilation Models Developed Using INDOT HFT Results

The generalized linear regression models given in Equation E.12:

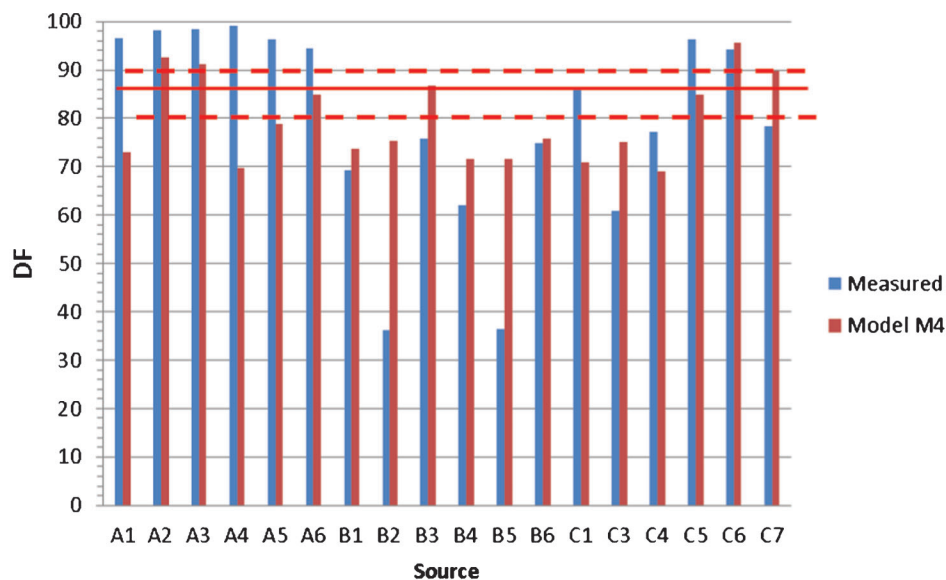


Figure E.7 Measured and predicted DF values.

$$\text{Dilation} = \beta_0 + \beta_1 P34 + \beta_2 P58 + \beta_3 P12 + \beta_4 P38 + \beta_5 P516 + \beta_6 P14 + \beta_7 P4 + \beta_8 P0 \quad (\text{E.12})$$

Where:

Dilation = Response variable = Percent dilation at 350 cycles  
 $\beta_i$  = Regression coefficients

P34, P58, P12, P38, P516, P14, P4 and P0 are predictor variables as described and calculated above.

**Model I1** Model I1 was developed using test results from all 18 aggregate sources and all predictors and the output for this model are given in Table E.9. If the P-value is <0.05 then there is a significant relationship between the predictor variables (PCMR values) and the response variable (in this case dilation). JMP puts an asterisks (\*) by the value if it is considered significant. The P-value for the model is listed under the Analysis of Variance section as Prob>F and the P-value corresponding to each predictor is listed in the last column under Parameter Estimates in JMP output (highlighted by a red box in Figure E.8). Model I1 has a P-value =0.0255 with an adjusted R<sup>2</sup> value of 0.59 indicating Model I1 is significant. However, only two predictors are significant (P14 and P4).

**Model I2** Model I2 is similar to Model I1 except that the two sources (A3 and B2) identified as outliers and the most insignificant predictors were excluded resulting in an improved model (see section E.2.2 for a detailed discussion on identifying outliers). Compared to Model I1, Model I2 contains more significant predictor variables and has a higher adjusted R<sup>2</sup> value of 0.853. The number of significant variables increased to four (P34, P38, P14, and P4), suggesting that these HFT results (predictor variables) correlate very well with the FT results

(response variables). This model is highly significant with a model P-value of 0.0001 (<0.05) indicating that the model is very stable. The JMP output of this model is displayed in Table E.10.

The formula for Model I2 is given in its general form in Equation E.13 and its more specific form as Equation E.14. The regression coefficients or  $\beta_i$  values for Model I2 are given in the Estimates column of the JMP output table under the Parameter Estimates section (Figure E.9). For Model I2  $\beta_0$  equals the intercept value, (0.0824663), and  $\beta_1$  is the regression coefficient for P34 (0.0063374), etc.

$$\text{Dilation} = \beta_0 + \beta_1 P34 + \beta_4 P38 + \beta_6 P14 + \beta_7 P4 \quad (\text{E.13})$$

Hence, Model I2 is:

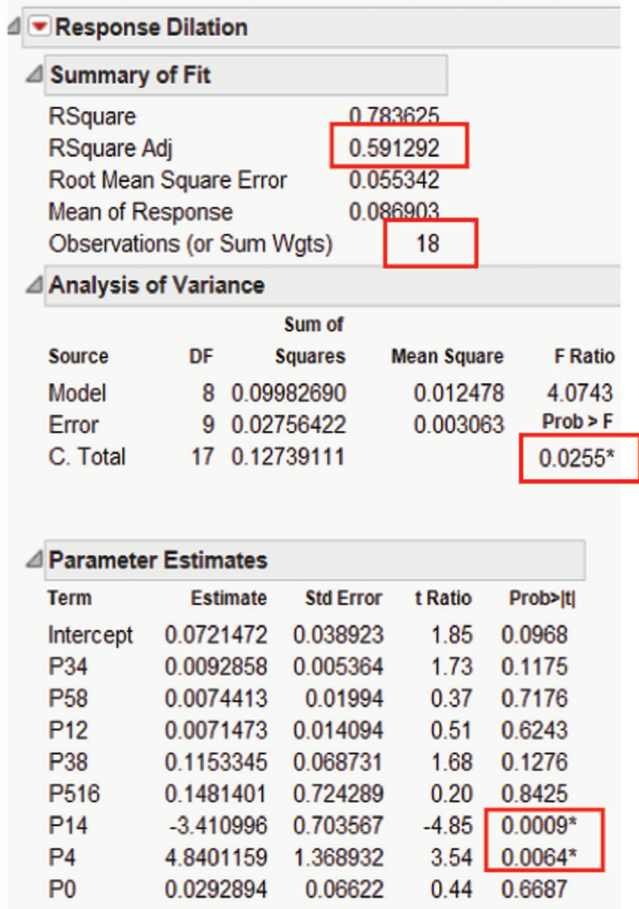
$$\text{Dilation} = 8.25E2 + 6.33E3 * P34 + 9.64E2 * P383.12 * P14 + 4.3 * P4 \quad (\text{E.14})$$

R<sup>2</sup>=0.89, adjusted R<sup>2</sup>=0.85 and n=16

Figure 6.4 shows the comparison of the actual measured dilation and dilation predicted by Model I2 and discussed further in Section 6.2.1.

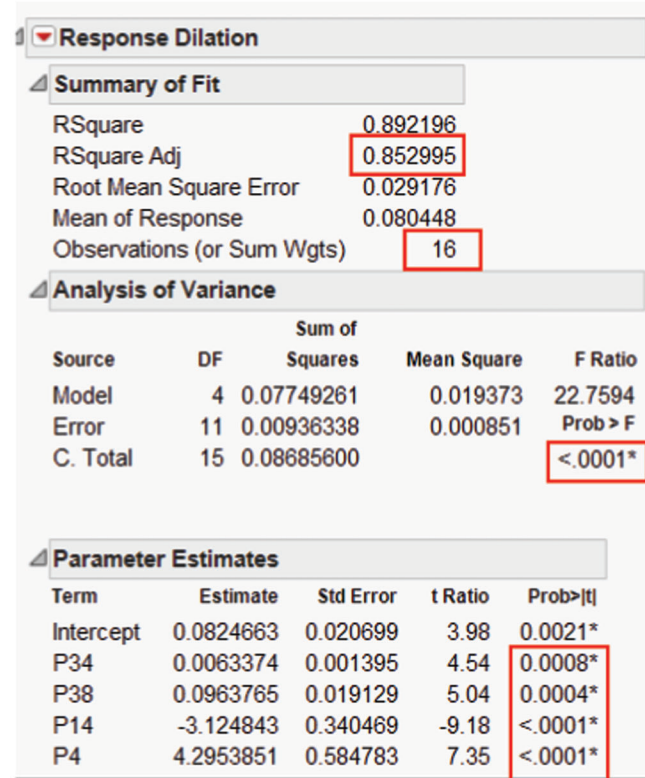
### E.2.2 Dilation Model Diagnostics

After fitting the regression models to the actual data, diagnostic tests were completed to determine whether the linear regression model assumptions were met. The assumptions which justify the use of linear regression models were linearity, independence, constant variance and normality. Linearity is detected from plots of the observed versus predicted values or a plot of residuals versus predicted values. The data points should be symmetrically distributed around a diagonal line. Normality can also be checked from scatter plots. There should be no quadratic relationship between the predictors and dependent variable. Violation of normality assumption is usually detected from normal probability



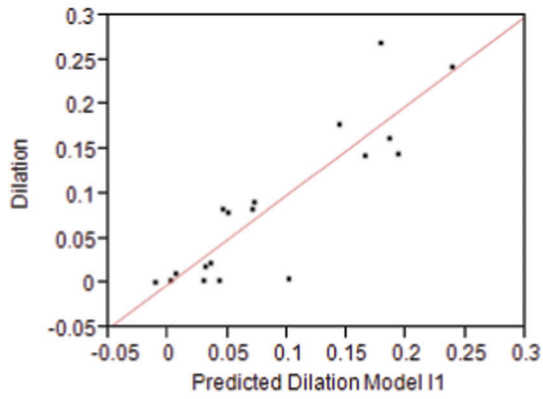
Response Dilation				
Summary of Fit				
RSquare				0.783625
RSquare Adj				0.591292
Root Mean Square Error				0.055342
Mean of Response				0.086903
Observations (or Sum Wgts)				18
Analysis of Variance				
Source	DF	Sum of Squares	Mean Square	F Ratio
Model	8	0.09982690	0.012478	4.0743
Error	9	0.02756422	0.003063	Prob > F
C. Total	17	0.12739111		0.0255*
Parameter Estimates				
Term	Estimate	Std Error	t Ratio	Prob> t
Intercept	0.0721472	0.038923	1.85	0.0968
P34	0.0092858	0.005364	1.73	0.1175
P58	0.0074413	0.01994	0.37	0.7176
P12	0.0071473	0.014094	0.51	0.6243
P38	0.1153345	0.068731	1.68	0.1276
P516	0.1481401	0.724289	0.20	0.8425
P14	-3.410996	0.703567	-4.85	0.0009*
P4	4.8401159	1.368932	3.54	0.0064*
P0	0.0292894	0.06622	0.44	0.6687

Figure E.8 JMP output of Model I1.



Response Dilation				
Summary of Fit				
RSquare				0.892196
RSquare Adj				0.852995
Root Mean Square Error				0.029176
Mean of Response				0.080448
Observations (or Sum Wgts)				16
Analysis of Variance				
Source	DF	Sum of Squares	Mean Square	F Ratio
Model	4	0.07749261	0.019373	22.7594
Error	11	0.00936338	0.000851	Prob > F
C. Total	15	0.08685600		<.0001*
Parameter Estimates				
Term	Estimate	Std Error	t Ratio	Prob> t
Intercept	0.0824663	0.020699	3.98	0.0021*
P34	0.0063374	0.001395	4.54	0.0008*
P38	0.0963765	0.019129	5.04	0.0004*
P14	-3.124843	0.340469	-9.18	<.0001*
P4	4.2953851	0.584783	7.35	<.0001*

Figure E.9 JMP output for Model I2.



**Figure E.10** Measured dilation versus predicted dilation by Model I1.

plot of the residuals and from histogram of residuals. The histogram of residuals should be bell-shaped. Outliers and influential points are usually detected using studentized residual.

As a rule of thumb, observation with a studentized residual of  $\pm 2$  is considered to be outliers. Violation of the assumption of constant variance is detected from the residual plot. The shape of this plot should not look like ‘megaphone’ (Zubery et al., 1997).

### E.2.2.1 Normality and Linearity

Model diagnoses were completed for Model I1 and I2 to see if the model assumptions were met and to detect outlier observations. The dilation versus predicted dilation for Model I1 is shown in Figure E.10 the data points are fairly distributed symmetrically around a diagonal line indicating that a linear model was appropriate.

Normality can also be checked from scatter plots. From the scatter plot shown in Figure E.11, it is apparent that there is no quadratic relationship between the predictors and dependent variable in this case dilation.

The normal probability plot and histogram of the residual dilations are shown in Figures E.12 and E.13 respectively. The two plots show that the distribution of the residuals is normal.

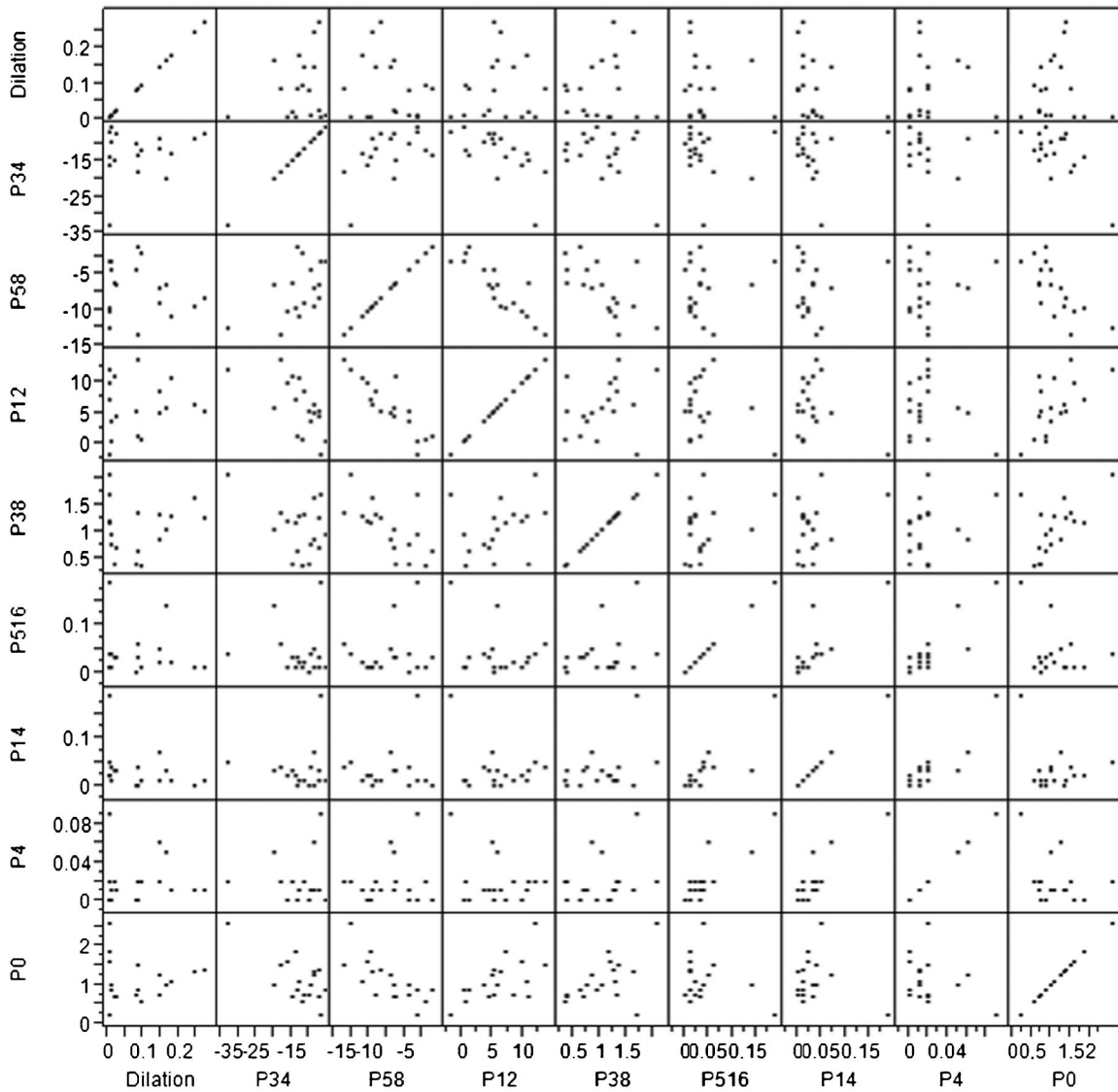


**Figure E.11** Scatter plot diagram.

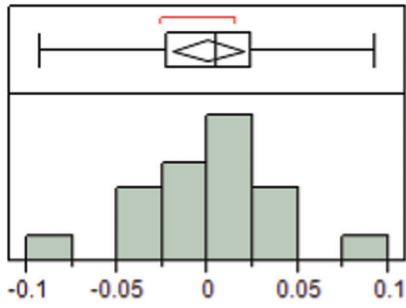


Figure E.12 Histogram of residuals for Model I1.

### E.2.2.2 Outliers

Outliers and influential points are usually detected using studentized residual. As a rule of thumb, observation with a studentized residual of  $\pm 2$  is considered to be outliers. The residual and studentized residual values of all data points are given in Table E.5. As indicated in the table source A3 and B2 are outlying observations. The relative location of outlier observations (A3 and B2) are shown in Figure E.14. It is clearly seen from the plots that the two sources are extreme observations. Model I2 was developed by excluding these outlier observations. The improvement in the residual plot is shown in Figure E.15.

Independence is not checked graphically or statistically rather it is experimental condition. HFT was done for all sources independently hence each observation is not dependent on any other data point. Hence all assumptions were met except that two sources (A3 and B2) are found to be outliers.

## E 2.3 Comparison of Dilation Models

Several other models were analyzed that considered various configurations, including and excluding various predictors, with and without outliers. Model I1 is presented as the initial model that considered all sources and all predictor variables. After several configurations were analyzed Model I2 was chosen as the best, most reasonable model because it was highly significant statistically, it considered several predictors and resulted in a high adjusted  $R^2$  value. The next step was to examine how useful each model would be for INDOT.

The predicted dilation for all sources using the two models are presented in Table E.6 and Figure E.16. Both models predicted the dialation acurately enough to predict pass/fail per INDOT's specification of 0.06% dilation failure criteria, for all but three sources (A3, B3 and C7). The models examined predicted failing dilation for A3, even though it clearly passed the FT test (0.007),

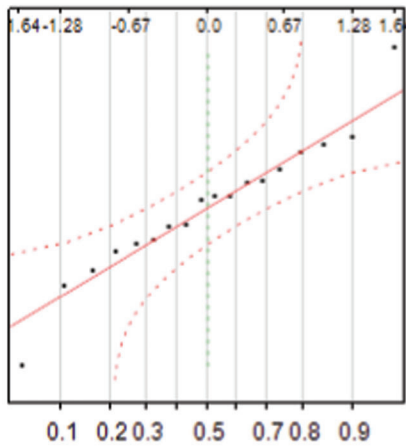


Figure E.13 Normal probability plot of residuals.

TABLE E.5  
Studentized residual for all aggregate sources

Source	Predicted dilation Model I1	Studentized residual
A1	0.029	-0.5
A2	-0.013	1.2
A3	0.100	-2.0*
A4	0.005	0.1
A5	0.042	-0.8
A6	0.031	-0.4
B1	0.185	-1.4
B2	0.177	2.0*
B3	0.044	1.0
B4	0.143	0.8
B5	0.238	0.1
B6	0.070	0.3
C1	0.164	-0.9
C3	0.192	-1.2
C4	0.071	0.7
C5	0.001	0.2
C6	0.035	-0.3
C7	0.049	0.6

\*Outlier observation.

and passing dilation for B3 and C7, even though they failed the FT test.

As displayed in Figure E.16, both models correctly predicted passing for all AP sources except A3 and failure for all B sources (known non-AP) except for B3. Also C7 is wrongly identified as an AP source by both models but clearly failed ITM 210. However, Model I2 is closer to predicting failure for B3 and C7 than Model I1. If the HFT acceptance criterion is set to  $\leq 0.05\%$  then Model I2 distinguishes all nondurable sources from durable sources as shown in Figure E.17.

## E.2.4 Durability Factor Models Developed Using INDOT HFT Results

To predict the DF the general linear regression model presented in Equation E.15 was considered:

$$DF = \beta_0 + \beta_1 P34 + \beta_2 P58 + \beta_3 P12 + \beta_4 P38 + \beta_5 P516 + \beta_6 P14 + \beta_7 P4 + \beta_8 P0 \quad (E.15)$$

Where:

DF= Response variable = Durability Factor

$\beta_i$ = Regression coefficients

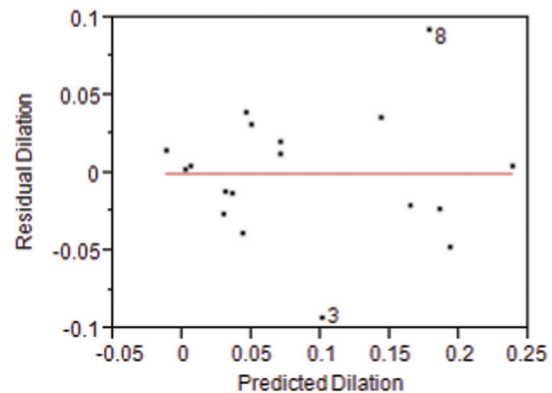


Figure E.14 Residual plot showing the location of outlier observations 3 (A3) and 8 (B2).

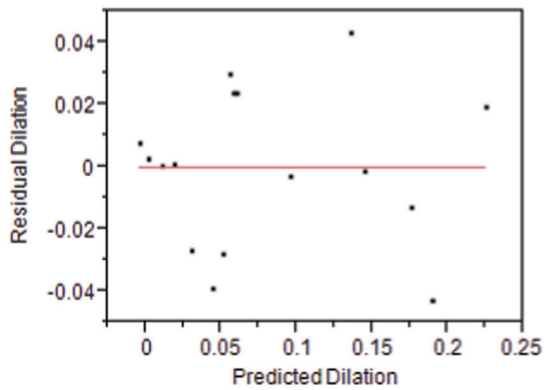


Figure E.15 Residual plot for Model I2.

P34, P58, P12, P38, P516, P14, P4 and P0 are predictor variables as described before.

**Model I3** In this model all sources and all predictors were considered. The JMP output is presented in Figure E.18.

The JMP output indicates that Model I3 is not significant (P-value = 0.0641, which is > 0.05) with an unimpressive adjusted  $R^2 = 0.4779$  and only one significant predictor (highlighted by red boxes in Figure E.18). This model was not considered for further analysis, but was used as a starting point for developing model I4.

**Model I4** Model I4 started out similarly as Model I3 but refined by dropping highly insignificant predictors, one by one, starting with the most insignificant variable. The number of significant predictors gradually increased from one to four, the adjusted  $R^2$  increased to 0.615 and the model became significant as shown in Figure E.19. The final form of Model I4 considered all sources and the significant predictors (P34, P38, P14, and P4).

**Model I5** In Model I5 all sources except the two outliers (A3 and B2) and all significant predictors were considered. (Outliers were identified in a similar manner as described in section E.2.2.2.) When the outliers (A3 and B2) are excluded from the analysis P0 became significant which was not significant in any of the previous models. As indicated in Figure E.20, this model is highly significant with a P-value of 0.0003, < 0.05, with an adjusted  $R^2$  value of 0.81.

## E.2.5 Comparisons of DF Models

Similar to the process shown in E.2.2.1 and E.2.2.2 Model diagnoses were completed for Model I4 and I5 to see if the model assumptions were met and to detect outlier observations. All assumptions were met.

The predicted DF for all sources using Model I4 and I5 are presented in Table E.7 and Figure E.21. If a DF of 86 is taken as a cut-off value, Model I5 distinguishes nondurable sources from durable sources with an exception of source A3.

TABLE E.6  
Measured and predicted dilation values

Source	Measured dilation, %	Predicted dilation Model I1, %	Predicted dilation Model I2, %
A1	0.0035	0.0292	0.0304
A2	0.0028	-0.0127	-0.0048
A3	0.0071	0.0998*	0.1068*
A4	0.0115	0.0054	0.0107
A5	0.0047	0.0422	0.0437
A6	0.0198	0.0305	0.0185
B1	0.1631	0.1852	0.1756
B2	0.2700	0.1770	0.1677
B3	0.0849	0.0444*	0.0551*
B4	0.1794	0.1430	0.1360
B5	0.2435	0.2377	0.2242
B6	0.0835	0.0701	0.0597*
C1	0.1440	0.1640	0.1450
C3	0.1458	0.1925	0.1887
C4	0.0922	0.0706	0.0950
C5	0.0044	0.0010	0.0015
C6	0.0232	0.0352	0.0508
C7	0.0809	0.0492*	0.0569*

\*Incorrect prediction by the Models per INDOT's pass/fail specification of 0.06% dilation.

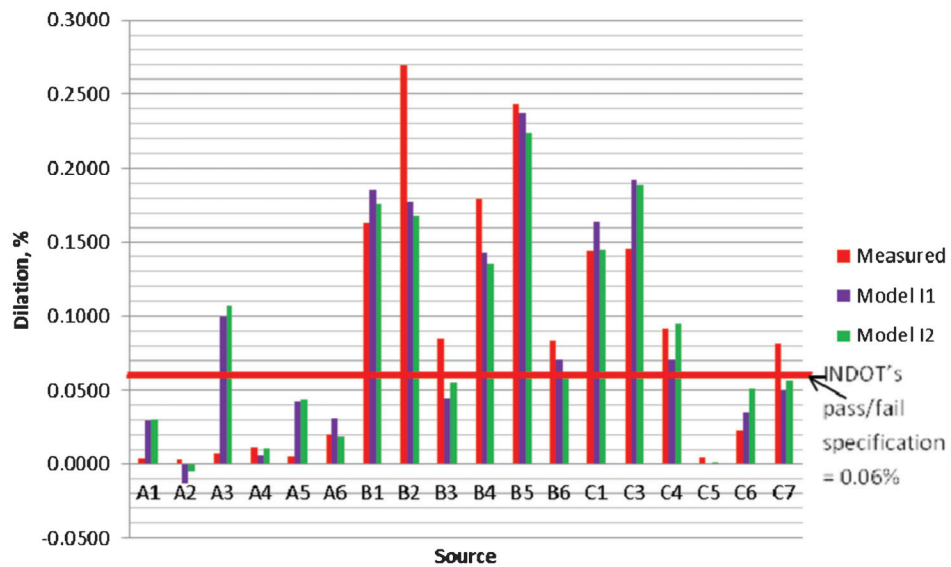


Figure E.16 Comparison of model outputs, measured dilations and the 0.06% dilation criteria.

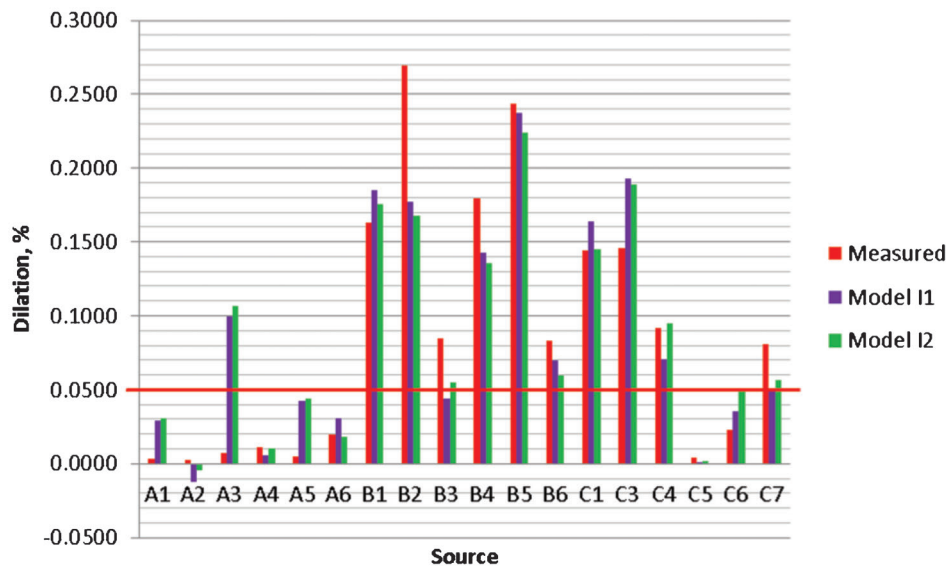


Figure E.17 Comparison of models with 0.05% dilation criteria.

**Response DF**

**Summary of Fit**

RSquare	0.723593
RSquare Adj	0.477899
Root Mean Square Error	14.61332
Mean of Response	79.44111
Observations (or Sum Wgts)	18

**Analysis of Variance**

Source	DF	Sum of Squares	Mean Square	F Ratio
Model	8	5031.3762	628.922	2.9451
Error	9	1921.9426	213.549	Prob > F
C. Total	17	6953.3188		0.0641

**Parameter Estimates**

Term	Estimate	Std Error	t Ratio	Prob> t
Intercept	82.007278	10.27795	7.98	<.0001*
P34	-1.627515	1.416454	-1.15	0.2802
P58	-1.286791	5.265203	-0.24	0.8124
P12	-1.334286	3.721744	-0.36	0.7282
P38	-34.93671	18.14894	-1.92	0.0864
P516	-25.53865	191.2534	-0.13	0.8967
P14	722.7497	185.7817	3.89	0.0037*
P4	-787.5899	361.4757	-2.18	0.0573
P0	4.7576207	17.48583	0.27	0.7917

Figure E.18 JMP output for Model I3.

**Response DF**

**Summary of Fit**

RSquare	0.705581
RSquare Adj	0.614991
Root Mean Square Error	12.54895
Mean of Response	79.44111
Observations (or Sum Wgts)	18

**Analysis of Variance**

Source	DF	Sum of Squares	Mean Square	F Ratio
Model	4	4906.1303	1226.53	7.7887
Error	13	2047.1885	157.48	Prob > F
C. Total	17	6953.3188		0.0020*

**Parameter Estimates**

Term	Estimate	Std Error	t Ratio	Prob> t
Intercept	83.985561	8.302299	10.12	<.0001*
P34	-1.503881	0.528411	-2.85	0.0138*
P38	-28.55475	7.721639	-3.70	0.0027*
P14	713.90884	143.6457	4.97	0.0003*
P4	-849.5036	247.6785	-3.43	0.0045*

Figure E.19 JMP output for Model I4.

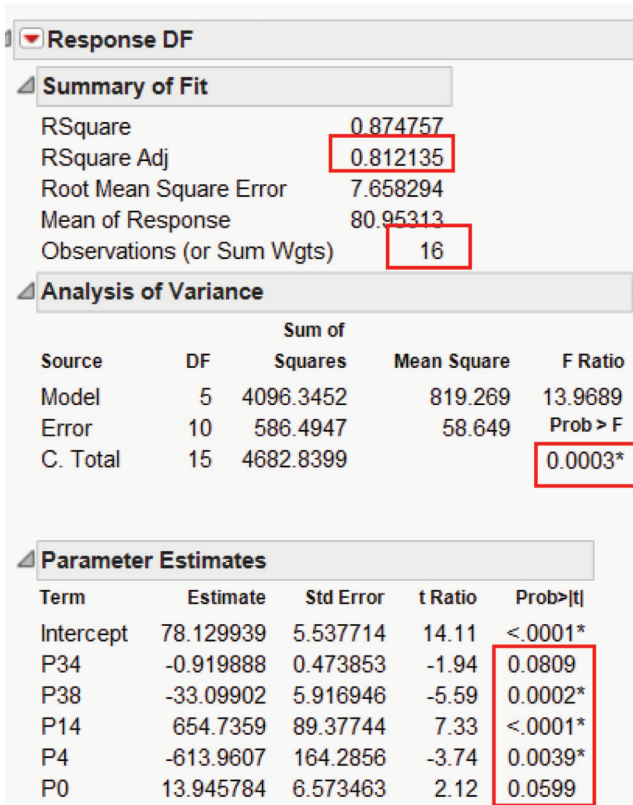


TABLE E.7  
Measured and predicted DF values

Source	Measured DF	Predicted DF Model I4	Predicted DF Model I5
A1	96.6	89.0	88.9
A2	98.2	105.1	100.4
A3	98.5	72.6*	70.8*
A4	99.0	97.3	96.0
A5	96.2	86.1	91.5
A6	94.3	99.5	95.8
B1	69.3	63.6	64.8
B2	36.2	58.1	63.4
B3	75.9	87.0	82.3
B4	61.9	65.4	63.1
B5	36.4	42.9	45.4
B6	74.8	84.0	85.1
C1	85.9	72.7	85.3
C3	60.8	54.5	50.2
C4	77.3	82.2	80.0
C5	96.3	93.5	96.4
C6	94.1	88.5	85.4*
C7	78.3	87.8	84.8

\*Incorrect prediction by the Models compared against DF=86.

Figure E.20 JMP output for Model 5.

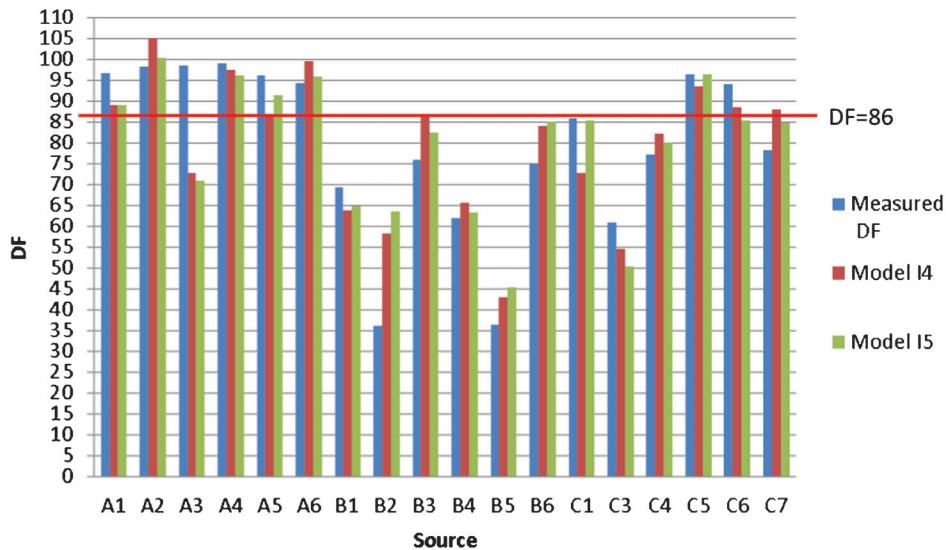


Figure E.21 Comparison of DF model outputs to actual DF measurements.

## APPENDIX F: RECYCLED CONCRETE AGGREGATE TESTING AND ANALYSES

### F.1 OBJECTIVE

Using recycled concrete aggregate (RCA) produced from crushed existing concrete in new concrete is becoming more widely accepted (Snyder, 2009). Previous research sponsored by INDOT has shown that RCA is a viable alternative for partial replacement of the coarse fraction of natural AP aggregate in new INDOT concrete paving mixtures (Verian, Whiting, Olek, Jain, & Snyder, 2013). However, often there is not enough lead time from when RCA is produced to when it is needed for a paving project to complete the ITM210 acceptance testing for AP aggregate (typically 90-days or more). This is especially true if the existing concrete pavement is a potential source for RCA for the new concrete being placed. If the HFT could be used to predict the freeze-thaw durability of RCA in less than two weeks, then the use of RCA in new concrete pavements becomes a much more feasible alternative.

The objective of this portion of the study was to determine if the HFT is a viable alternative for screening the freeze-thaw durability of RCA, and to gauge its potential for development as part of the INDOT acceptance criteria for RCA as coarse aggregate in concrete paving.

### F.2 RECYCLED CONCRETE AGGREGATE SELECTION

The availability of different RCA sources for this study was somewhat limited but with the help of INDOT and the concrete paving industry, six RCA sources from a variety of locations, concrete sources and producers were identified. Similar to the objectives used for collecting the natural aggregate sources, an attempt was made to collect crushed concrete as aggregate that would represent both freeze-thaw durable and nondurable aggregates.

The six RCA sources used in this study were produced from different concrete structures that had been removed from service, crushed by different producers and collected from different locations from around the state (as detailed in Table F.1). Five of the sources were crushed from INDOT highway pavements (R-1 through R-5) and one was a non-INDOT source, crushed from miscellaneous concrete infrastructure from Indianapolis Department of Public Works contracts and stockpiled near Indianapolis (R-6).

Generally RCA can be described as containing four types of particles: 1) original aggregate, 2) original aggregate with some amount of paste or mortar clinging to it, 3) mortar/paste and 4) other waste products. The presence of old paste and mortar usually decreases the specific gravity and increases the absorption of the RCA aggregate from what these properties were for the original aggregate (Issa & Bendok, 2000). The 'other waste products' most prevalent in RCA used in this project that were produced from crushed concrete pavements included some amount of asphalt. However if the RCA comes from a 'mixed-

use' stockpile, or is not handled carefully then a number of waste products in addition to asphalt are possible including brick, steel, wood, soil and more.

Estimating the percentage of old paste and mortar, asphalt and other waste products that an RCA source contains may provide valuable insights into the properties of the RCA that relates to its performance, but that work was beyond the scope of this study.

All the RCA sources used in this study had some amount of asphalt particles. R-6 also contained pieces of wood, soil, and other contaminants. Any obvious contaminants were removed from the RCA sample before testing, but trace amounts of asphalt particles remained. R-6 had more fines clinging to the aggregate particles than the other RCA sources and was washed several times before used in testing or in batching ITM210 concrete beams (additional details are provided in Appendix D). Other than HFT and ITM 210 freeze-thaw testing, the specific gravity and percent absorption were measured for each aggregate source.

The original aggregate in five of the six RCA sources was gravel (as shown in Table F.1). One of these five sources, R-6, had a mix of gravel and a limited amount of crushed carbonate aggregate. One RCA source had crushed carbonate rock as the original aggregate (R-5).

### F.3 AGGREGATE TEST RESULTS

#### F.3.1 Specific Gravity and Absorption

The bulk specific gravity and the percent absorption were measured according to AASHTO T85 for each RCA source using a gradation that reflected the gradation used in batching the ITM 210 concrete beams (as shown in Table 3.2). As is common for RCA, the specific gravity tended to be lower and the absorption higher than for many natural aggregates. As shown in Table F.2, the bulk specific gravity at SSD conditions shown in ranged from 2.387 to 2.471, all of which were lower than any of the 18 sources of natural carbonate quarried aggregates tested (given in Table 5.1). The percent absorption for the RCA ranged from 2.9% to 5.1%, which is higher than 15 of the 18 carbonate quarried aggregate sources but very similar to the absorption of three of the carbonate quarried aggregate sources tested.

#### F.3.2 INDOT HFT Chamber Results

The Hydraulic Fracture Test (HFT) was performed on samples of all six RCA sources using INDOT's HFT equipment and procedure described in Section 3.2.5. The HFT results were used to calculate the percent change of mass retained on each sieve (PCMR). The PCMR is the change in mass on each sieve from before any testing (0 cycles) to after 50 cycles of testing, divided by the initial mass. For the 3/4 in., 5/8 in. and 1/2 in. (P34, P58 and P12) the change in mass from 0 to 50 cycles was divided by the initial mass on that sieve. For the sieves smaller than 1/2 in., that had no initial mass, the mass on each sieve after 50 cycles is divided by the total initial mass (see Appendix E for additional details and equations for developing PCMR). These PCMR values (P34, P58, P12, P38, P516, P14, P4, and P0) relate to the

TABLE F.1  
Sources of recycled concrete for RCA

Source No.	Location		Structure	Original aggregate type
	Nearest city	District		
R-1	Lafayette, IN	Crawfordsville	SR26 INDOT pavement	Gravel
R-2	Lafayette, IN	Crawfordsville	US 52 INDOT pavement	Gravel
R-3	Lebanon, IN	Crawfordsville	I-65 INDOT pavement	Gravel
R-4	Elkhart, IN	Fort Wayne	SR19 INDOT pavement	Gravel
R-5	Gary, IN	Laporte	SR912 INDOT pavement	Crushed carbonate rock
R-6	Indianapolis, IN	Greenfield	Misc structures from Indianapolis Dept. of Public Works	Primarily gravel, some crushed carbonate rock

TABLE F.2  
RCA properties

Source No.	Specific gravity (SSD)	Absorption %
R-1	2.471	3.63
R-2	2.457	2.91
R-3	2.445	4.34
R-4	2.387	5.14
R-5	2.430	4.04
R-6	2.432	4.77

mass change on the 3/4 in., 5/8 in., 1/2 in., 3/8 in., 5/16 in., 1/4 in., #4 sieves and in the pan, respectively, and were used as model inputs to predict freeze-thaw results of percent dilation or durability factor. A summary of the HFT result is presented in Table F.3.

#### F.4 CONCRETE FREEZE-THAW TEST RESULTS

All six RCA sources were tested for FT durability using ITM 210. Mix design, materials and plastic concrete properties are detailed in Appendix D. Dilation and durability factor for R-1 through R-5 were measured at 350 cycles of freezing and thawing, per ITM 210 requirements. For R-6, two of the three beams broke prior to 350 cycles and the dilation of the third specimen was unusually high. The measurements of the fundamental transverse frequency became so erratic that a sound reading could not be obtained after 336 cycles in order to calculate the durability factor. Therefore dilation and durability factor at 350 cycles for this source were estimated by extrapolation of the average readings before specimen 2 and 3 broke, as shown in Figures F.1 and F.2.

All RCA sources except R-6 met INDOT's acceptance criteria of  $\leq 0.060\%$  expansion and are considered FT durable (as shown in Figure F.3). These same five sources all had a DF of 88 or higher. Source R-6 failed the INDOT criteria with an estimated dilation of 0.64% and had a very low estimated DF of 30.

#### F.5 REGRESSION MODEL DEVELOPMENT

The model inputs developed from the RCA test data were plugged into the HFT models developed from the 18 natural aggregate sources and described in Chapter 6. The HFT model outputs did not match the measured data for the RCA materials, as shown in Table F.4. When the measured values were plotted against modeled values, there were no linear trends (R-squared values  $< 0.01$ ). Hence the models developed for the natural aggregate sources did not accurately predict RCA freeze-thaw durability. It is not surprising that the models for natural aggregate did not work for crushed concrete because of the much softer nature of reclaimed mortar and the likelihood that some particle "pre-fracturing" is likely in RCA due to the crushing process. These differences between RCA and natural aggregate

TABLE F.3  
Summary of HFT and freeze-thaw test results used as model inputs

RCA source	Response variables		Predictor variables							
	Freeze-thaw test result		HFT result (PCMR values)							
	Dilation	DF	P34	P58	P12	P38	P516	P14	P4	P0
R-1	0.019	98.4	-14.39	-8.27	5.60	1.39	0.07	0.08	0.06	1.51
R-2	0.006	99.6	-27.46	-7.82	7.68	1.24	0.09	0.14	0.06	2.49
R-3	0.040	94.2	-10.41	-10.29	6.38	1.21	0.15	0.09	0.06	1.80
R-4	0.006	88.4	-19.24	-15.55	6.01	2.44	0.08	0.10	0.07	2.27
R-5	-0.002	96.0	-17.60	-5.50	6.03	1.03	0.05	0.03	0.04	1.67
R-6	0.640	30.0	-21.56	-11.60	8.74	1.75	0.18	0.17	0.12	2.82

would result in very different particle size redistribution during the HFT testing process. Therefore new models needed to be developed exclusive to the RCA data.

The RCA test data was analyzed statistically and regression models were developed to predict percent dilation and durability factor from the HFT results. Separate predictive models were developed for percent dilation and durability factors. The test results were modeled using the statistical analysis software package JMP, developed by SAS.

#### F.5.1 Dilation Models

The predictive model considered is shown in Equation F.1

$$\text{Dilation} = \beta_0 + \beta_1 P34 + \beta_2 P58 + \beta_3 P12 + \beta_4 P38 + \beta_5 P516 + \beta_6 P14 + \beta_7 P4 + \beta_8 P0 \quad (F.1)$$

Where:

Dilation = Percent dilation at 350 cycles

$\beta_i$  = Regression coefficients

P34, P58, P12, P38, P516, P14, P4 and P0 are percentages of mass change on various sieve sizes, as described in section F.3.2.

This model has eight predictor variables and nine regression constants ( $\beta_0$  to  $\beta_8$ ). To determine nine regression constants, a minimum of nine observations are needed. In this model each observation is a different RCA source and only six observations are available (i.e., only six RCA sources were tested). It is not possible to determine nine constants with only six observations; there are not enough degrees of freedom. One solution was to reduce the number of predictor variables, which means using a reduced model.

A reduced model has lower predictive power, but it was determined that this was the best option for creating models based on the data available. The results from the four coarser sieve sizes (3/4 in., 5/8 in., 1/2 in. and 3/8 in.) were used to develop PCMR values (P34, P58, P12 and P38) as predictor variables for this modeling. The rationale behind this approach was that the coarser aggregate is more readily affected by the stresses induced by both cyclical freezing and thawing and the HFT, and would be more influential in the development of a predictive model than the smaller sized material.

**Model RCA1** The four predictors used in this model to predict the dilation from the HFT results, P34, P58, P12 and P38, are included in the model shown in Equation F.2

$$\text{Dilation} = -1.447 + 4.65E - 02P34 + 1.21E - 01P58 + 3.29E - 01P12 + 9.24E - 01P38 \quad (F.2)$$

The JMP output of this model is shown in Figure F.5. As it can be seen from this table, the adjusted  $R^2$  is 0.9978, and the model is significant and all predictors are significant. This model successfully predicts dilation from HFT results. The predicted versus measured dilation plot seen in Figure F.6 shows a very good correlation.

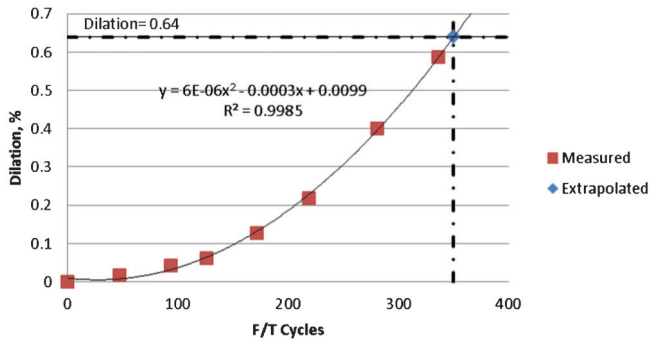


Figure F.1 Dilation versus FT cycles for source R-6.

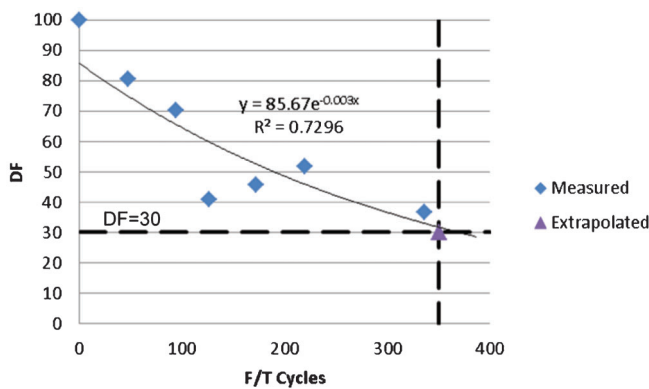


Figure F.2 DF versus FT cycles of RCA.

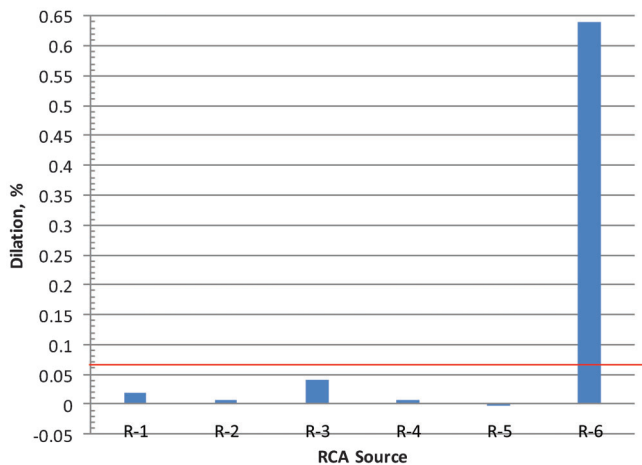


Figure F.3 Plot of dilation compared against INDOT's acceptance criteria.

TABLE F.4. Measured and predicted values for dilation and DF using models developed from testing quarried carbonate sources

Source	Dilation		DF	
	Measured	Predicted	Measured	Predicted
R1	0.019	0.134	98.4	82.0
R2	0.006	-0.151	99.6	72.9
R3	0.04	0.110	94.2	16.7
R4	0.006	0.185	88.4	-8.9
R5	-0.002	0.149	96	-32.6
R6	0.64*	0.100	30*	38.9

\*Based on extrapolation of the data measured up to 336 cycles.

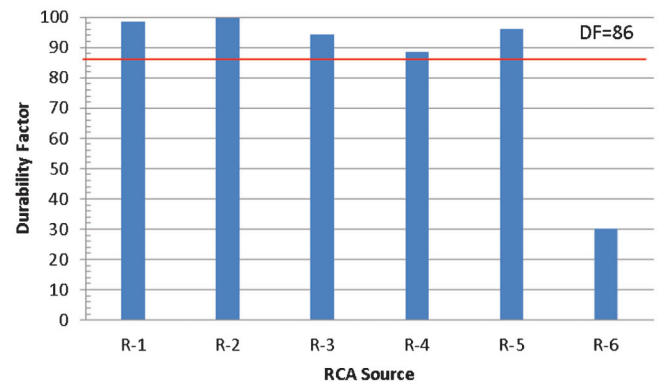


Figure F.4 Plot of durability factor results of RCA.

**Response Dilation**

**Summary of Fit**

RSquare	0.999557
RSquare Adj	0.997787
Root Mean Square Error	0.012046
Mean of Response	0.118167
Observations (or Sum Wgts)	6

**Analysis of Variance**

Source	DF	Sum of Squares	Mean Square	F Ratio
Model	4	0.32771173	0.081928	564.6252
Error	1	0.00014510	0.000145	Prob > F
C. Total	5	0.32785683		0.0316*

**Parameter Estimates**

Term	Estimate	Std Error	t Ratio	Prob> t
Intercept	-1.446811	0.035603	-40.64	0.0157*
P34	0.0464616	0.001726	26.91	0.0236*
P58	0.1210935	0.006272	19.31	0.0329*
P12	0.3291131	0.007508	43.84	0.0145*
P38	0.9238546	0.042741	21.61	0.0294*

Figure F.5 JMP output of Model RCA1.

TABLE F.5  
Measured and predicted dilation and DF using models developed from RCA test results

Source	Dilation		DF	
	Measured	Predicted	Measured	Predicted
R1	0.019	0.010	98.4	98.8
R2	0.006	0.004	99.6	98.6
R3	0.04	0.041	94.2	95.5
R4	0.006	0.008	88.4	89.2
R5	-0.002	0.006	96.0	94.6
R6	0.64	0.640	30.0	30.0

### F.5.2 Durability Factor Models

In this model four predictors are used to predict the DF from the HFT results. The assumptions used in choosing the predictors is that the coarser aggregate is more responsive to both FT and HFT testing, therefore the changes in mass on coarser sieves better predict the freeze thaw resistance of the RCA. The coarser sieves included in this study are 3/4 in., 5/8 in., 1/2 in. and 3/8 in. Therefore P34, P58, P12 and P38 were selected as predictor variables in the model, as shown in Equation F.3.

$$DF = \beta_0 + \beta_1 P34 + \beta_2 P58 + \beta_3 P12 + \beta_4 P38 \quad (F.3)$$

Where:

DF= Response variable = Durability Factor after 350 FT cycles

$\beta_1$ = Regression coefficients

P34, P58, P12, P38 are predictor variables.

**Model RCA2** The output of Model RCA2, which is presented in Figure F.7, had an adjusted  $R^2$  value of 0.9629; however JMPs advanced statistical analysis indicated that the model and the predictors are not significant. If the P-value is  $<0.05$ , then there is a significant relationship between the predictor variables (PCMR values) and the response variable (in this case DF). JMP puts an asterisks (\*) by the value if it is considered significant. The P-value for the model is listed under the Analysis of Variance Section as Prob>F and the P-value corresponding to each predictor is listed in the last column under Parameter Estimates in JMP output. Model RCA2 has a P-value of 0.0.1012 which is much greater than 0.05, indicating that Model RCA2 is not significant, and the P-value for three of the predictors are greater than 0.05, indicating that they are not significant.

The predicted versus measured DF plot presented in Figure F.8 shows very good correlation.

### F.5.3 Summary and Discussion of the Models

The dilation and DF models were developed using only six RCA sources, which is a very small data pool for the development of a generic model. As previously discussed, the limited number of observations (sources) available for analysis limited the number of HFT test outputs (predictor variables) that could be considered to develop models. This raises doubts as to whether the developed models considered all of the HFT results that may be important in predicting durability.

The range of freeze-thaw test results for the five durable RCA sources did a fairly good job representing the range of values considered durable (as shown in Table F.5). The dilation values for the five durable RCA sources ranged from -0.002 to 0.040 (all within INDOT's  $<0.06$  specification) and the DF ranged from 99.6 to 88.4.). However, no marginally durable sources were tested, and there was only one nondurable source tested, which had extraordinarily high dilations and low DF. This strongly bi-model data set leaves a big gap in the data that was unrepresented, with no data representing either mid-range values or marginal material.

### F.6 CONCLUSIONS

The RCA testing and model development show that RCA is responsive to testing in the HFT, and that those responses can be measured using the procedures developed for carbonated quarried aggregates. However the models developed for predicting freeze-thaw durability of the carbonated quarried aggregates cannot be used to predict the freeze-thaw durability of RCA.

Preliminary modeling shows promise that a reliable model can be developed that predicts ITM210 freeze-thaw durability using HFT results. However, the new models developed for RCA are very preliminary and more data from additional sources are needed to validate or refine these models. Additional RCA sources that fail FT testing, sources that have marginal freeze-thaw performance and sources that fail the FT testing with mid-range values for dilation and DF need to be tested both in ITM 210 and in the HFT with the test results used for further model development.

At this time both the predictive models developed are considered very preliminary. It is recommended that the dilation model presented in Equation F.2 be used for research and preliminary screening purpose only. Further HFT and FT testing of additional RCA sources that represent a greater spectrum of FT performance is needed to improve these models prior to using as part of the acceptance criteria for RCA as coarse aggregate in INDOT concrete paving projects.

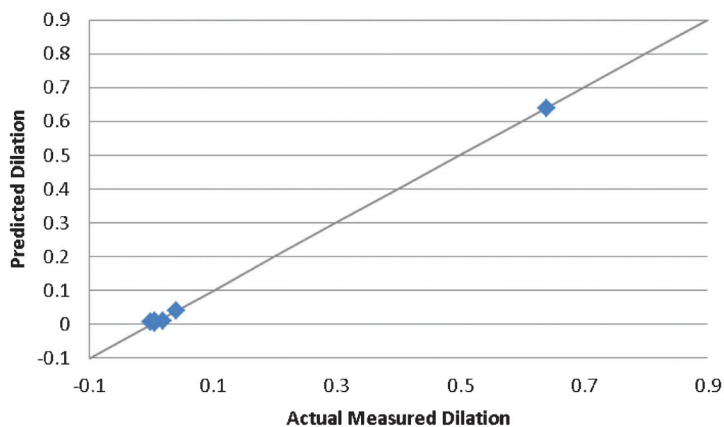


Figure F.6 Measured versus predicted dilation for Model RCA1.

**Response DF**

**Summary of Fit**

RSquare	0.995435
RSquare Adj	0.977174
Root Mean Square Error	4.072547
Mean of Response	84.43333
Observations (or Sum Wgts)	6

**Analysis of Variance**

Source	DF	Sum of Squares	Mean Square	F Ratio
Model	4	3616.4077	904.102	54.5111
Error	1	16.5856	16.586	Prob > F
C. Total	5	3632.9933		0.1012

**Parameter Estimates**

Term	Estimate	Std Error	t Ratio	Prob> t
Intercept	252.39213	12.03703	20.97	0.0303*
P34	-4.841985	0.58367	-8.30	0.0764
P58	-12.79037	2.12037	-6.03	0.1046
P12	-33.56328	2.538217	-13.22	0.0481*
P38	-103.8944	14.45037	-7.19	0.0880

Figure F.7 JMP output of Model RCA2.

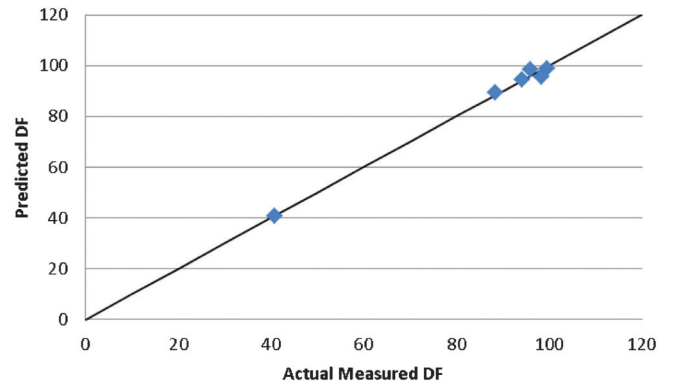


Figure F.8 Measured versus predicted dilation for Model RCA2.

## APPENDIX G: INDOT HFT EQUIPMENT AND MODIFICATIONS

### G.1 MODIFICATIONS TO INDOT CHAMBER

Prior to any modifications to the INDOT chamber the ownership of the equipment was established and legally transferred to Purdue (see Figure G.1). As with most projects, the HFT equipment developed under this SPR projects using INDOT SPR funds will be transferred to INDOT upon completion of the project.

The schematics developed by the Purdue Machine Shop for the new HFT lid are shown in Figure G.2 and Figure G.3. Figure G.4 is a conceptual view of a cross-section of the inside of the lid with the angle of the slope highly exaggerated.

### G.2 CURRENT INDOT HFT EQUIPMENT

The following are detailed descriptions of the existing INDOT HFT equipment that was used for testing in this study. Figure 3.10 is repeated here as Figure G.5 for the reader's convenience.

**Pressure chamber assembly** The pressure chamber assembly is connected to the water supply and drainage lines and associated valves. The bottom of the pressure chamber assembly is firmly attached to the table stand by four bolts.

**Lid assembly** The lid assembly includes the chamber lid, excess fill water drain valve and line, chamber pressure line and valve, ball valve, actuator pressure valve, and pressure line for actuator, actuator switch, and exhaust pipe. Inside of lid has an O-ring to seal the pressure chamber assembly to prevent leakage of air and water when the chamber is pressurized. The inside surface of the top assembly is slightly conical with highest point at the exhaust opening—trapped air (if any) will immediately escape upon release of pressure.

**Water supply and drainage assembly** The water supply line connects the pressure chamber to a water source and the drainage line is connected to the chamber and drains water to a bucket after test is completed. The connections of these lines are controlled by three valves, A, B, and C (as shown in Figure G.6).

**Pressure transducer** A small pressure transducer is installed in water supply and drainage assembly as shown in Figure G4 and G5. The transducer is used in calibrating the pressure release rate of the chamber.

**Chamber pressure gauge** This gauge is attached directly to the pressure chamber. It measures the pressure in the chamber as shown in G.4. This gage is important to check the actual pressure the aggregate specimen is experiencing during testing.

**Fill overflow line** Excess water from the chamber will drain out through this line and is controlled by a drain valve (Valve D, shown in Figure G.6). This valve is closed before the chamber is pressurized.

**Pressure release assembly** This assembly consists of an electrically-operated pneumatic actuator, ball valve, electric switch (to trigger the actuator) and pressure line to supply nitrogen to operate the actuator (see Figure G.5). The pneumatic actuator is mounted on the lid assembly in a cross type of connection and operates the ball valve. When the electric power switch is triggered, the actuator opens the ball valve through bursts of pressurized nitrogen gas.

**Exhaust line** When the ball valve is opened rapidly during depressurization, water and nitrogen gas is released from the chamber through the exhaust line. As shown in Figure G.8, the exhaust pipe extends up to the ceiling. It then extends across the room about 30 ft. (9 m) and down into a bucket on the floor.

**Nitrogen cylinders and pressure regulators** The pressure required to pressurize the HFT chamber is supplied from a high-pressure compressed nitrogen cylinder. The pressure supplied to the chamber is controlled by the pressure regulator attached to the cylinder (Regulator 1) and a valve (Valve E) attached on lid assembly. Valve E remains open during the pressurization cycle and must be closed before the pressure is released. The pressure required to operate the pneumatic actuator is supplied from the low-pressure nitrogen cylinder and is regulated by the pressure regulator (Regulator 2) attached on the cylinder (Figure G.8).

**Slide table** The slide table shown in Figure G.8 is used to place the lid assembly onto when removed from the chamber body. Figure G.9 shows the lid assembly off the chamber body resting on the slide table.

**Martin Marietta Aggregates**



**Indiana District Quality Control**

4700 East 96<sup>th</sup> Street  
Indianapolis, IN 46240  
Telephone (317) 846-5942 ext. 102

March 19, 2012

Mr. Bob Rees  
Indiana Department of Transportation  
Office of Materials Management  
120 S. Shortridge Rd.  
Indianapolis, IN 46219

Re: Donation of Hydraulic Fracture Testing Apparatus

Dear Mr. Rees,

In the spirit of continued research and development in the area of aggregates technology, Martin Marietta Materials releases ownership of the Hydraulic Fracture Testing (HFT) apparatus currently being used by Purdue Research for SPR 3402. Ownership is freely given to Purdue University. Martin Marietta Materials is not liable for any engineering or changes to the apparatus, and is released from all liability as a result of the use of this apparatus.

Thank you for the opportunity to assist in this important research.

Sincerely,

Scott A. Woodard  
Quality Assurance Supervisor, Indiana District

File

**Figure G.1** Letter transferring ownership of the HFT equipment to Purdue.

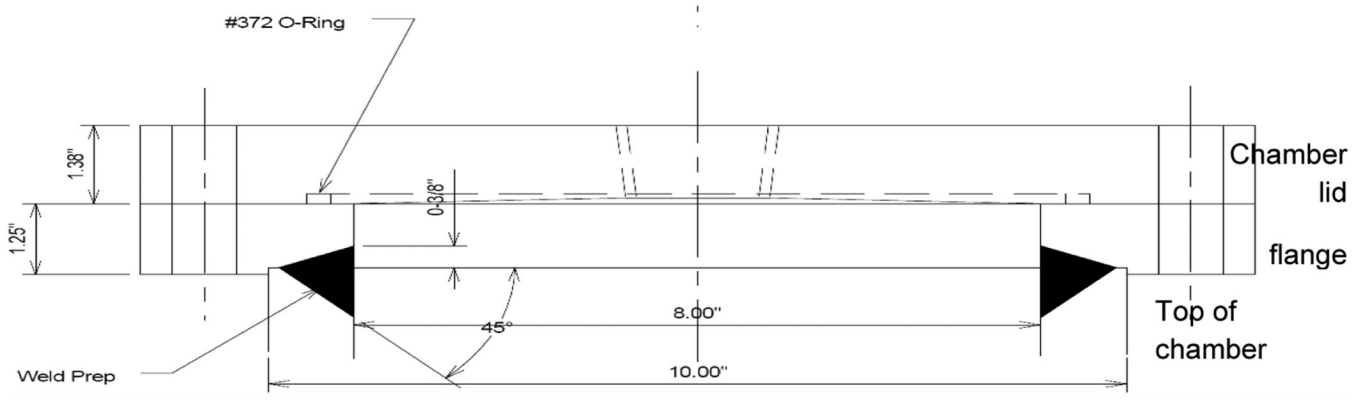


**Figure G.2** Schematic side view of the top of the modified INDOT HFT chamber.

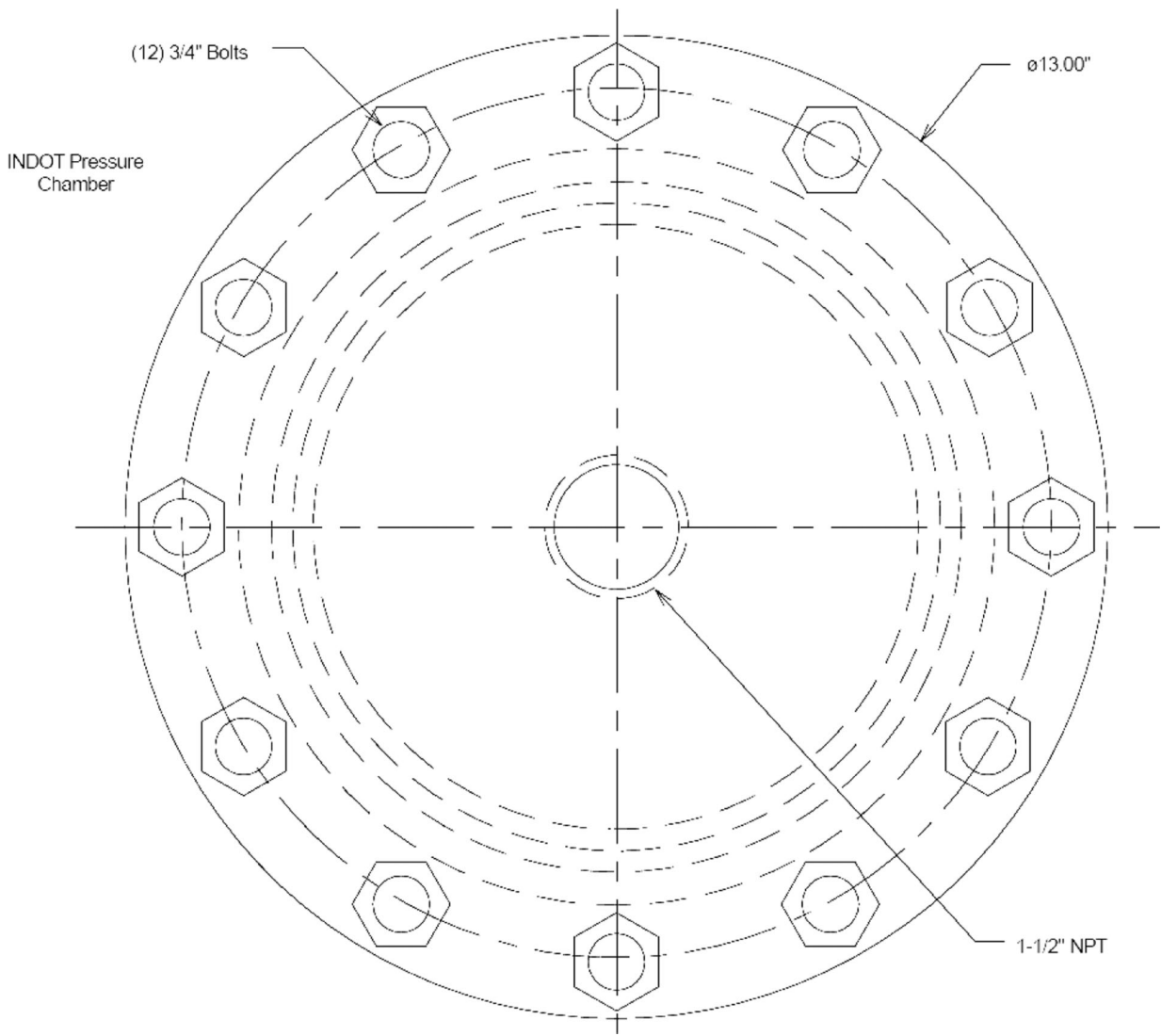


**Figure G.3** Schematic view of the new cover for the modified INDOT HFT chamber.



**Figure G.4** Diagrammatic representation of inside of the lid with the angle of the slope highly exaggerated.

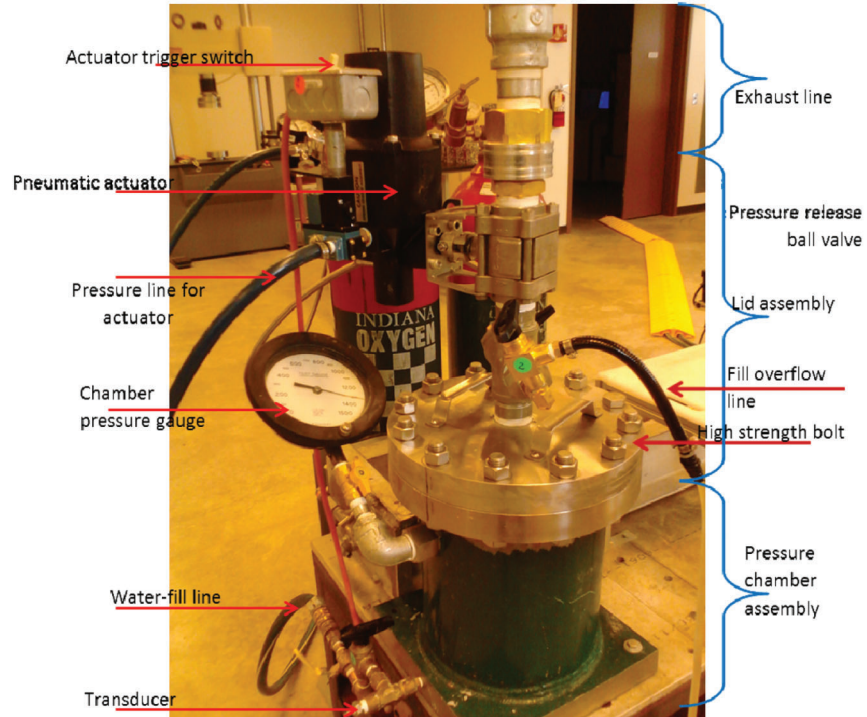


**Figure G.5** Annotated photo of INDOT HFT equipment fully assembled, ready for testing.

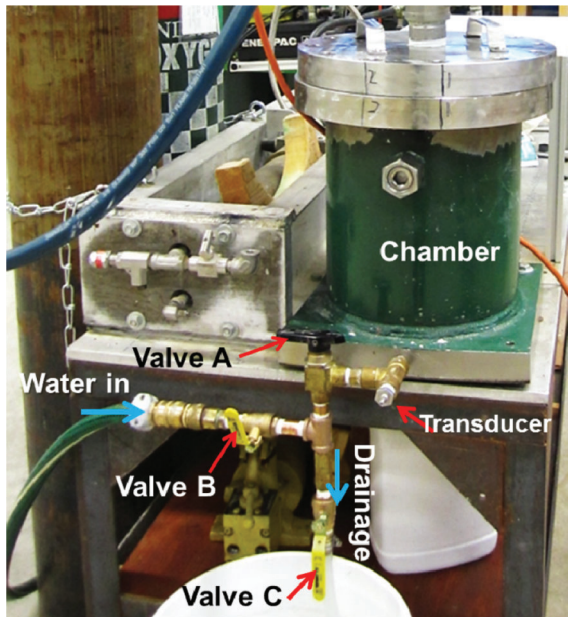


**Figure G.6** INDOT HFT chamber showing water fill and drain assembly.

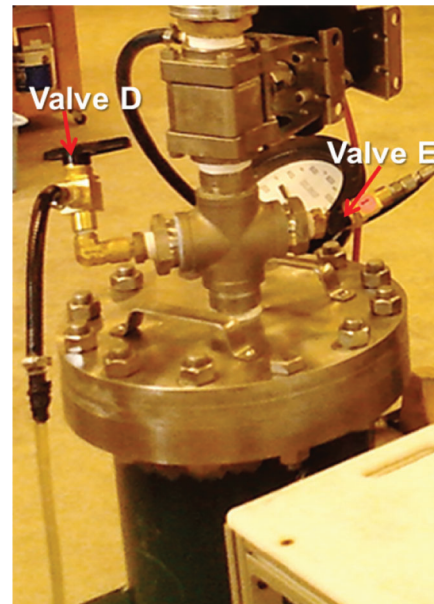


**Figure G.7** INODT HFT chamber showing excess water drain line and valve.

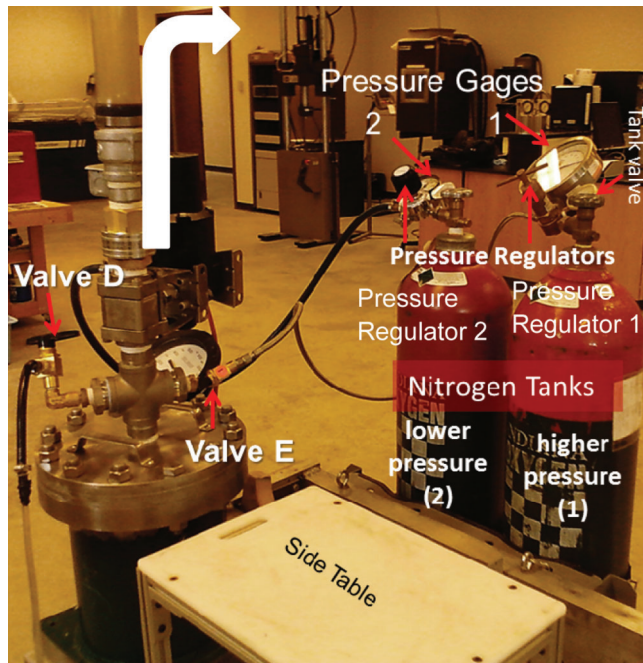


**Figure G.8** INDOT HFT chamber showing exhaust pipe, nitrogen cylinders, pressure regulators and side table.

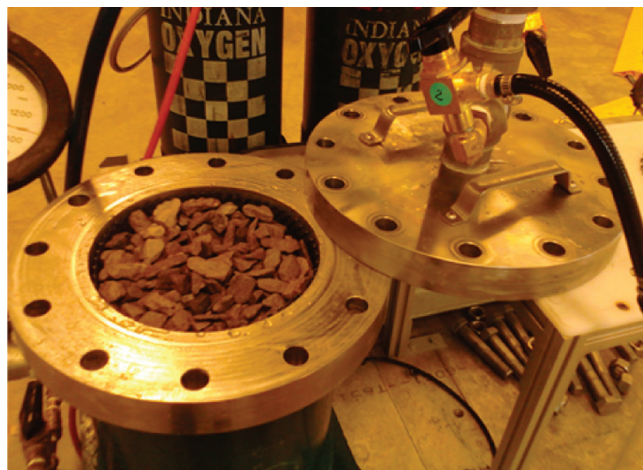


**Figure G.9** INDOT HFT chamber filled with aggregate with lid assembly resting on slide table.

## About the Joint Transportation Research Program (JTRP)

On March 11, 1937, the Indiana Legislature passed an act which authorized the Indiana State Highway Commission to cooperate with and assist Purdue University in developing the best methods of improving and maintaining the highways of the state and the respective counties thereof. That collaborative effort was called the Joint Highway Research Project (JHRP). In 1997 the collaborative venture was renamed as the Joint Transportation Research Program (JTRP) to reflect the state and national efforts to integrate the management and operation of various transportation modes.

The first studies of JHRP were concerned with Test Road No. 1—evaluation of the weathering characteristics of stabilized materials. After World War II, the JHRP program grew substantially and was regularly producing technical reports. Over 1,500 technical reports are now available, published as part of the JHRP and subsequently JTRP collaborative venture between Purdue University and what is now the Indiana Department of Transportation.

Free online access to all reports is provided through a unique collaboration between JTRP and Purdue Libraries. These are available at: <http://docs.lib.purdue.edu/jtrp>

Further information about JTRP and its current research program is available at: <http://www.purdue.edu/jtrp>

## About This Report

An open access version of this publication is available online. This can be most easily located using the Digital Object Identifier (doi) listed below. Pre-2011 publications that include color illustrations are available online in color but are printed only in grayscale.

The recommended citation for this publication is:

Desta, B., Whiting, N. M., & Snyder, M. B. (2014). *Hydraulic fracture test to determine aggregate freeze-thaw durability* (Joint Transportation Research Program Publication No. FHWA/IN/JTRP-2014/15). West Lafayette, IN: Purdue University. <http://dx.doi.org/10.5703/1288284315515>